UNIVERSITEIT VAN PRETORIA
UNIVERSITY OF PRETORIA
YUNIBESITHI YA PRETORIA

Nickel (II) phthalocyanine-multi-walled carbon nanotube hybrids as supercapacitors

by

Alfred Tawirirana Chidembo

A thesis submitted in fulfillment of the requirements for the degree of

Master of Science

at the University of Pretoria

Department of Chemistry

Faculty of Natural and Agricultural Science

November 2009

Supervisor: Dr. K.I. Ozoemena

Dedication

To my dear family who have stuck by me and supported me during the course of my studies.

UNIVERSITEIT VAN PRETORIA
UNIVERSITY OF PRETORIA
YUNIBESITHI YA PRETORIA

Declaration

I declare that the dissertation, which I hereby submit for the degree Magister Scientae in the faculty of Natural and Agricultural Sciences at the University of Pretoria is my own work and has not previously been submitted by me for a degree at this, or any other tertiary institution.

Alfred T. Chidembo

s27280552

Acknowledgements

First and foremost I would like to thank the Almighty God, ever loving father, for guiding me during my studies and in my life. For it is not because of my own wisdom or strength that I have managed to be where I am today but through his mercy and protection.

My sincere appreciation and gratitude go to my supervisor, Dr. Kenneth Ozoemena, for believing in me when no one else did. For giving me the opportunity to further my studies and mostly for the intellectual guidance and concern; it has truly been an exciting learning curve for me.

To my mother, I thank you for the love and constant prayers. To my brothers and sisters, I thank you for the moral support and encouragement. To my sister Eugenia, I could not have done this without your encouragement and support, the two hour phone calls every weekend were priceless.

To my friend Munyaradzi Mugadza, there are friends who stick closer than a brother, and you have done just that for me, ever since we were kids. Thanks a lot. To all my friends and colleagues, I thank you from the bottom of my heart.

Finally, I would like to thank the National research Foundation (NRF) for the financial assistance.

Abstract

The thesis examines for the first time the supercapacitive properties of three different nickel (II) phthalocyanine complexes, nickel (II) tetraamino phthalocyanine (NiTAPc), nickel (II) phthalocyanine and nickel (II) tetra *tert-butyl*phthalocyanine as

(a) nanocomposites with multiwalled carbon nanotubes and as

(b) an electropolymer supported on multiwalled carbon nanotube platform (MWCNT-polyNiTAPc).

The supercapacitive properties of nickel (II) tetraaminophthalocyanine (NiTAPc)/multi-walled carbon nanotube (MWCNT) nanocomposite films have been found to possess a maximum specific capacitance of 981 F g^{-1} (200 mF cm^{-2}), a maximum power density of 700 Wkg^{-1}, a maximum specific energy of 134 Wh kg^{-1} and excellent stability of over 1500 charge-discharge continuous cycling. When compared to MWCNTs modified with unsubstituted nickel (II) phthalocyanine (MWCNT-NiPc) or nickel (II) tetra *tert-butyl*phthalocyanine (MWCNT-*t*BuNiPc), MWCNT-NiTAPc exhibited superior supercapacitive behaviour, possibly due to the influence of nitrogen-containing groups on the phthalocyanine. The MWCNT-polyNiTAPc electrode had a maximum (112 mF cm^{-2}) capacitance which was higher than that observed for MWCNT-polyNi(OH)TAPc (84.9 $mFcm^{-2}$) but lower that of the MWCNT-NiTAPc (200 mF cm^{-2}).

Table of Contents

List of Abbreviations

AFM = Atomic force microscopy
Ag = Silver wire pseudo-reference electrode
Ag|AgCl = Silver/Silver chloride reference electrode
BET = Brunauer, Emmett and Teller
BPPGE = Basal plane pyrolytic graphite electrode
C.E = Counter electrode
CNT = Carbon nanotube
CV = Cyclic voltammetry
CV = Cyclic voltammogram
DMF = Dimethylformamide
EDLCs = Electrical double layer capacitors
FTIR = Fourier transform infrared
HOMO = Highest occupied molecular orbital
IHP = Inner Helmholtz plane
IR = Infrared
LUMO = Lowest occupied molecular orbital
MPc = Metallophthalocyanine
MWCNT = Multiwalled carbon nanotube
NiTAPc = Nickel (ii) tetraaminophthalocyanine

NiTAPc-poly = Electropolymerized Nickel (ii) Tetraaminophthalocyanine film

NiTAPc-poly-OH = Electropolymerized Nickel (ii) tetraaminophthalocyanine film in alkaline solution

tBuNiPc = Nickel (ii) tetra-*tert-butyl*phthalocyanine

NiPc = Nickel (ii) phthalocyanine

PANI = Polyaniline

PTFE = Polytetrafluoroethylene

PPy = Polypyrrole

OHP = Outer Helmholtz plane

PVDF = Polyvinylidene fluoride

R.E. = Reference electrode

SEM = Scanning electron microscope

SWCNT = Single walled carbon nanotube

TBAP = Tetrabutylammonium perchlorate

UV-Vis = Ultraviolet-visible

W.E. = Working electrode

XRD = X-ray diffraction

List of figures

List of Schemes

List of tables

CHAPTER 1

INTRODUCTION

[1]

---

[1] The following publications resulted from part of the research work presented in this chapter and are therefore not referenced further in this thesis:

1. Alfred T. Chidembo, Kenneth I. Ozoemena, Bolade O. Agboola, Vinay Gupta, Gregory G. Wildgoose and Richard G. Compton, *Energy Environ. Sci.*,2010, **3**, 228-236
2. Alfred T. Chidembo and Kenneth I. Ozoemena, *Supercapacitive behaviour of electropolymerized film of nickel (II) phthalocyanine supported on multi-walled carbon nanotube platforms* (paper submitted for publication)

1.1 General Overview of Thesis

The past few years have seen an increased focus on developing sustainable energy devices that are environmentally friendly. Pollution from combustion of fossil fuels has triggered this massive attention on 'green energy'. The three main electrochemical energy storage and conversion (or delivery) systems (i.e. supercapacitors, batteries and fuel cells) are currently attracting major research interests as they have been forecasted to drastically ease the current global energy crisis and reduce man's dependence on fossil fuels (crude oil) for his main energy source.

Supercapacitors exhibit unique energy storage and conversion properties when compared to batteries and fuel cells, notably in terms of power density and fast charging and discharging. The electrode from which a supercapacitor is fabricated impacts heavily on its properties. A significant amount of research on carbon nanotubes and other carbon materials as potential supercapacitor electrodes has therefore been undertaken over the past few years. Hybrid capacitors that make use of CNTs and metal oxides or conducting polymers have also been probed for the same applications. However, no reports have been made on the use of phthalocyanines as supercapacitor electrode materials.

In this thesis, three types of nickel (II) phthalocyanines, unsubstituted nickel (II) phthalocyanine (NiPc), nickel (II) tetra-*tert*-butylphthalocyanine (tBuNiPc) and nickel (II) tetraaminophthalocyanine (NiTAPc) were interrogated with acid-functionalised multi-walled carbon nanotubes (MWCNTs), and their supercapacitive properties investigated using cyclic voltammetry, electrochemical impedance spectroscopy and galvanostatic charge/discharge experiments. This approach is expected to take advantage of the remarkable characteristics of the MWCNTs and MPc to make a novel and robust nanocomposite with higher capacitance compared to its constituents.

1.1.1 Aim of Thesis

The main aim of this thesis is to employ electrochemical techniques (cyclic voltammetry (CV), galvanostatic charge/discharge (CD) and electrochemical impedance spectroscopy (EIS)) to interrogate the supercapacitive properties of:

(i) NiTAPc/MWCNT, NiPc/MWCNT and tBuNiPc/MWCNT composites supported on a basal plane pyrolytic graphite electrode (BPPGE) platform and

(ii) Electrodeposited NiTAPc onto a BPPGE surface pre-modified with MWCNT.

This introduction section provides a general overview of supercapacitors, carbon nanotubes and metallophthalocyanines, electrochemical techniques (CV, CD and EIS), electrode modification strategies, spectroscopic and microscopic characterization of supercapacitor materials. In chapter two the procedure adopted for the experiment is provided. Chapter three discusses the results obtained.

The choice of nickel (II) phthalocyanine complexes supported on MWCNTs has been motivated by many factors such as: (i) cost effectiveness and ease of preparation of MPc complexes, notably NiTAPc, (ii) the high popularity of Ni complexes as supercapacitor materials compared to Fe and Co complexes, (iii) the ability to be stably immobilized onto basal plane pyrolytic graphite substrate via $\pi - \pi$ interaction, (iv) the high surface area, high conductivity and interconnectivity of CNTs that enhance capacitive properties.

1.2 Supercapacitors

Electrochemical capacitors also known as supercapacitors, ultracapacitors or power capacitors are energy devices that have high cycling stability, energy and power density.[1] Supercapacitor and ultracapacitor are the two terms that are mainly used to describe these energy storage devices.

1.2.1 A Brief Historical Perspective

The first patent on the supercapacitor was granted to Becker at General Electric Corp. in 1957, in which they proposed a capacitor based on porous carbon material. This was the first electrical device using double-layer charge storage.[2] Becker's device was however never commercialized. SOHIO were the next big company to work on supercapacitors where they attempted to market their device using high surface carbon materials.[3] Other companies such as NEC, ECOND and Panasonic also marketed their own devices with Panasonic introducing the "Goldcap" double layer capacitor in 1978 in Japan. In the 1990's, Cap-XX, Nippon Chemi-con (NCC) of Japan and Nesscap were the major role players in manufacturing supercapacitors.

In 2002 Maxwell Technologies of the USA purchased the Montena Components of Rossens, Switzerland, an electrochemical capacitor manufacturer making it one of the leading US producers of electrochemical capacitors. Today, Maxwell Technologies has become one of the major manufacturers of supercapacitors in the world. Perhaps, the greatest potential for growth and development of the supercapacitor lies in the automotive industry where hybrid electric vehicles (HEVs) are increasingly becoming popular as well as in memory protection of electronic devices.

1.2.2 Design and Operation Principle

Supercapacitors operate on the same principle as traditional capacitors although they make use of electrodes that have a much higher surface area thereby increasing the capacitance and energy. A supercapacitor is made of two electrodes that are separated by a thin insulator called a separator. The two electrodes are required to be electrochemically inert. The separator is made of porous material so as to facilitate the movement of the electrolyte ions into the pores.

An electrolyte is a material that provides conductivity between the positive and negative electrodes of a cell.[4] The two electrodes, at some distance apart are immersed in an electrolyte. Energy storage is achieved by the separation of charges when a voltage is applied to the electrodes. Negative ions will diffuse to the positive electrode and the positive charges to the negative electrode. This is illustrated in Figure 1.1. The voltage applied forces the formation of an electrochemical double layer (Helmholtz layer) at the inner surface of the electrodes where the charge is stored. The double layer has a thickness of about 5-10 Å.[5] To explain the mechanism of charge storage at the electrode/electrolyte interface an area of one of the two electrodes will be examined in this section.

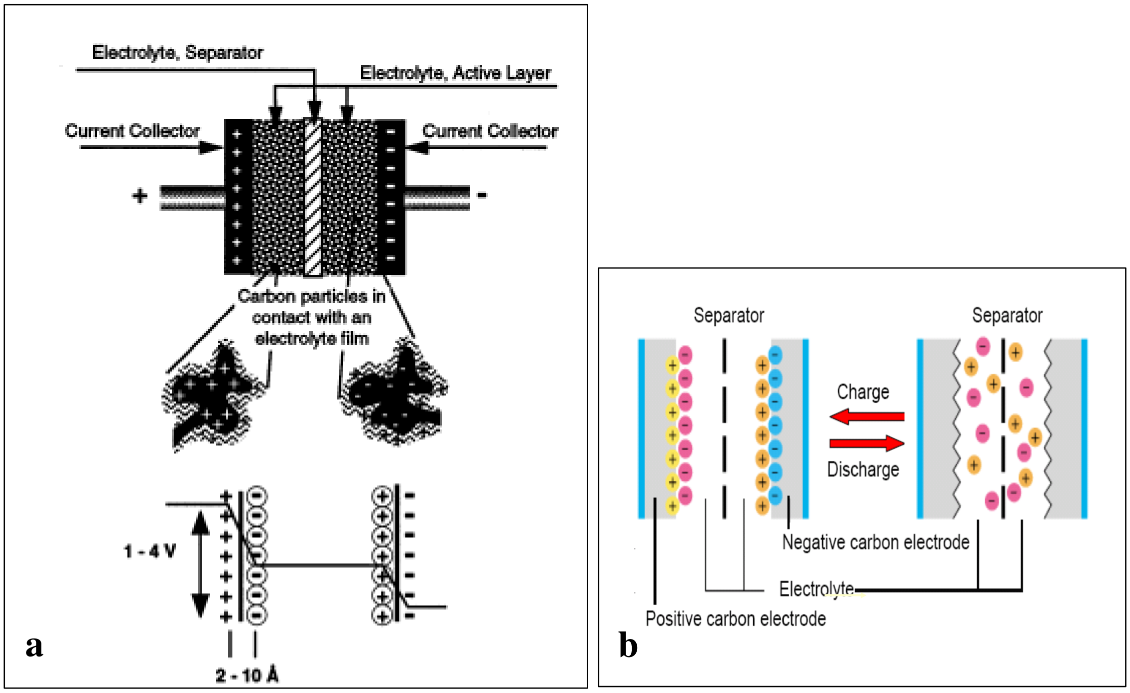

Figure 1.1: Schematic diagram showing the mechanism of a supercapacitor made of porous carbon material. Figure adapted from Kotz and Carlen.[5] **(b)** operating principle of an electrical double layer capacitor. Figure adapted from Frackowiak and Béguin.[6]

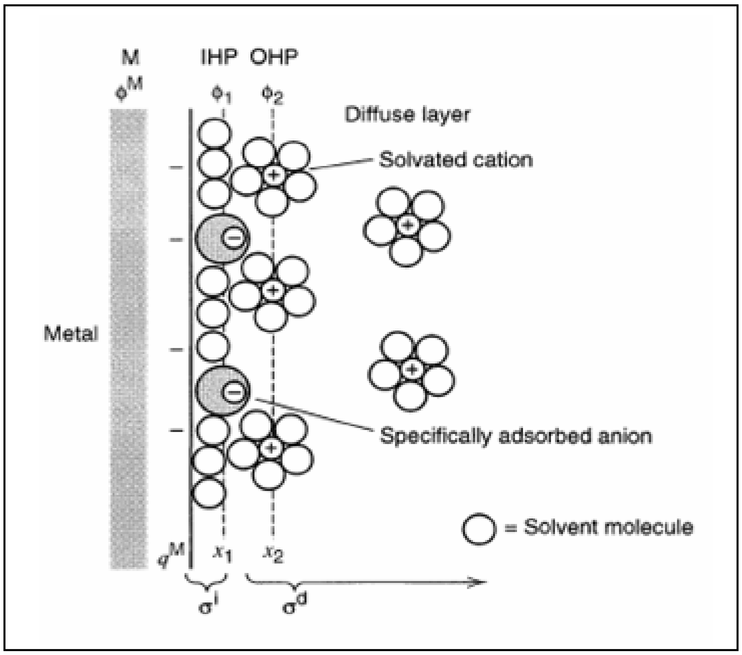

Figure 1.2: Proposed model of the electrical double layer region under conditions where anions are specifically adsorbed. Figure adapted from Bard and Faulkner.[7]

An array of charged species and oriented dipoles existing at the metal-solution interface is called the electrical double layer. The electrical double layer forms at the electrode-electrolyte interface where the electrode surface accommodates one layer and the solution another as shown in Figure 1.2.[4] The result is a separation of charge between the electrode surface and the solution. The double layer capacitance is generally a function of potential, which makes it different from a standard capacitor. The inner layer at the electrode surface known as the compact, Helmholtz, or Stern layer is composed of solvated molecules and other ions or molecules that are thought to be adsorbed. The inner layer can be divided into two Helmholtz planes, the inner Helmholtz plane (IHP) and the outer Helmholtz plane (OHP).

From Fig. 1.2, the IHP is located at a distance x_1 and the OHP at a distance x_2. The OHP is the location for the maximal charge density.[8] The IHP is the closest distance of approach of specifically adsorbed ions. As solvated ions interact with the charged metal only long-range electrostatic forces dominate, so that their interaction is essentially independent of the chemical properties of the ions. These ions are said to be nonspecifically adsorbed. The structure of the double layer can affect the rates of electrode processes in as much as it can be affected by the structure of the electrode and the electrolyte layer itself. Due to the different mechanisms of charge storage, different classes of supercapacitors have emerged. The situation in figure.1.2. can be represented by a simple circuit.

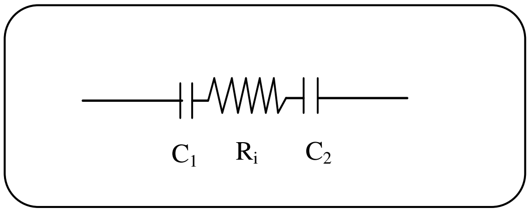

Figure 1.3: Simple circuit showing the connection of electrodes in a two electrode system. Figure adapted from Winter and Brodd. [4]

C_1 and C_2 are the double layer capacitances of the anode and cathode respectively and R_i is the internal resistance of the cell. Equation 1 best describes the calculation of total capacitance for capacitors connected in series.

$$\frac{1}{C}=\frac{1}{C_1}+\frac{1}{C_2} \quad \text{...} \quad (1)$$

The amount of electrical charge stored in a capacitor is reported in Farads (F), pico Farads (pF) or microfarads (μF). The *specific capacitance* is usually expressed in F/g or F/cm^2. However, typical values for specific capacitance (F/cm^2) are usually in the range of 15-50 μF/cm^2.[9] The capacitance, C, is defined as the ratio between the stored charge, Q, to the applied voltage.

$$C=\frac{Q}{V} \quad \text{...} \quad (2)$$

In a normal capacitor, capacitance, C, is given by equation (3).

$$C=\frac{A}{4\pi d} \quad \text{...} \quad (3)$$

where *A* is the area of the plates in square metres and *d*, the distance between the electrode plates in metres. *C* in this case has the units for length. In cases where the electrode plates are separated by a dielectric medium (ε = Fm^{-1}), the capacitance is given by equation (4) where the units for capacitance are in F.

$$C=\frac{A\varepsilon}{4\pi d} \quad \text{...} \quad (4)$$

To achieve high capacitance values for electrochemical capacitors, the area (A) of the electrodes has to be increased since the distance, *d* is number of factors and few of these will be mentioned here. The capacitance of a two electrode system and a single cell electrode vary significantly by a factor of four.[10] It is therefore imperative that in reporting these values, one states the type of electrode measurement used. The choice of electrolyte also has to be done carefully as the decomposition voltage of the electrolyte determines the voltage at which the supercapacitor operates (i.e. the operating voltage of a supercapacitor). Different electrolytes have been studied with aqueous electrolytes being restricted to a maximum voltage of 1 V due to the thermodynamic electrochemical window of water (1.23 V). The possibility of achieving higher voltages comes from organic electrolytes where the maximum working voltage is limited to 2.5-2.7 V.[10] However, organic electrolytes increase the resistance and have lower conductivity. The amount of maximum usable power of supercapacitors that use organic electrolytes is low due to the high resistance. The energy, E stored in a capacitor is directly proportional to the capacitance.

$$E = \frac{1}{2}CV^2 \quad \text{……………………………………………………} \quad (5)$$

In general, the power P is the energy represented per unit time. From equation 5, high values of C and V automatically imply a higher energy.

1.2.3 Energy and Power Densities: The Ragone Plot

Energy density (expressed in Wh/kg) and *Power Density* (expressed in W/kg) are two terms that are mainly used in energy systems to compare energy contents and rate capabilities respectively. Both quantities have their density as a quantity per unit mass or per unit volume. A Ragone plot (Fig.1.4) has been developed to show the relationship between power and energy densities for various energy devices and also highlights the performance characteristics of these energy storage and conversion systems.

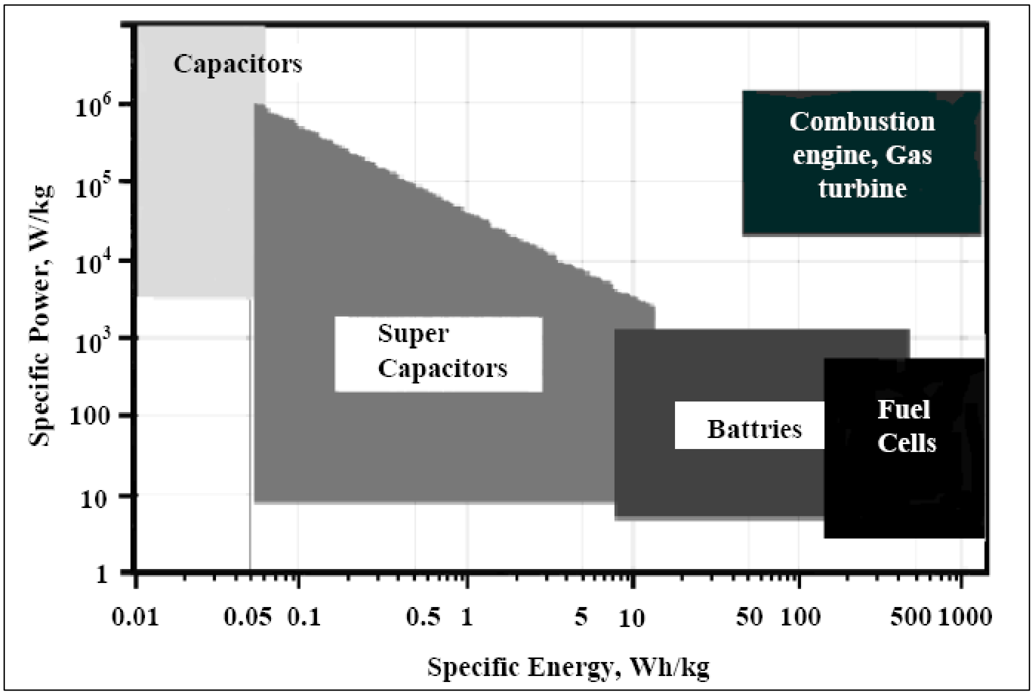

Figure 1.4: A simplified Ragone plot of specific power versus specific energy for various energy storage devices.[4, 5]

Conventional capacitors from the diagram above show high power density but lower energy density when compared with batteries and fuel cells. This implies that batteries can store more energy than a capacitor but the delivery time of this energy is longer, hence a lower power density. A capacitor, although it stores less energy can quickly discharge and rapidly release large amounts of power resulting in a high power density. The importance of the supercapacitor as a link between traditional capacitors and batteries is therefore highlighted in the Ragone plot. Although a supercapacitor provides greater capacitance, it still falls short of reaching the energy densities of batteries and fuel cells. For this reason, this work will focus only on the supercapacitor in an attempt to improve the capacitance at the electric double layer and consequently the energy density of the device.

1.2.4 Relevance of Supercapacitors in Energy Devices

Supercapacitors serve as intermediate systems that bridge the power/energy gap between traditional capacitors (high power) and batteries (high energy).[5] Supercapacitors, due to their long cycle life and stability, find numerous applications in car audio systems, photo and video cameras, solar lanterns, lightweight electronic fuses, starting power of fuel cells, memory protection of computer electronics etc. Furthermore, they are non toxic and are applicable in a large temperature range.

Supercapacitors have a shorter charging time and high power density compared with fuel cells and batteries.

A closer look at the Ragone plot clearly indicates the following points:

(a) Fuel cell is a high-energy system;

(b) Supercapacitor is high-power system; and

(c) Batteries posses intermediate power & energy properties;

(d) No single electrochemical energy storage system can match the internal combustion engine

To be able to match the performance characteristics similar to those of the internal combustion engine, the new trend is to combine these electrochemical energy storage systems in electronic devices and hybrid electric vehicles. For example, the diagram (Figure 1.5) below explains how this is done with supercapacitors and batteries.

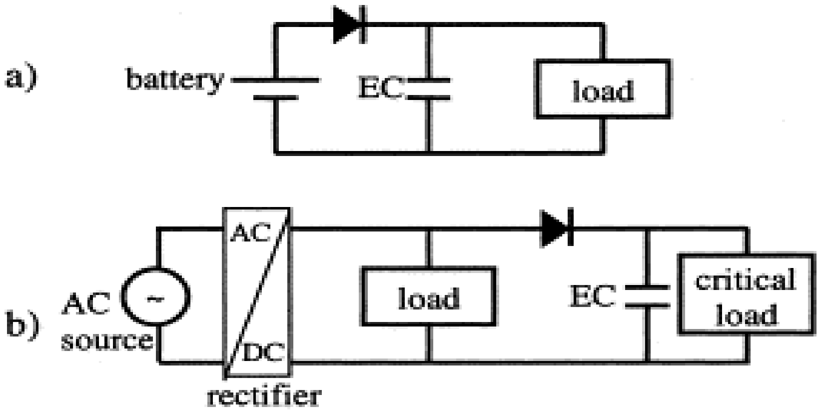

Figure 1.5: (a) A battery powered device where the EC supercapacitor provides power backup of the load in case of disconnection of the battery. **(b)** An AC-voltage powered device involving heavy switching currents. The EC protects the critical load (e.g. memory) from large voltage drops. Figure adapted from Kotz and Carlen.[5]

1.2.5 Classification of Supercapacitors

Supercapacitors are classified into two different categories namely, (i) Electric Double Layer Capacitors (EDLCs) and (ii) pseudocapacitors. Recently, a third category has been added that incorporates hybrid capacitors. The operation mechanism of EDCLs involves the non-Faradaic separation of charges at the "double-layer" (i.e., electrode/electrolyte interface) while pseudocapacitors involve fast Faradaic, redox reaction of electroactive materials at the interface. Hybrid capacitors involve both mechanisms.

EDLCs make use of high surface area carbon materials such as activated carbon, carbon nanofibres, carbon aerogels and carbon nanotubes (CNTs). Pseudocapacitors employ metal oxides such as RuO_2, NiO_2 and MnO_2 and conducting polymers as electrode materials.[4, 10] An active research interest involves the integration of EDLC and pseudo-capacitive materials to obtain high-performance supercapacitors (Hybrid capacitors) compared to the individual capacitor system.[9]

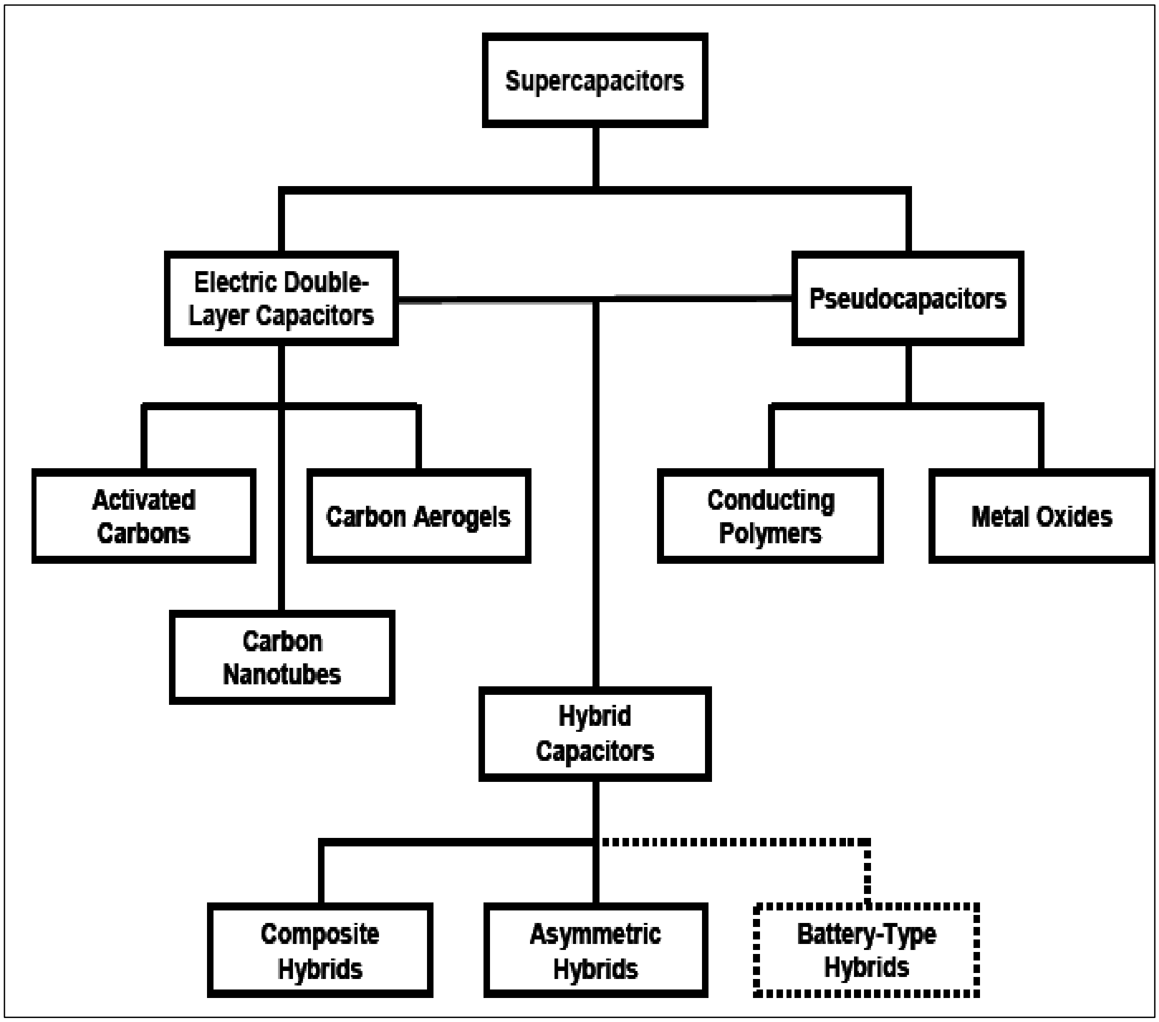

Figure 1.6: General classes of supercapacitors. Figure adapted from Halper and Ellendogen.[11]

1.2.5.1 Electric Double Layer Capacitors (EDLCs)

Activated carbons, carbon aerogels, carbon xerogels, carbon nanotubes, and carbon nanofibres have attracted a lot of interest from researchers in the supercapacitor industry. After the engineers at SOHIO had used carbon as a material of choice for the manufacture of supercapacitor electrodes, it has become one of the most frequently used electrode material in different modifications. The investigation of carbon based electrodes for supercapacitors have largely been fuelled by the attractive properties of carbon.

Carbon is a low cost material that has an impressive surface area of about 2500 m^2 /g ideal for supercapacitor electrodes.[5] Its porous nature means that carbon based electrodes can store charge in the pores that exist in the electrode. The availability of pores in any electrode material for supercapacitors is of vital importance with the pore size and pore volume playing a pivotal role in charge storage.[12] An *et al*. reported micropores (<2nm) and macropores (>50 nm) to be inappropriate for supercapacitor electrodes. Micropores provide a slow rate of electrolyte diffusion while the macropores[13] are too large to retain hydrated ions. Mesopores are therefore ideal for storing charge in supercapacitors.[14] According to Frackowiak *et al*.[9] ionic conductivity relates the mobility of ions inside the pores. The rate of electrochemical accessibility is dictated by the mobility of ions inside the pores. Larger pores are easily accessible whereas smaller pores are difficult to access, making the movement of ions difficult. A network of resistors was therefore postulated by Frackowiak *et al*. due to the non-uniformity in resistance throughout the electrode material as a whole.

(a) Activated carbons

Activated carbons, in the activation process can be tailored in such a way that the distribution of pores, pore size and pore volume can be controlled. Activated carbons achieved by treatment with KOH have been reported to exhibit a high oxygen content that influences the electrochemical characteristics. Shi[15] suggested the strong dependence of power density of activated carbons to the porous structure. Shi *et al*. went on to study the relationship between BET surface area, total pore volume, average pore size, pore volume and pore distribution and capacitance. They found that there is no linear relationship between the specific double layer capacitance and surface area. They also reported that the specific double layer capacitance per unit of external surface area is strongly dependant on the porous structure. Since activated carbon is usually in powder form, binders such as polyvinylidene fluoride (PVDF) [16] and polytetrafluoroethylene (PTFE) [17, 18] are necessary for making a paste that can be used as a practical electrode.

(b) Carbon aerogels

Carbon aerogels are highly mesoporous materials that consist of a continuous rigid solid framework and an open, continuous network of pores. Amongst their favorable characteristics are the good electrical conductivity, controllable pore structure and highly useable surface area.[18] These qualities make carbon aerogels good candidates for supercapacitor electrodes.

(c) Carbon nanotubes

Carbon nanotubes have emerged as leading materials for electrodes since their first use as supercapacitor electrodes was reported by Niu *et al*.[19] The highly porous nature, chemical and thermal stability as well as high surface area give carbon nanotubes an edge over other materials being investigated as supercapacitor electrodes. The porous nature of carbon nanotubes allows easy access of ions from the electrolyte into the pores of the electrode. Both single walled carbon nanotubes (SWCNTs) and multiwalled carbon nanotubes (MWCNTs) have undergone immense research as potential electrode materials. Niu *et al*. reported the use of MWCNTs as supercapacitor electrodes with capacitance as high as 102 and 49 F/g at 1 and 100 Hz respectively in 38% H_2SO_4 as the electrolyte and a maximum specific capacitance of 113F/g. Frackowiak *et al*.[20] reported a maximum capacitance value of 135 F/g. In both cases, the two electrode system was employed.

The capacitance of CNTs can be significantly enhanced by functionalizing them first. Functionalization involves the treatment of CNTs with nitric acid/ sulphuric acid mixture under harsh conditions resulting in defects on the walls of the carbon nanotubes, an essential property for charging the double layer and also enhancing wettability of CNTs. By functionalizing the CNTs, surface carboxyl groups are added resulting in pseudocapacitance and a deviation from ideal double layer capacitive behaviour. Excessive oxidation however lowers conductivity due to the damage caused on the CNT structure.[10] Apart from functionalization of CNTs, the use of binders such as PVDF and PTFE have been reported to increase specific capacitance of CNT based supercapacitors.[18]

1.2.5.2 Pseudocapacitors

Pseudocapacitance has been described by Conway as arising from surface faradaic processes. In such instances, the charge, Q, passed during the oxidation and reduction process is continuously, and reversibly, dependant on the electrode potential.[21] Electrosorption of H or metal adatoms and redox reactions of electroactive species are some of the processes associated with pseudocapacitance[6]. The charging and discharging of a pseudocapacitor takes place through Faradaic processes involving electron transfer across the electrode-solution interface. The contribution of pseudocapacitance to the final capacitance of an electrode cannot be underestimated. However, cyclic life of the capacitor is reduced due to the redox processes that take place in the electroactive electrode material. Conducting polymers and metal oxides such as RuO_2 and other oxides of transition metals are good examples of materials that give rise to pseudocapacitance.

(a) Metal Oxide based Supercapacitors

Research into possible supercapacitor electrode materials has intensified over the years and several materials have been investigated. Metal oxides e.g. MnO_2[22, 23], IrO_2[24], RuO_2[25, 26] and NiO[27, 28] have been studied as potential electrode for supercapacitor applications. The most popular novel metal oxides for supercapacitor electrodes are RuO_2 and IrO_2. These metals give rise to high capacitance values ranging from 720-760 Fg^{-1}(three electrode system) and can be probed over a wider potential window compared with carbon materials. Although these materials exhibit favorable characteristics, they are very expensive and this limits their applications.[29] As an alternative, inexpensive metal oxides such as MnO_2 [30], NiO[31] and Fe_30_4 [32] have been reported in literature.

The capacitance of metal oxides can be enhanced by mixing them with high surface area carbon materials to make nanocomposites which combine double layer capacitance and pseudocapacitance. Zheng *et al*.[31] in their work, reported that MWCNTs greatly improved electrochemical properties, power density, specific capacitance and cycle performance of NiO. Recently, it has been discovered that metal hydroxides can achieve higher capacitance as compared to metal oxides.[33]

(b) Conducting Polymer Based Supercapacitor

Polymeric materials such as polyaniline, [34, 35] polypyrrole (PPy) [36] and polythiophenes[37] are promising materials for supercapacitor electrodes. Conducting polymers have desirable characteristics such as

(i) high specific capacitance,
(ii) high conductivities,
(iii) "fast" charge-discharge processes,
(iv) good thermal and chemical stability
(v) high energy density and power density.[38]

Polyaniline (PANI) is the most frequently used polymer as an electrode material for supercapacitors due to its ease of polymerization in aqueous media and high environmental stability. PANI can also exhibit different oxidation states giving rise to pseudocapacitance. [39] Compared to carbon materials; PANI however has poor cycling stability.[40] Capacitance values as high as 775 F/g have been reported by Gupta and Miura using the three electrode system.[34]

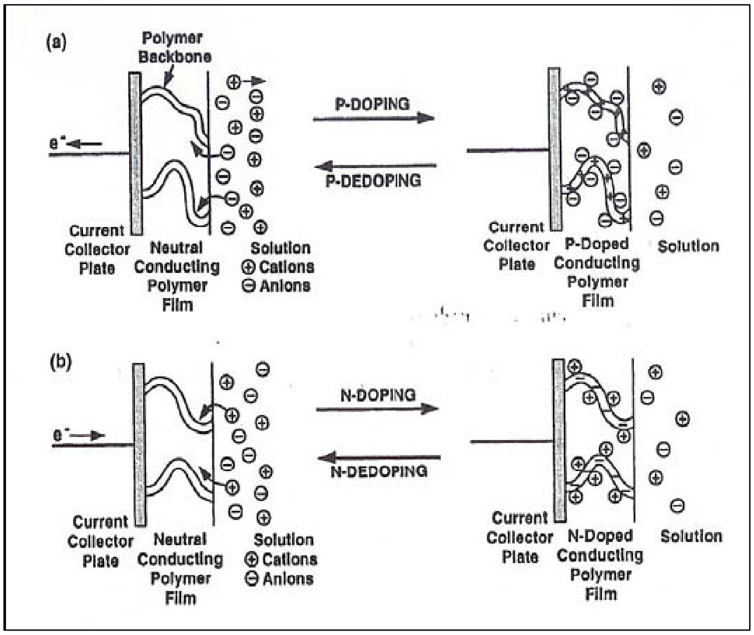

Figure 1.7: Development of a quasi linear double layer at a charged conducting polymer chain. Figure adapted from Conway.[41]

The mechanism of operation of polymer based supercapacitors is shown in Figure 1.7. There are two polymer configurations, where one is negatively charged (n-doped) and the other is positively charged (p-doped). In their work on polymer based redox supercapacitors, Arbizzani *et al.*[42] reported the limited use of n-doped compared to p-doped polymers. However a combination of n-doped and p-doped configurations as negative and positive electrodes respectively has been reported to be more promising.[43] Conducting polymers have also been used to make composites with CNTs.[40]

1.2.5.3 Hybrid Capacitors

Hybrid capacitors exploit the advantages of both pseudocapacitors and electrical double layer capacitors resulting in better performing supercapacitors that outperform both EDLCs and pseudocapacitors. The carbon materials provide a backbone with high surface area and favorable pore distribution while the pseudocapacitive material enhances the capacitance through faradaic reactions on the surface of the electrode.[44, 45] Research in hybrid capacitors promises to overtake research in EDLCs and pseudocapacitors.

(a) Composite hybrids

The modification of CNTs with conducting polymers or metal oxides for supercapacitor electrodes has also been shown to improve capacitance.[36] In such instances, the carbon nanotubes function as electron acceptors while the polymer acts as an electron donor. Supercapacitor studies of CNTs/conducting polymers have been well documented.[40, 46, 47]

In this work, the best qualities of MWCNTs and metallophthalocyanines have been combined to form a hybrid capacitor with higher capacitance and remarkable cycling stability.

(b) Asymmetric

Asymmetric hybrid supercapacitors combine both faradaic and non-Faradaic processes to achieve high power and energy densities than EDLCs and pseudocapacitors. In asymmetric supercapacitors, the two electrodes are each made up of different material. Arbizzani, Mastragostino and Soavi[48] reported the use of p-doped poly (3methylthiophene) as a positive electrode and activated carbon as a negative electrode. The hybrid capacitor outperformed the EDLCs. This arrangement affords the opportunity to exploit the favorable characteristics of the individual electrodes.

(c) Battery-Type

Asymmetric and battery-type capacitors operate in the same principle where two electrodes made up of different material are used. Battery-type supercapacitors however employ a battery electrode and a supercapacitor electrode. Such capacitors are a result of the need for storage systems which can maintain high cycle life, high energy density and fast charge characteristics. The most common materials for the battery electrode are metal hydroxides. Little research has been done on this type of supercapacitor although it has been forecasted to bridge the gap between batteries and supercapacitors.[49]

1.3 Carbon Nanotubes

The rediscovery of tubular carbon nanostructures[50] in 1991 by Sumio Iijima sparked a lot of interest from researchers around the world. The first evidence of tubular nano-sized filaments similar to carbon nanotubes was first reported by the Russian scientists, L.V. Radushkevich and V.M. Lukyanovich in 1952.[50a]. Wiles and Abrahamson in 1978 are also reported to have discovered fibres on graphite anodes and these fibres are now known as carbon nanotubes.[50b] Iijima, an NEC electron microscopist in Tsukuba, Japan, rediscovered carbon nanotubes in the soot of the arc discharge method. Carbon nanotubes exist in two main forms, multi-walled carbon nanotubes (MWCNTs) and single-walled carbon nanotubes (SWCNTs). Iijima claimed to have discovered MWCNTs in 1991 by Iijima and SWCNTs two years later[51]. They reported MWCNTs to be hollow nanostructures made up of concentric cylinders of graphite that resembled graphitic shells with an adjacent shell separation of ~ 0.34 nm and diameters of ~ 1nm. SWCNTs which are more similar to ideal fullerenes on the contrary, only have single graphitic shells.

Smalley and co-workers [52] in their publication provided more insight into the synthesis of bundles of aligned SWCNTs with a yield higher than 70%. Carbon nanotubes cannot be viewed in isolation but as structures related to fullerenes. The connectivity between these two interesting forms of carbon lies in their functionality, with carbon nanotubes acting as nanowires and carbon fullerenes as quantum dots.[53] Figure 1.8 shows a typical SEM image of normal carbon nanotubes.

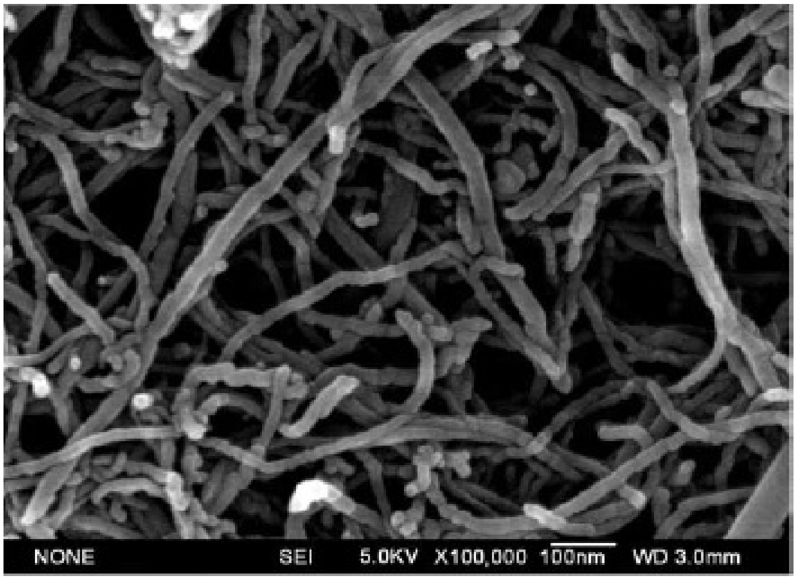

Figure 1.8: SEM image showing normal carbon nanotubes. Figure adapted from Jiang *et al*.[54]

1.3.1 Structure of carbon nanotubes

Carbon nanotubes are made up of sp^2 carbon atoms which are bonded together to make up graphite sheets which are rolled up to form carbon nanotubes as shown in figure 1.9. The roll–up vector determines the valuable electronic properties of the nanotubes.[57] Carbon nanotubes are mainly synthesized using three different methods namely, arch-discharge, laser ablation and chemical vapor deposition (CVD) and can exist in different atomic structures (figure 1.10).

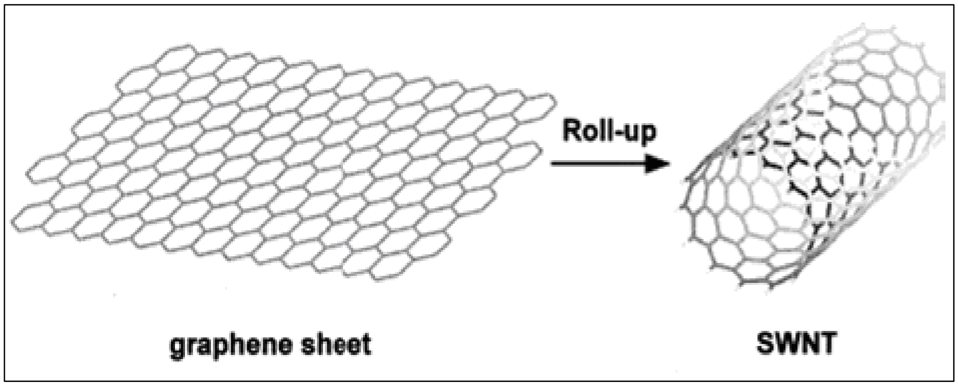

Figure 1.9: Schematic of a 2D graphene sheet illustrating the folding of graphene sheet making up SWCNT. Figure adapted from Odom *et al*.[55]

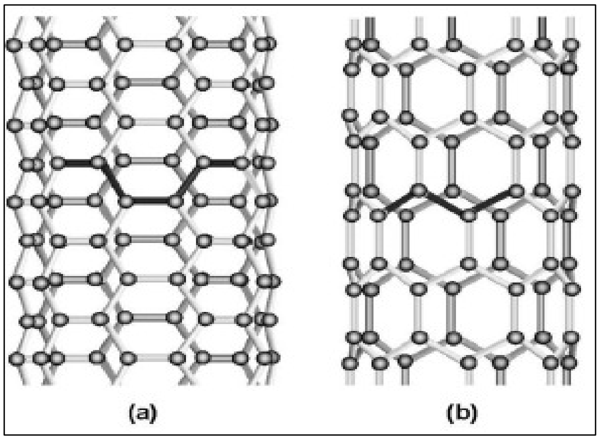

Figure 1.10: Illustrations of atomic structures **(a)** armchair and **(b)** a zigzag nanotube. Figure adapted from Popov. [56]

1.3.2 Properties of carbon nanotubes

The field of carbon nanotube research is still growing and the amount of interest in this area has been phenomenal. Carbon nanotubes have unique properties such as the remarkable ability to either have conducting or semiconducting properties. This behaviour stems from the chirality and diameter of the nanotubes.[53] Additionally, carbon nanotubes have great thermal stability, high tensile strength and elasticity. Wong *et al*.[58] matched the theoretically predicted properties of carbon nanotubes with experimental data using atomic force microscopy (AFM). Knowledge of these properties enabled the scientists to link the materials with possible applications. In their study, Wong *et al*. concluded that MWCNTs are able to store and absorb considerable energy.

Perhaps the most important property of carbon nanotubes that make them ideal supercapacitor electrodes is their high surface area. Peigney and co-workers[59] reported the specific surface area of individual carbon nanotubes and bundles of carbon nanotubes as a function of tube diameter, the number of walls and the number of carbon nanotubes in a bundle. The functionalization of carbon nanotubes opens the way for research into their use as composites with other materials.

1.3.3 Applications

The wide varieties of applications that carbon nanotubes receive are attributable to their remarkable properties. CNTs have the unique ability of promoting electron transfer in electrochemical reactions that has prompted their use in electrochemical sensing. The electrocatalytic activities of CNTs have also been probed thoroughly by researchers with molecules such as

NADH and H_2O_2 receiving a lot of attention.[60-63]. Ozoemena *et al*. have recently reported the use of carbon nanotubes – metal phthalocyanine composites for the detection of dopamine [64] and electrocatalytic detection of V-type nerve agent sulfhydryl hydrolysis products.[65] The elecro-reduction of ferricyanide and the oxidation of NADH, epinephrine and nor-epinephrine using MWCNT abrasively loaded onto basal plane pyrolytic graphite electrodes was performed by Moore et al. in 2004.[65a]. MWCNT when grown using metal catalysis usually result in the nanotubes containing iron impurities. The metal impurities were however shown to aid the electrocatalysis of hydrogen peroxide at MWCNT-modified electrodes by Banks *et al* [65b].

The use of carbon nanotubes and nanostructured carbons in energy storage devices has been reported by Frackowiak and Béguin.[66] Three important energy devices, lithium batteries, supercapacitors and fuel cells all make use of carbon nanotubes. In lithium – ion batteries, CNTs find their place in the construction of the negative electrode where MWCNTs play a pivotal role in the formation of a double layer.[67] Good electronic conductivity make CNTs good materials for electrode construction for the storage of hydrogen where SWCNTs are believed to store as much as 110 $mAhg^{-1}$ of hydrogen electrochemically.[68]

1.4 Metallophthalocyanines (MPcs)

The name *Phthalocyanine* was conceived by Linstead. The prefix *phthal* comes from the Greek word *naphtha* (rock oil) and *cyanine* (blue). Phthalocyanines (Pcs) are 18π – electron aromatic macrocycles that have a characteristic blue green colour that makes them materials of choice for making dyes. Pcs were discovered by accident in 1928 at the Grangemouth plant for Scottish Dyes Ltd. The glass-lined vessel containing reagents for the preparation of phthalimide from phthalic anhydride cracked resulting in the formation of a blue-green material. Two employees, Dandridge and Dunsworth, studied the material and discovered the material to be remarkably stable and insoluble. In 1929, a patent was granted to Dandridge and Dunsworth on the preparation and properties of the material.[69, 70]

The possibility of attaching around seventy metal ions in the central cavity of the phthalocyanine moiety makes the redox chemistry of these molecules very interesting to study. Reduction and oxidation reactions of MPc complexes either take place at the central metal atom, in the phthalocyanine ring itself or both. MPcs that have Zn and Cu as the central atoms have been reported by Ozoemena as having no accessible d-orbitals. This means that any redox reactions that occur will only involve the macrocyclic ring.[71]

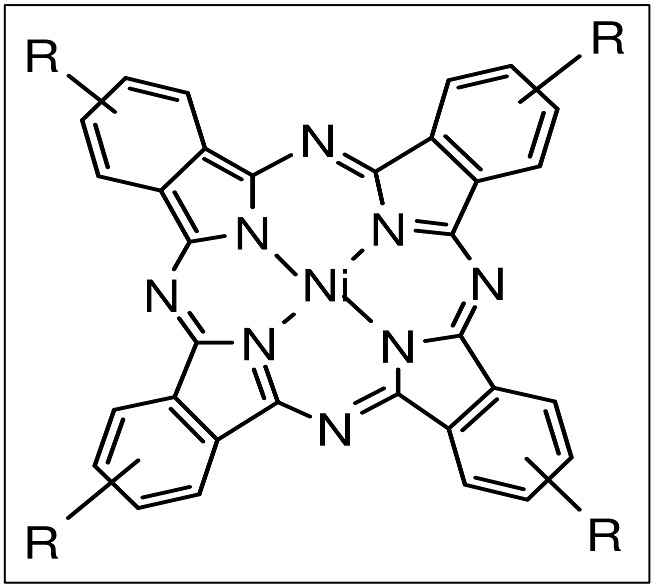

Figure 1.12: Molecular structure of nickel (II) phthalocyanine studied in this thesis where R = H (NiPc), R = $-NH_2$ (NiTAPc),R = -t Butyl (tBuNiPc).

1.4.1 Applications

Phthalocyanines owe their wide variety of applications to their properties such as insolubility not only in water but other organic solvents as well. The macromolecules furthermore have exceptional stability. Over the past years, phthalocyanines have been used in the dye industry. With the increase in technology, MPcs have been used as industrial catalysts as light absorbing materials for compact discs, [72] as photoconducting materials in photovoltaic cells[73], in liquid crystal displays, sensors[74] and fuel cells.[75]

CHAPTER TWO

REVIEW OF METHODS OF CHARACTERIZATION OF SUPERCAPACITOR MATERIALS

2.1 Physico-chemical Characterisation of Supercapacitor Materials

2.1.1 X-Ray Powder Diffraction

X-Ray powder diffraction is a technique that has experienced significant growth over the past thirty years. The development of the Rietveld [76] method has catapulted development of this technique to where it is today. In material sciences, some materials are only present in powder form. To elucidate their structures, techniques such as powder diffraction have had to be employed thereby playing a pivotal role in unlocking the structure of materials. X-ray diffraction finds its primary use in the fingerprint characterization of crystalline materials and the determination of their structure.

Any crystalline substance has a unique X-ray powder pattern which can be known as its "fingerprint". The technique is also used for the determination of the bonding and packing of atoms in crystals. The area under the peaks gives important information about the quantity of each phase in a sample.[77]

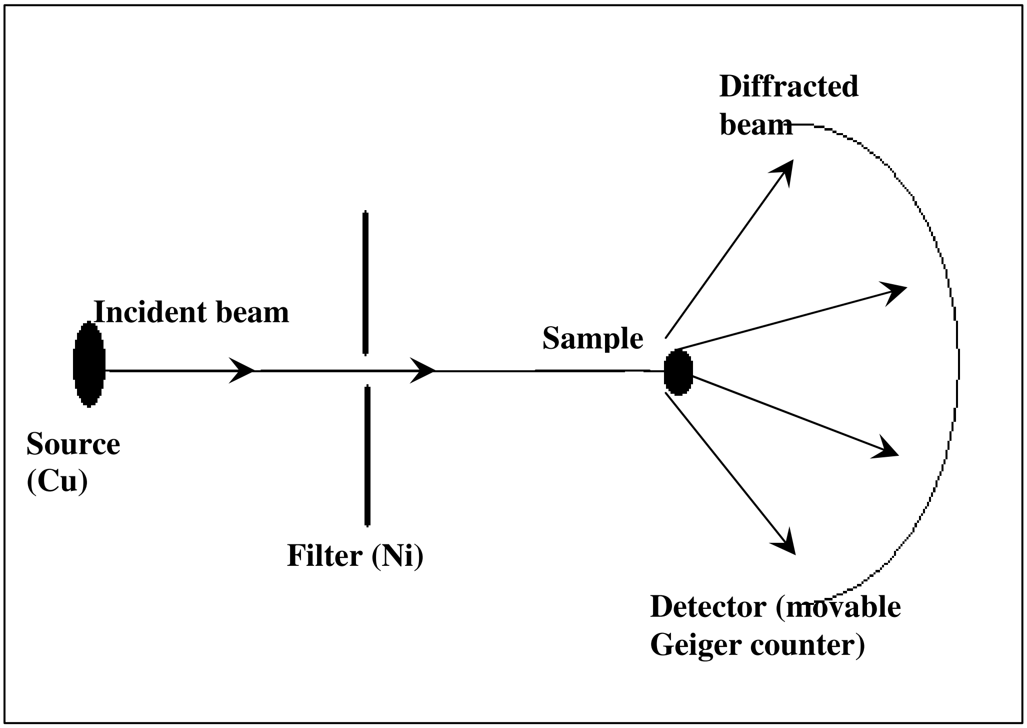

Figure 2.1: Schematic diagram showing how an X-ray diffractometer works. Figure adapted from Whittingham[78]

The X-ray radiation most commonly used is that emitted by copper, whose characteristic wavelength for the K radiation is =1.5418Å. Diffraction occurs in every possible orientation of 2 theta when the incident beam strikes powder sample. Electrons in the atoms of the powder sample oscillate with the same frequency as the incident beam. Destructive interference and constructive interference are experienced when the waves are out of phase and in phase respectively. Upon diffraction, the beam may be detected by using a moveable detector, which is connected to a chart recorder. The counter is set to scan over a range of 2theta values at a constant angular velocity. Routinely, a 2θ range of 5 to 70 degrees is sufficient to cover the most useful part of the powder pattern. The particle size is best estimated by the Debye-Scherrer equation,

$$L = \frac{K_s \lambda}{B \cos \theta} \quad \text{.................................... (9)}$$

Where L is the average particle size, K_s is the scherrer's constant, λ = 1.54056 Å, B is the width of a strong peak in radians and θ the corresponding Bragg angle.[79] For supercapacitor electrode materials, broad peaks are ideal as these imply the amorphous nature of the material and consequently a higher surface area. The peak height observed in the XRD pattern is related to the crystal size of the material under investigation.[80]

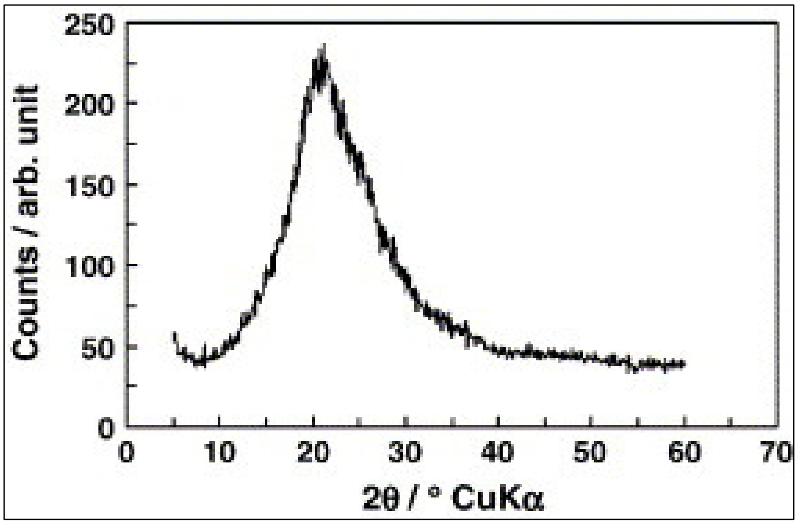

Figure 2.2: Typical X-ray diffraction pattern for polyaniline nanowires studied as potential supercapacitor electrodes. Figure adapted from Gupta and Miura.[34]

In this work, X-ray diffraction provided useful information regarding the presence of Nickel metal in the hybrids.

2.1.2 Infra-Red Spectroscopy

Infrared spectroscopy (IR) has become a well accepted technique for the study of surface reactions. Its huge success as an analytical tool has been largely due to its ability to examine adsorbed molecules on solid surfaces.[81] IR makes use of infrared radiation to fingerprint a sample. Infrared radiation is transmitted through the sample and upon hitting it; some of the radiation is adsorbed while some of it passes through the sample. A spectrum is then recorded in the form of a plot of absorbance versus wavenumber. This results in a molecular fingerprint being created as no two samples can produce identical spectra.[82]

Fourier Transform Infrared Spectroscopy (FTIR) can therefore provide a wealth of information regarding the identity and quality of a sample in addition to the components in a mixture. Some of the advantages of FTIR over other dispersive techniques include; high sensitivity due to the high signal-to-noise ratio, high rate of data generation, simplicity and reduced heating effect of the beam. For functionalized carbon nanotubes, stretching absorption peaks of importance are mainly the C=O, C-O ester groups usually observed around 1700 and 1000 cm^{-1}. Phthalocyanines on the other hand are usually characterized by UV-Vis spectroscopy as discussed in the following section.

2.1.3 UV-Vis Spectroscopy

UV-Vis spectroscopy is one of the oldest and important analytical techniques used for the quantitative determination of a variety of species. The technique finds a lot of applications in many areas such as physics, chemistry and biochemistry. The technique is popularly used for phthalocyanines where the B and Q band are thoroughly analysed. This is discussed in more detail in chapter 3.

The Bouguer-Lambert-Beer law forms the mathematical-physical basis of light-absorption measurements on gases and solutions in the UV-Vis and IR region.[83] Beer's law is represented as follows

$$A = -\log T = \log \frac{P_0}{P} = \varepsilon bc \ldots\ldots\ldots\ldots\ldots\ldots\ldots\ldots\ldots\ldots\ldots \quad (10)$$

Where A is the absorbance, P_0 and P, the incident radiant power and transmitted radiant power respectively, ε is the molar absorptivity, b, the path length of the sample and c, the concentration of absorber. A monochromatic beam of radiation with power P_0 is passed through a homogeneous medium. As the beam is transmitted through the box, some n ions, molecules or atoms absorb the radiation thereby decreasing the power of the incident ray to P.[84] The full derivation of Beer's law is not shown in this work but Strong [85] discussed this in detail. Typical solvents used in UV-Vis spectroscopy are *n*-heptane, water and trifluoroethanol, usually transparent from ca. 800 nm in the UV-Vis region.

2.1.4 Scanning Electron Microscopy

The Scanning Electron Microscope (SEM) is a powerful and versatile tool used for the imaging of surfaces. This is particularly important in the field of nanotechnology and supercapacitor studies where carbon nanotubes are frequently used. The SEM uses electrons instead of light in producing an image. The instrument allows for the observation of materials on a very small scale ranging from nanometers to micrometers. An ability to produce three-dimensional images is one of the most outstanding capabilities of the SEM apart from the high resolution, higher magnification and ease of sample observation. A large depth of field of the SEM allows for the focusing of larger areas of the specimen at one time resulting in three-dimensional images.

Although SEM is the most widely used technique in surface imaging, the technique has a lower sensitivity to surfaces when compared with other imaging techniques.[81] When an electron beam is focused on a sample, the electron beam causes the emission of secondary electrons, X-rays, backscattered electrons and photons of various energies. The secondary electrons are of particular interest as these result in the formation of an image. The X-rays upon analysis can yield vital elemental information. The electron beam can be focused on one position or moved in a raster across the surface of the specimen to form images. SEM provides useful information on supercapacitor electrodes. The porous structure of electrodes and alignment of carbon nanotubes are observed using this imaging technique. Such structures are essential for the storage of charge in the electrical double layer.

2.1.5 Transmission Electron Microscopy (TEM)

TEM uses the same principle as that of a light microscope. However, instead of light, TEM uses electrons. An electron beam with uniform current density is directed onto a specimen. As electrons interact with the thin specimen, an image is recorded on an imaging device. The amount of power used to generate electrons allows for higher magnification and better resolution.

An electron gun is responsible for producing the electrons that are irradiated onto the specimen. Two condenser lenses are responsible for focusing the beam into a pinpoint beam. A condenser aperture then restricts the beam by knocking out high angle electrons. As the beam comes into contact with the specimen, part of it is transmitted and focused by the objective lens forming an image. The image is then passed through the intermediate and projector lenses which enlarge it before it hits the phosphor screen where it can be seen. The image contrast is due to the thickness of the specimen. Darker areas on the image correspond to fewer electrons being transmitted through due to the thicker or denser nature of the material at that point. Lighter areas of the image are a result of more electrons being transmitted through the material in areas that are thinner or less dense.[75]

TEM provides information on the diameter and length of carbon nanotubes. The method also allows the user to observe the effect of functionalizing carbon nanotubes for supercapacitor electrodes. The activation and functionalization of carbon nanotubes results in shorter nanotubes which can be observed on the images provided by TEM and consequently a higher surface area is ideal for supercapacitor electrodes.[86]

2.1.6 Atomic Force Microscopy (AFM)

AFM is an imaging technique that relies heavily on the forces that exist between the tip and the sample under investigation. In AFM, a tip is fixed to the end of a flexible cantilever. As the tip moves across the surface of the sample, changes in surface height are measured by a laser beam in the quadrant photodetector.[81]

At the same time forces between the tip and the surface are detected by the tip. The different types of forces that can be encountered are as follows:

- Van der Waals Forces – these forces are present in all materials and play a major role in imaging by AFM.

- Electrostatic force- as ions are brought closer to each other, the attractive forces between them increase sharply.
- Adhesive forces – As AFM tips are used over and over again, they lose their shape and sharpness resulting in a greater contact area between the tip and the sample. This leads to the presence of “adhesive forces”.
- Double Layer forces – A positively charged layer called an “ionic atmosphere” can be formed at the solid – liquid interface when imaging is performed in an aqueous medium.[87] In the case of supercapacitor electrodes, it is essential to have information on the topology of the electrode material. Surface roughness can be detected using AFM and this is particularly important when coupled with electrochemical impedance spectroscopy (EIS) data to model the circuit suitable for a supercapacitor electrode.

2.2 Electrochemistry: Characterization of Supercapacitor Electrodes

Electrochemistry is the interplay between chemistry and electricity where reactions involving electrical currents and potential are dealt with.[88] Electrochemical reactions are invariably oxidation/reduction reactions carried out under special circumstances. Oxidation and reduction can simply pertain to the donation of electrons by one atom to the other. The two always occur together. When oxidation or reduction occurs, electrons carry electrical currents which can be used to carry out useful work like lighting a bulb.[89] Electrochemical reactions take place between the electrode surface and the solution. Studies in supercapacitor development all focus mainly on the type of reactions taking place at the electrode-solution interface. Electrochemistry finds numerous applications in developing sensors, corrosion studies, environmental protection and development of energy devices such as fuel cells and batteries. There are many electrochemical techniques that exist but in this work, cyclic voltammetry, electrochemical impedance spectroscopy and galvanostatic charge-discharge will be discussed.

2.2.1 Cyclic Voltammetry (CV)

Cyclic voltammetry (CV) is a potentiodynamic experimental method and probably the simplest and most versatile electroanalytical technique used by electrochemists for the study of electroactive species. A number of methods have in the past been employed for the measurement of reaction kinetics but CV has stood out due to the ease of measurement and its effectiveness in observing redox behaviour over a wide potential window. The first step in characterizing any electroactive material is to perform cyclic voltammetry over the chosen potential window.

(a) Instrumentation

In a three electrode system, a working electrode is immersed in the electrolyte, a potential is applied to it and the resulting current recorded, yielding a cyclic voltammogram. A three electrode cell consists of a working electrode, a reference electrode (usually SCE or Ag/AgCl) and an auxiliary or counter electrode (platinum) as shown in figure 2.15.

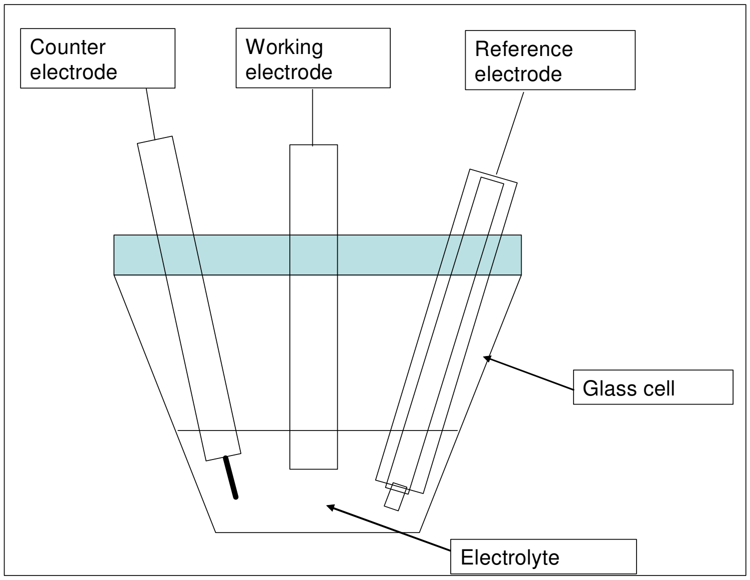

Figure 2.3: Schematic diagram of a three electrode cell used in this work.

A potentiostat applies a potential to the working electrode which is measured against the reference electrode.[90] The auxiliary electrode generates the current required to sustain electrolysis at the working electrode. [91] An excitation signal which is presented as a linear potential scan with a triangular waveform is passed between the two electrodes (figure 2.4). A cyclic voltammogram is obtained by measuring the current at the working electrode where the reaction takes place during the potential scan.[92] The voltammogram is a display of current versus potential (figure 2.5).

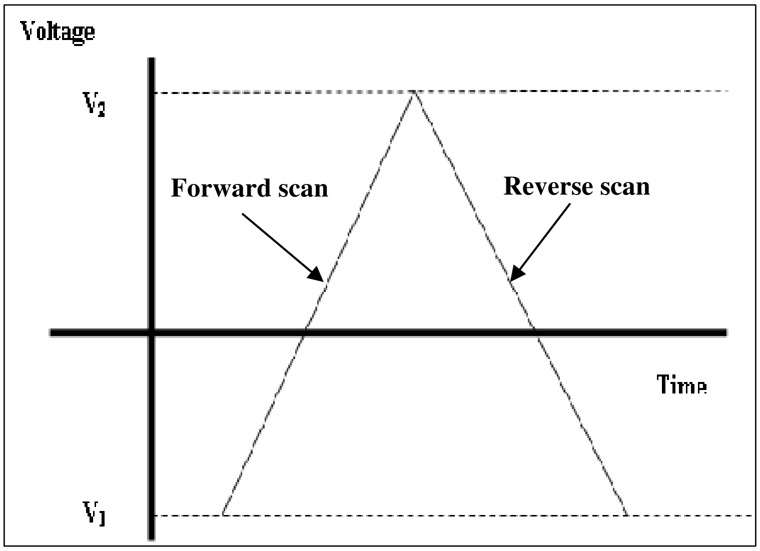

Figure 2.4: A typical cyclic voltammogram excitation signal recorded for a reversible single electrode transfer reaction is in a solution containing only a single electrochemical reactant. Figure adapted from Kissinger and Heineman.[90]

(b) Fundamentals of cyclic voltammetry

Nicholson and Shain have contributed significantly to the understanding of cyclic voltammetry and the development of the technique.[93] Nicholson and Shain performed quantitative simulations of CV in 1964 and the field of electrochemistry has never been the same since then. Perhaps the easiest and simplest explanation of how cyclic voltammetry operates has been given by Kissinger and Heineman.[90] They reported how a typical cyclic voltammetry experiment progresses using 6 mM $K_3Fe(CN)_6$ in KNO_3. A typical cyclic voltammogram they obtained is shown in Figure 2.5.

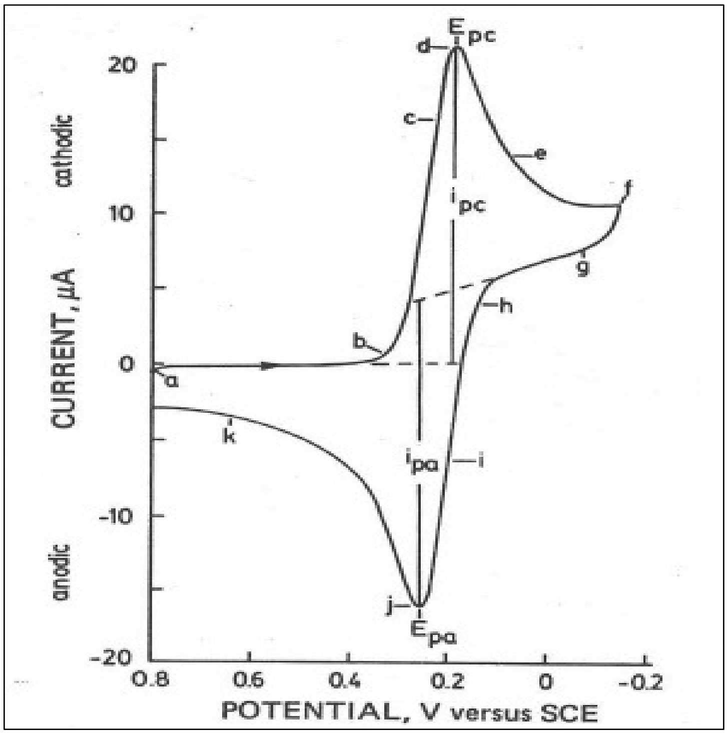

Figure 2.5: Typical cyclic voltammogram for a redox active species, $K_3Fe(CN)_6$ in 1 M KNO_3 versus SCE. Figure adapted from Kissinger and Heineman.[90]

The scan was performed over a potential window of -0.2 to 0.8 V. At 0.8 V, $Fe(CN)_6$ is not electrolyzed, upon the switching on of the electrode. The forward scan begins at this potential moving towards more negative potentials to reduce $Fe^{III}(CN)_6^{3-}$ as shown at point *(b)*. The chemical reaction at (*b*) is shown below.

$$Fe^{III}(CN)_6^{3-} + e \longrightarrow Fe^{II}(CN)_6^{4-} \quad ....(11)$$

From *b-d* the current increases rapidly until the concentration of $Fe^{III}(CN)_6^{3-}$ diminishes and that of $Fe^{II}(CN)_6^{4-}$ increases causing the current to reach a peak (*d*). The current rapidly decreases (*d-g*) as the electrode becomes an oxidant. The reverse scan then begins, this time with $Fe^{II}(CN)_6^{4-}$ being oxidized back to $Fe^{III}(CN)_6^{3-}$ in the process

$$Fe^{II}(CN)_6^{4-} \longrightarrow Fe^{III}(CN)_6^{3-} + e \quad ....(12)$$

An anodic current (*i-k*) results and as concentration of $Fe^{II}(CN)_6^{4-}$ decreases, another peak is observed (*j*). The solution surrounding the electrode is now deficient of $Fe^{II}(CN)_6^{4-}$ but abundant in $Fe^{III}(CN)_6^{3-}$ completing the cycle and ready to start a new one. A complete voltammogram is therefore recorded. A cyclic voltammogram is characterized by some important parameters such as cathodic (E_{pc}) and anodic (E_{pa}) peak potentials, the cathodic (i_{pc}) and anodic (i_{pa}) peak currents, the cathodic half-peak potential ($E_{p/2)}$) and half wave potential ($E_{1/2}$) .

Two limiting cases exist where CV is employed. The electrode processes can either be reversible or irreversible. All reversible voltammograms have the typical shape as that shown in Figure 2.5. A reversible voltammetry can be characterized by ‘fast’ electrode kinetics in relation to the rate of mass transport to the electrode. Reversible electrochemical behaviour also implies that the Nernstian equation (13) is obeyed on every point of the voltammogram.

$$E = E_f^0(A/B) + \frac{RT}{F}\ln\frac{[B]_0}{[A]_0} \qquad (13)$$

Where E is the applied potential, $E^0{}_f$ the formal electrode potential and $[A]_0$, $[B]_0$ the concentrations of reactant and product respectively. R is the gas constant, T, the absolute temperature and F, Faraday's constant. Other characteristics for a reversible reaction are that $\Delta E = E_{pc} - E_{pa} = 59$ mV (for single electron reactions) is independent of scan rate (v).The ratio of i_{pc} to i_{pa} is equal to 1.[94] Irreversible reactions are due to slow electrode kinetics at the electrode-electrolyte interface. ΔE varies with scan rate and the reverse peak is absent for an irreversible reaction. Quasi-reversible reactions are characterized by a shift in ΔE with shift in scan rate and $i_p/v^{1/2}$ is independent of scan rate.

Cyclic voltammetry is probably one of the most useful techniques in electrochemistry that should be performed in the preliminary stages of any electrochemistry project. Its ease of operation, good sensitivity and fast generation of results makes it a popular tool for qualitative analysis of electrode reactions. However, cyclic voltammetry should be used in conjunction with other electrochemical techniques to provide a full picture of both qualitative and quantitative diagnosis of electrode reactions. Ideal capacitor behaviour is characterized by a rectangular cyclic voltammogram. Electrode materials that exhibit pseudocapacitance deviate from the rectangular shape resulting in a distorted voltammogram where reversible peaks are identified as illustrated in figure 2.6.

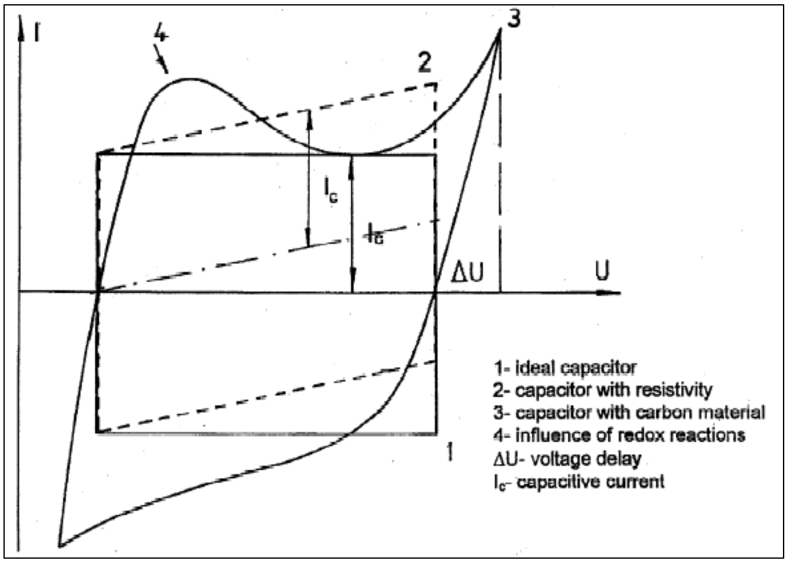

Figure 2.6: Typical voltammograms for electrochemical capacitors. Figure adapted from Frackowiak and Béguin.[9] [9]

2.2.2 Galvanostatic Charge/Discharge (CD)

The Galvanostatic charge /discharge (CD) method is probably the most dependable electrochemical method that can be used for calculating specific capacitance of electrodes.[61]. A typical constant charge/discharge profile of an ideal supercapacitor is characterized by linear charging and discharge profiles as shown in figure 2.7. Furthermore, a mirror image of the charging curve and the discharging curve indicates a typical supercapacitor. In contrast, a supercapacitor that is characterized by pseudocapacitance exhibits non-linear charge and discharge profiles.[95]

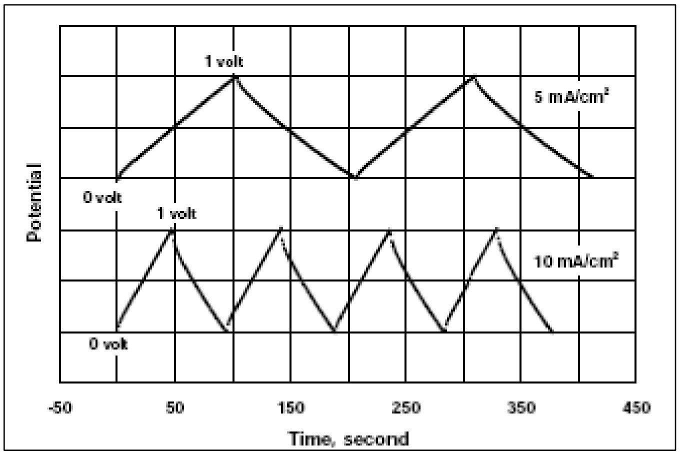

Figure 2.7: Typical constant charge/discharge profile for nafion based supercapacitor. Figure adapted from Lakatos- Varsanyi and Hanzel.[96]

The concept of Galvanostatic charge/discharge is analogous to that of cyclic voltammetry although the latter results in an *E*-*i* plot. An excitation signal is applied to the system and causes the potential to scan from the starting potential to the final potential and back again resulting in the first scan. Different currents can be chosen resulting in different current densities that can be used to calculate specific capacitance. The potential window used in Galvanostatic charge/discharge experiments should always be consistent with that used in cyclic voltammetry.

Galvanostatic charge/discharge experiments are used to calculate specific capacitance, specific energy and specific power. Ragone plots are then plotted after calculating the values of specific power against specific energy using the formulae.

$$SC(F/g) = \frac{[i(A) \times \Delta t(s)]}{[\Delta E(V) \times m(g)]} \quad \text{.................................} \quad (14)$$

$$SE(Whkg^{-1}) = \frac{[i(A) \times t(s) \times \Delta E(V)]}{m(kg)} \quad \text{......................} \quad (15)$$

$$SP(Wkg^{-1}) = \frac{[i(A) \times \Delta E(V)]}{m(kg)} \quad \text{..........................} \quad (16)$$

Where *I,* is the discharge current in ampere, Δ*t* is the discharge time in seconds, Δ*E*, the potential difference in volts and *m*, the mass of the electroactive material in grams. For specific energy and specific power the mass, m is in kg.[97] The energy deliverable efficiency (*η* %) can be calculated using equation 17.

$$\eta \ (\%) \quad = \quad \frac{t_{\mathrm{d}}}{t_c} \mathrm{x}100 \qquad \text{...................................} \quad (17)$$

where t_d and t_c are discharge time and charging time, respectively.

2.2.3 *Electrochemical Impedance Spectroscopy (EIS)*

Electrochemical impedance spectroscopy has been branded one of the most powerful tools in electrochemistry.[46] It is the study of the variation of total impedance of an electrochemical cell with frequency of a small-amplitude AC perturbation. EIS can be applied to a host of areas of study such as corrosion studies[98, 99, 100], organic coatings[101, 102], energy storage devices, [103, 104] sensors [105, 106] and the study of liquid-liquid interfaces.[107]

EIS provides a wealth of information when it comes to the study of interfacial characteristics and pseudocapacitance of the electrode.

(a) Fundamentals of Impedance Spectroscopy

Ohm's law gives a simple relation between dc-potential (E) and dc-current (I)

$$R = \frac{E}{I} \quad \text{..........} \quad (18)$$

Ohms law is only limited to one circuit element which is an ideal resistor. When performing experiments, other elements come into existence and these have to be considered as well. The expression above changes when an ac-signal is applied to a cell.

$$Z(\omega) = \frac{\Delta E(\omega)}{\Delta I(\omega)} \quad \text{..........} \quad (19)$$

Where Z (ω) is the complex impedance. ΔE (ω) is the change in potential and ΔI (ω), the change in current.

Electrochemical impedance is usually measured by applying an AC potential to an electrochemical cell and measuring the current through the cell. A sinusoidal potential excitation (figure 2.8(a)) is applied to the electrode interface making the cell's response pseudo-linear. The current response leads or lags the voltage by a phase angle of θ.

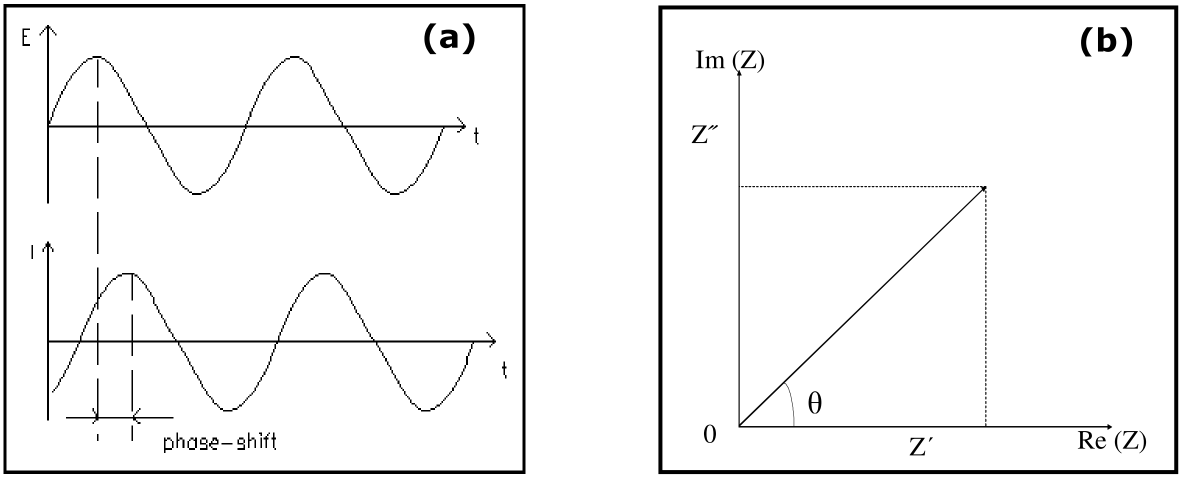

Figure 2.8: (a) Response in a linear system. **(b)** Plot of Z″ versus Z' representing Z with rectangular or polar coordinates. Figure adapted from Gamry Instruments[108]

The capacitance of the electrode is given by

$$Z = \frac{1}{j\omega C} \quad \text{...} \quad (20)$$

The total impedance is given by the following equation that incorporates both the real and imaginary components of the impedance. The angular frequency ω is expressed as $2\pi f$.

$$Z(\omega) = Z'(\omega) + j.Z''(\omega) \quad \text{..} \quad (21)$$

Z is the total impedance, Z', the imaginary impedance and Z″ the real impedance.[109] Z is therefore a vector quantity that is plotted in the plane with either polar or rectangular coordinates (figure 2.8 (b)) with $\theta = \tan^{-1}(Z''/Z')$. The phase difference, θ, between the voltage and the current is equal to zero for a pure resistor and 90° for a pure capacitor.[110]

(b) Data representation

The relationship between the impedance and frequency is very useful and can be displayed in various ways. A Bode plot is a plot of log $|Z|$ and θ against log ω (figure 2.9 (b)). Bode plots are very useful and give more explicit information regarding frequency. A *Nyquist plot,* displays Z_{Im} *vs.* Z_{Re} for different values of ω (figure 2.9 (a)).[7] Both these representations will be dealt with in more detail in chapter 3.

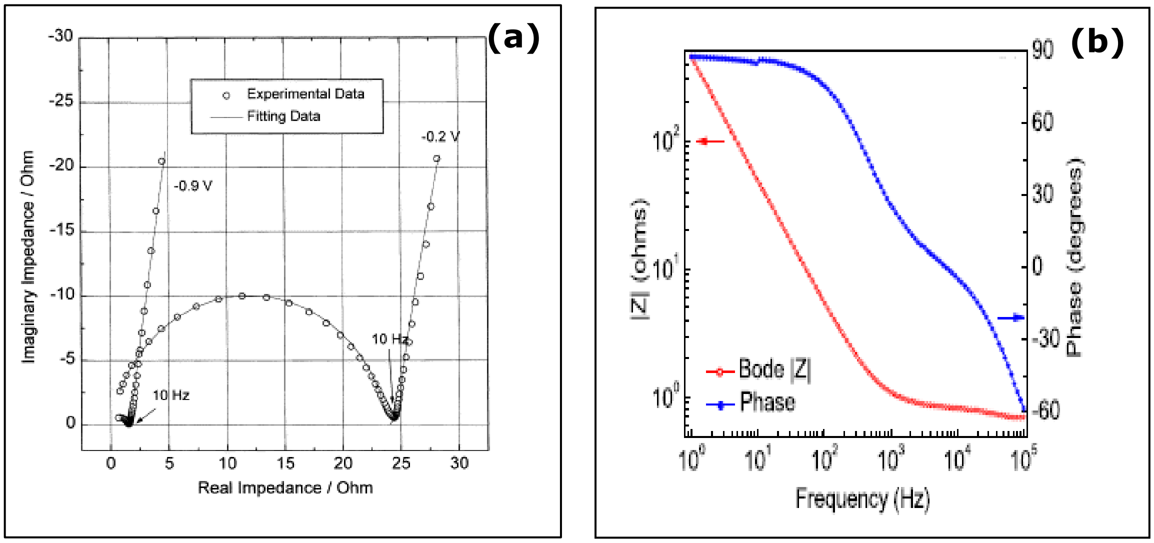

Figure 2.9: (a) Nyquist plot for a supercapacitor made of activated carbon and numerical data fitting Figure adapted from Qu.[80] **(b)** Bode |Z| and Bode angle plots of a typical supercapacitor. Figure adapted from Du and Pan.[111]

(c) EIS Fitting

The Kramers-Kronig (K-K) test is ideally the first test that one should undertake to determine whether EIS experimental data is stable in time and linear. The test checks whether data points recorded at the beginning of an experiment are in agreement with those recorded at the end. A few assumptions have been employed to check the validity of the experimental data. These assumptions are (i) that the impedimetric response is only related to the excitation signal; (ii) that the impedimetric response is linear (or the perturbation is small, e.g., < 10mV, for non-linear systems; (iii) that the system does not change with time, say due to ageing, temperature changes, non-equilibrium conditions, etc and (iv) that the system is finite for all values of ω, including zero and infinity.[112] The K-K test results in a value of pseudo χ^2. Bad fit results in a high value of χ^2 indicating the corruption of the data recorded. An equivalent series that fits the experimental data will therefore not be found. Values of χ^2 lower than 10^{-6} are considered to be good while those higher than 10^{-4} are considered to be bad. The relative error and χ^2 functions are very important and accurate ways of establishing the relationship between the experimental and the modeling data.

EIS data is commonly analyzed by fitting it to an equivalent electrical circuit model as shown in Fig 2.10. Most of the circuit elements in the model are common electrical elements such as resistors, capacitors, and inductors. To be useful, the elements in the model should have a basis in the physical electrochemistry of the system. The simplest circuit used is the Randles circuit.

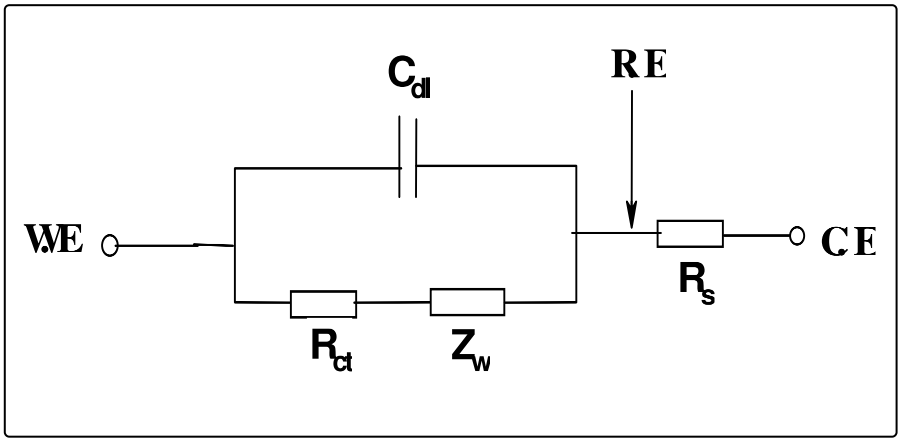

Figure 2.10: Randles equivalent circuit depicting an ideal situation.

The Randles circuit is made up of (i) the electrolyte resistance between working and reference electrodes R_s, (ii) the double layer capacitance (C_{dl}), and (iii) the Faradaic impedance consisting of charge-transfer resistance R_{ct} at the working electrode-electrolyte interface and the Warburg Impedance Z_w, which reflects the influence of the mass transport of the electroactive species on the total impedance of the electrochemical cell. The charge transfer resistance is closely associated with the surface area of the electrode and its conductivity. A summary of all the circuit elements is given in the table 2.1.

Table 2.1: A summary of some of the circuit elements used in the description of equivalent circuits.

Element	**Symbol**
Charge transfer Resistance	R_{CT}
Solution Resistance	R_S
Capacitance	C
Inductance	L
Constant Phase Element	Q
Warburg Diffusion	W

For practical situations where the electrode surface is not smooth, the modified Randles circuit is applied wherein one or both elements (C_{dl} and Z_w) are replaced by a constant phase (CPE) element representing pseudocapacitance.

The impedance of CPE (Z_{CPE}) is defined as [113,114]

$$Z_{CPE} = \frac{1}{[Q(j\omega)^n]} \quad \text{...} \quad (22)$$

where Q is the frequency-independent constant relating to the surface electroactive properties, ω is the radial frequency, the exponent n arises from the slope of log Z vs log f (and has values $-1 \leq n \leq 1$). If $n = 0$, the CPE behaves as a pure resistor; $n = 1$, CPE behaves as a pure capacitor, $n = -1$ CPE behaves as an inductor; while $n = 0.5$ corresponds to Warburg impedance (Z_w) which is associated with the domain of mass transport control arising from the diffusion of ions to and from the electrode|solution interface. Generally speaking, CPE occurs by several factors such as (i) the nature of the electrode (e.g., roughness and polycrystallinity), (ii) distribution of the relaxation times due to heterogeneities existing at the electrode/electrolyte interface, (iii) porosity and (iv) dynamic disorder associated with diffusion.[115]

EIS, like any other technique, has its advantages and limitations. The technique is very sensitive, non-destructive and accurate but less understood. Furthermore it is used in situ and has a fast rate of generating results. However it is not a stand alone technique and needs to be complimented by other techniques such as cyclic voltammetry. The interpretation of data can also prove to be intricate. In conclusion, the three electrochemical techniques discussed above when coupled together; provide useful information for probing supercapacitor electrodes.

2.2.4 Chemically modified electrodes (CMEs)

There are many well documented methods of electrode modification, which include:

(i) **Dip-dry or Immersion**. One of the simplest methods of modifying an electrode is to dip the electrode surface into a solution of a polymer/modifier. The electrode is then withdrawn from the modifier's solution and the solvent is allowed to dry. The main drawback of this method is that the amount of material on the electrode cannot be controlled.

(ii) **Drop-dry**. A known amount of the electroactive material is deposited onto the electrode surface and allowed to dry.

(iii) **Spin-Coating**. The electrode modifier upon deposition is evaporated by spinning the electrode on a spin coater. This method is used mainly in the semiconductor industry. A uniform film thickness is obtained.

(iv) **Electrodeposition or potential cycling**. This method involves the coating of the electrode surface by electrochemically running voltammetric scans in the solution of the modifier (i.e. not the electro-active probe).

(v) **Covalent attachment**. In this method, the formation of covalent bonds between specific functional groups on the electrode surface and the electroactive material is the main objective. It is essential to use a coupling agent to achieve the desired interactions. It is possible to form multimolecular layers at the electrode surface through this method.

The choice of the method to use to modify an electrode depended on the molecule to be attached on the surface and the type of surface. In this thesis, drop dry method and electrodeposition were adopted because of their several advantages for the work proposed in this thesis.

CHAPTER THREE

EXPERIMENTAL

3.1 Materials and Reagents

Multi-walled carbon nanotubes (MWCNT, purity > 90 %, 110-170 nm in diameter, 5-9 µm in length) obtained from Sigma Aldrich were acid-functionalised (converted mainly into carboxylated) by undergoing very stringent acid treatment following the established methods.[116,117] 1 g of MWCNTs in 140 ml of 2.6 M HNO_3 was refluxed for 48 hours. The carbon nanotube sediments were separated from the reaction mixture, washed with distilled water, and sonicated in a concentrated H_2SO_4/HNO_3 mixture (3:1 ratio, 98% and 70% purity, respectively) for 24 hours. Thereafter, the sediments were washed with distilled water, stirred for 30 minutes in a H_2SO_4/H_2O_2 mixture (4:1, 98% and 30% purity, respectively) at 70 °C, and washed again with deionised water. Finally, the purified paste-like MWCNTs were then oven-dried at 50 °C for 48 hours.

Nickel (II) tetraaminophthalocyanine (NiTAPc) was synthesised and characterised following the well-known procedure introduced by Achar and Jayasree.[118] For a comparative study, unsubstituted nickel phthalocyanine (NiPc) was purchased from Aldrich. Nickel (II) tetra-*tert-butyl* phthalocyanine (tBuNiPc) was obtained from its metal-free precursor, tetra-*tert-butyl* phthalocyanine (tBuPc) kindly donated by Prof T. Fukuda, Graduate School of Science, Tohoku University, Japan). Introduction of nickel into the core of the tBuPc was achieved using a similar metallation process described before.[119] Briefly, this involved refluxing a DMF solution containing a mixture of H_2tBuPc and excess of nickel acetate for about an hour. The DMF was then evaporated and the dark green residue purified using a short silica gel column ($CHCl_3$ + small percentage of methanol as eluent) to afford the desired NiTTBPc.

As expected, the formation of the nickel complex was easily established UV-visible spectrophotometrically in $CHCl_3$ by observing the total collapse of the split Q-bands (663 and 696 nm) of the metal-free tBuPc complex (D_{2h} symmetry) to the single Q-band (668 nm) of the metal, NiTTBPc, complex (D_{4h} symmetry). Ultra-pure water of resistivity 18.2 MΩcm was obtained from a Milli-Q Water System (Millipore Corp., Bedford, MA, USA) and was used throughout the experiments.

3.2 Equipments and methods

Field emission scanning electron microscopy (FESEM) images were obtained from JEOL JSM 5800 LV (Japan) while the energy dispersive x-ray spectra were obtained from NORAN VANTAGE (USA) at the Microscopy and Microanalysis Laboratory of the University of Pretoria. Transmission Electron Microscopy was performed on the JEOL JEM-2001 F/HT transmission electron microscope. Atomic Force Microscopy (AFM) experiments were performed with AFM 5100 System (Agilent Technologies, USA). TGA was performed with a Mettler Toledo A851 (Switzerland). Simultaneous TGA/DTA data machine was used for thermal and gravimetric analyses. Powder samples (ca. 10mg) were placed in an open 70 μL alumina pan and heated from 25-1000°C at a scan rate of 10°C / min in nitrogen atmosphere. The Perkin-Elmer GX 2000 FTIR spectrometer attached to the Perkin-Elmer Auto Image Microscope system equipped with liquid Nitrogen cooled MCT detector was used for FTIR analysis. UV-Vis spectroscopy was performed using the Cary 300 UV-Vis spectrophotometer driven by the Varian software 3.0.

The samples were prepared for XRD analysis using a back loading preparation method. XRD experiments were performed using a PANalytical X'Pert Pro powder diffractometer with X'Celerator detector and variable divergence and receiving slits with Fe filtered Co-Kα

radiation. The samples were scanned at the required 2θ angle ranges. The phases were identified using X'Pert Highscore plus software.

Electrochemical experiments were carried out using an Autolab Potentiostat PGSTAT 20 (Eco Chemie, Utrecht, Netherlands) driven by the GPES software version 4.9. Electrochemical impedance spectroscopy (EIS) measurements were performed with Autolab Frequency Response Analyser (FRA) software between 100 kHz and 10 mHz using a 5 mV rms sinusoidal modulation. Bare or modified BPPGE disk (d = 5mm in Teflon) was used as the working electrode and was fabricated at the Chemistry Department of the University of Pretoria from BPPG plate (Le Carbone, Sussex, UK). Electrical contact with the disk was maintained through an inserted copper wire held in place with conducting silver varnish L 100 (Kemo® Electronic, Germany). An Ag/AgCl in saturated KCl and platinum wire was used as reference and counter electrodes, respectively. All solutions were bubbled with nitrogen for 5 minutes prior to each electrochemical experiment. Experiments were performed at 25 ± 1 °C.

3.3 Preparation of Nickel Phthalocyanine -MWCNT composites and electrode fabrication

Prior to modification with NiTAPc, MWCNTs or MWCNT-NiTAPc, the BPPGE surface was cleaned by gentle polishing on a p1200C Norton carborundum paper (Saint-Goban Abrasives, Isando, South Africa) followed by cleaning with cellotape process of removing graphite layers and finally rinsing in acetone to remove any adhesives. All modifiers were prepared in dry distilled DMF and used within 48 hours of preparation. MWCNT-NiTAPc composite was obtained by grinding equal amounts of MWCNT-COOH and NiTAPc (1:1 mass/mass ratio) using mortar and pestle for about 5 minutes. The mixture was then dissolved in DMF (1 mg MWCNT-NiTAPc mixture/1ml of DMF) and ultrasonicated for 30 minutes. The drop-dry method was then employed to load the MWCNT-NiTAPc hybrid onto the BPPGE surface by placing about 20 μL drop of the mixture onto the BPPGE surface and dried in the oven at ~ 50 °C for 5 minutes. The same procedure was repeated with tBuNiPc and NiPc.

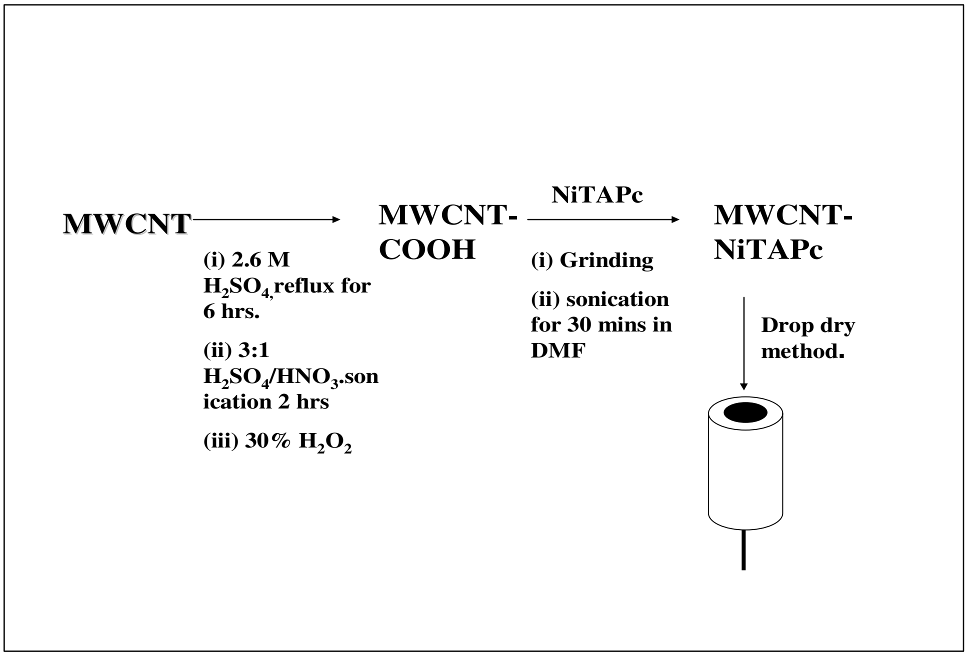

Scheme 3.1: Schematic representation for the synthesis of the MWCNT-NiTAPc nanocomposite and electrode preparation using the drop-dry method.

3.4 Preparation of poly-Nickel Phthalocyanine -MWCNT composites and electrode fabrication

The BPPGE was placed into a solution containing 1 mM NiTAPc and 0.1 M tetra-n-butylammonium perchlorate (TBAP) which acted as a supporting electrolyte. The NiTAPc film was deposited onto the electrode by cycling under continuous cycling conditions of -0.2 to 0.9 V at 100 mVs^{-1} for 40 cycles.[120] The resulting electrode (BPPGE-polyNiTAPc) was then washed with acetone and distilled water and dried in an oven at 50 °C. The BPPGE-MWCNT electrode was obtained by first drop-drying 20 μL of MWCNT dissolved in DMF and allowed to dry in an oven at 50 °C for ca. 10 minutes. The resulting electrode was then placed in a solution of DMF/NiTAPc and cycled from -0.2 to 0.9 V at 100 mVs^{-1} for 40 cycles. The electrode was then rinsed and washed using acetone and distilled water to obtain the desired BPPGE-MWCNT-polyNiTAPc electrode.

The BPPGE-MWCNT-polyNiTAPc was then transferred to a fresh solution of 0.1 M NaOH and cycled in the potential window of -0.2 to + 0.8 V for 50 scans at 100 mVs^{-1} to obtain the BPPGE-MWCNT-polyNi(OH)TAPc electrode. Well defined peaks appear at around 0.4 V are observed. As the cycling continues, the peaks grow steadily until they reach a steady state where no further growth is observed. This is typical of cyclic voltammograms recorded for electroformed nickel macrocyclic-based films in alkaline solution and shows that the film has been formed as a result of the anodic polymerization of the macrocyclic complex.

It has been postulated that the polymerization of nickel macrocyclic complexes in alkaline media is very similar to that of the nickel hydroxide electrode.[121] The nickel-nitrogen tetra coordination of the complex is thought to be lost in the polymerization process. Another postulate by Roslonek and Taraszewka proposes that upon electropolymerisation, the complexes are attached *via* oxo-bridges.[122] Capacitance studies for the BPPGE-polyNiTAPc, BPPGE-MWCNT-polyNiTAPc, BPPGE-polyNi(OH)TAPc and BPPGE-MWCNT-polyNi(OH)TAPc electrodes were all performed in 1 M H_2SO_4.

CHAPTER FOUR

RESULTS AND DISCUSSION

4.1 Physico-chemical Characterization

4.1.1 X-Ray Diffraction

Carbon nanotubes are made up of graphite sheets rolled up together as already discussed in chapter one. Broader diffraction peaks observed in the XRD patterns (figure.4.1) for the materials indicate the amorphous nature of the four materials implying a small grain size. A decreased grain size consequently contributes to the high surface area of the materials studied. It is a well known fact that materials required for capacitance studies should have a high surface area.[4] A typical powder diffraction for functionalized carbon nanotubes and normal MWCNTs is shown in figure.4.1 (a). The normal MWCNTs and functionalized MWCNTs show very similar structures with a strong peak (100) at 31° and a weak peak (004) at 51°. The peaks indicate that the MWCNTs consist of small domains of ordered graphene sheets. From the similarities in the structures of the two forms of MWCNTs we deduced that the crystal structures of the two are the same. Functionalization therefore did not alter the novel structure of the CNTs as has also been previously reported by Jiang *et. al*.[123]

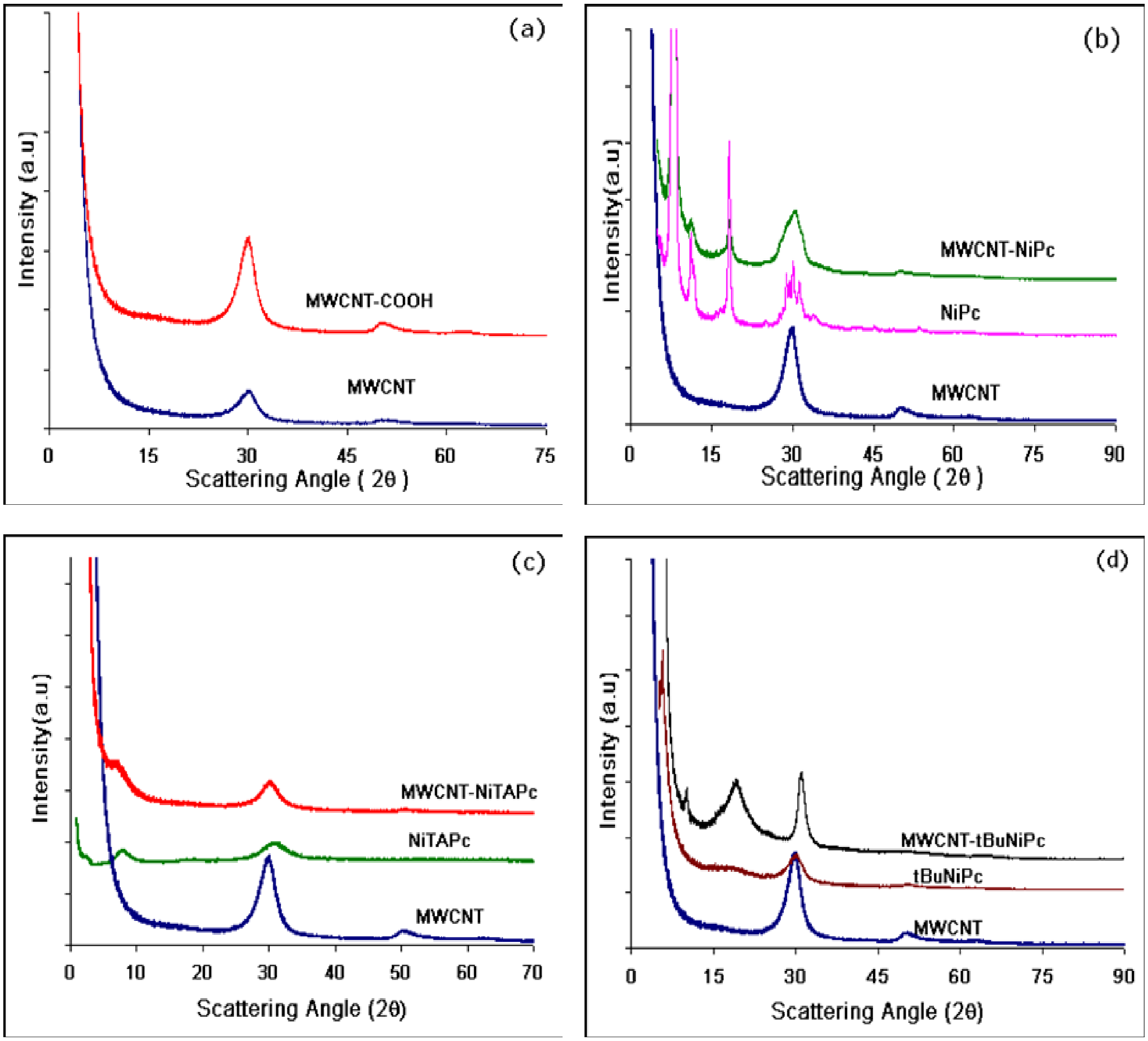

Figure 4.1: X-ray diffraction analyses for the functionalised MWCNT, Ni (II) phthalocyanines and MWCNT-Ni (II) phthalocyanine nanocomposites

Qu suggested the dependency of specific capacitance of the electrode material on the crystal orientation of the surface.[80] From the XRD patterns; the orientation for the graphite sheets has not been altered by the functionalization of the MWCNTs even when coupled with the phthalocyanines. The MWCNT-NiPc, MWCNT-NiTAPc and MWCNT-tBuNiPc nanocomposites clearly have different XRD patterns from the MWCNTs. However, the contribution of the MWCNTs is significant. The strong peak at 31° is evident in all the XRD patterns. For MWCNT-NiPc, peaks due to the NiPc are clearly visible. A strong peak at 7.9° was observed. Other peaks at $2\theta = 11.3^\circ$ and 18.4° were also observed for NiPc. The same peaks were also observed in the hybrid although at lower intensity. This phenomenon indicates a change in polycrystalline structure resulting in an amorphous compound.[124]

For the MWCNT-COOH and MWCNT-NiTAPc, the XRD patterns show that there is very little order between the graphene sheets.[125] The XRD patterns of the neat MWCNT and NiTAPc slightly differ from the MWCNT-NiTAPc (see figure. 4.1 (c)) hybrid confirming the formation of a new compound. The main peak at 8.75° for NiTAPc shifted to 7.44° for MWCNT-NiTAPc indicating a change in crystallinity and interplanar spaces. The tBuNiPc exhibits a strong peak is at $2\theta = 5.8^\circ$. This peak shifts to $2\theta = 10.2^\circ$ with a significant loss in intensity. This implies the formation of a new compound (MWCNT-tBuNiPc) that is more amorphous in nature with smaller grains. This information is in accordance with HRSEM images.

4.1.2 TGA Analysis

In order to obtain important information on the thermal stability of the MWCNT-COOH, MWCNT-MPc and MPc complexes, TGA was performed. The curves in figure 4.2 show that the MWCNT-NiTAPc, MWCNT-tBuNiPc, tBuNiPc and NiTAPc initially lose weight at 100°C. This phenomenon can be attributed to the desorption of physically adsorbed water from the complexes. The complexes lose about 10% of the water content compared with 3% for MWCNT-COOH. Further decomposition of MWCNT-NiTAPc complexes is observed at about 540 °C where the weight of the complex decreases more rapidly compared with the MWCNT-COOH. The same behaviour is observed for the bulk MPcs.

The TGA analysis shows that the MWCNTs are very stable. After heating to about 500 °C, only 10% of the original weight had been lost due to pyrolysis. The Phthalocyanines however disintegrated more than the MWCNTs with NiPc losing ca. 90% of the mass after heating to 800 °C. The larger tBuNiPc and NiTAPc molecules lost significant weight only after heating up to 1000 °C although the initial pyrolysis occurred at 400 °C and 450 °C respectively, higher than that of the MWCNT hybrids.From the TGA curves, the hybrids all started to disintegrate at lower temperatures as compared with the MWCNTs and the constituent Nickel phthalocyanines. The low decomposition temperature of the MWCNT-MPc hybrids is due to the increased internal energy caused by the structural twist of the planar MPcs to match well with the cylindrical structure of the MWCNTs via π-π interactions.[126]

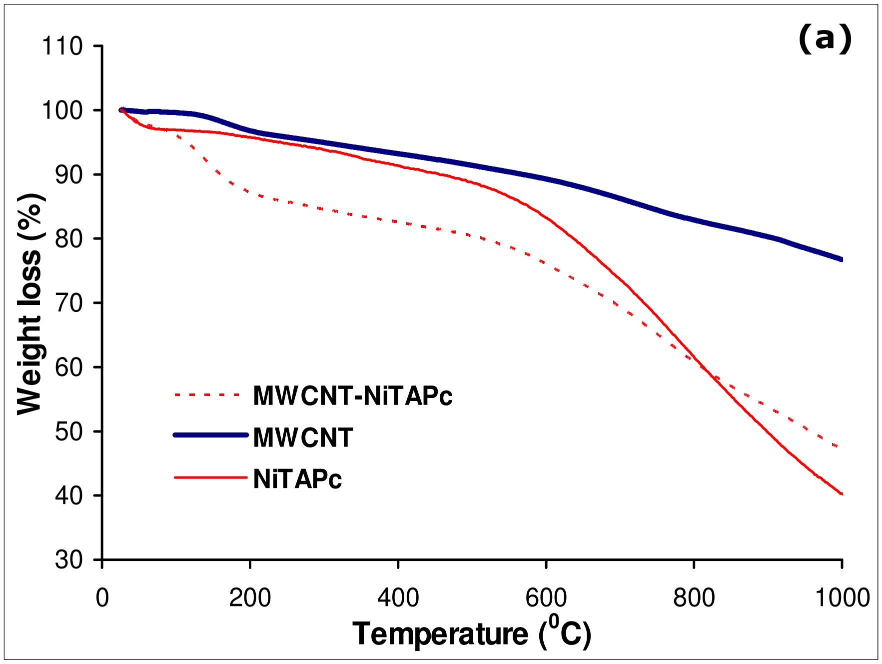

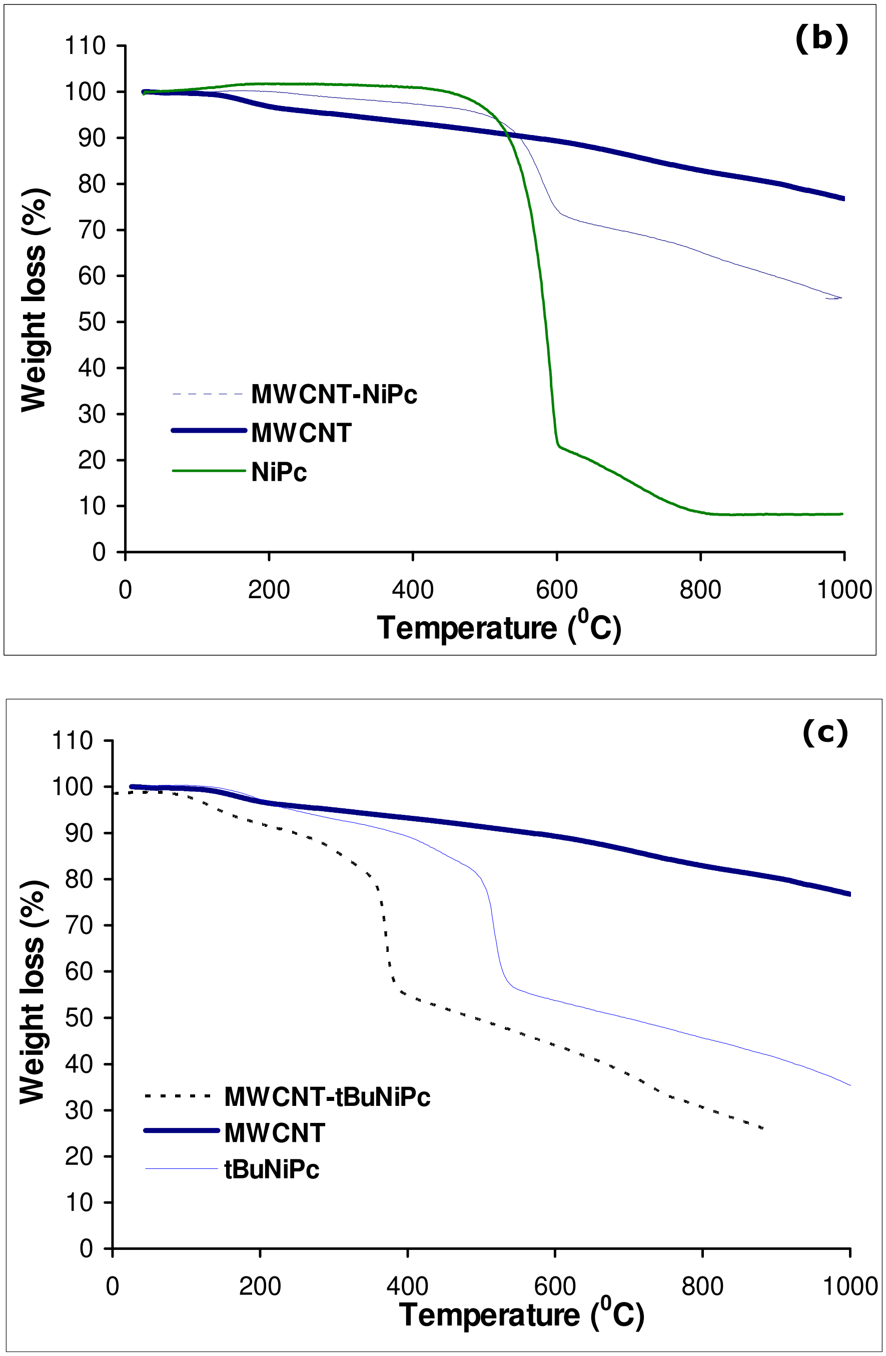

Figure 4.2: TGA analyses for the functionalised MWCNT, Ni (II) phthalocyanines and the MWCNT-Ni (II) phthalocyanine nanocomposites. **(a)** MWCNT, NiTAPc and MWCNT-NiTAPc, **(b)** MWCNT, NiPc and MWCNT-NiPc, **(c)** MWCNT, tBuNiPc and MWCNT-tBuNiPc.

4.1.3 UV-Vis Spectroscopy

The UV-visible spectrum observed for phthalocyanines originates from molecular orbitals within the aromatic 18π electron system and from overlapping orbitals on the central metal atom [127]

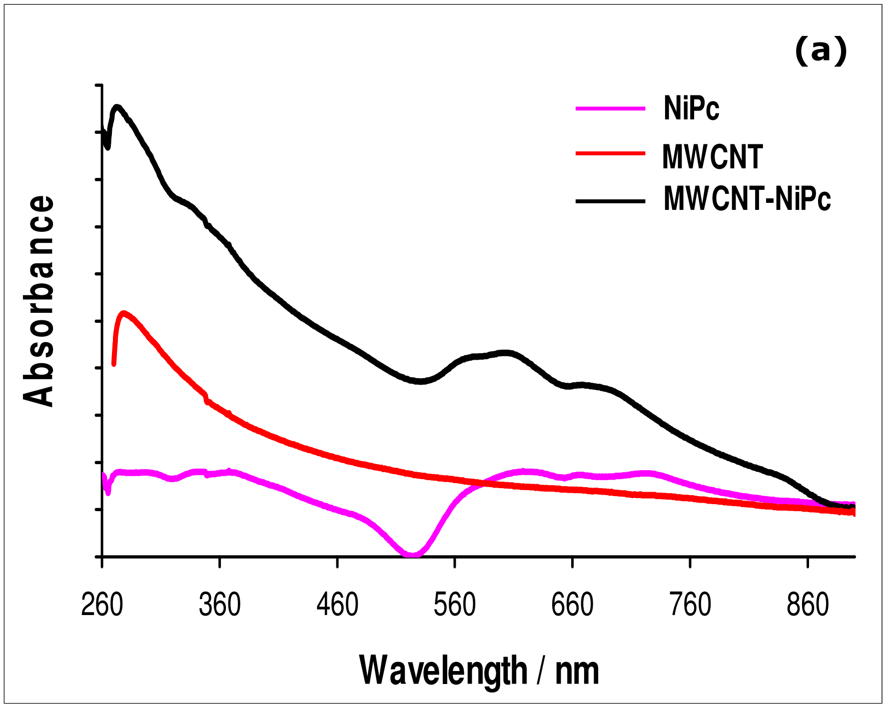

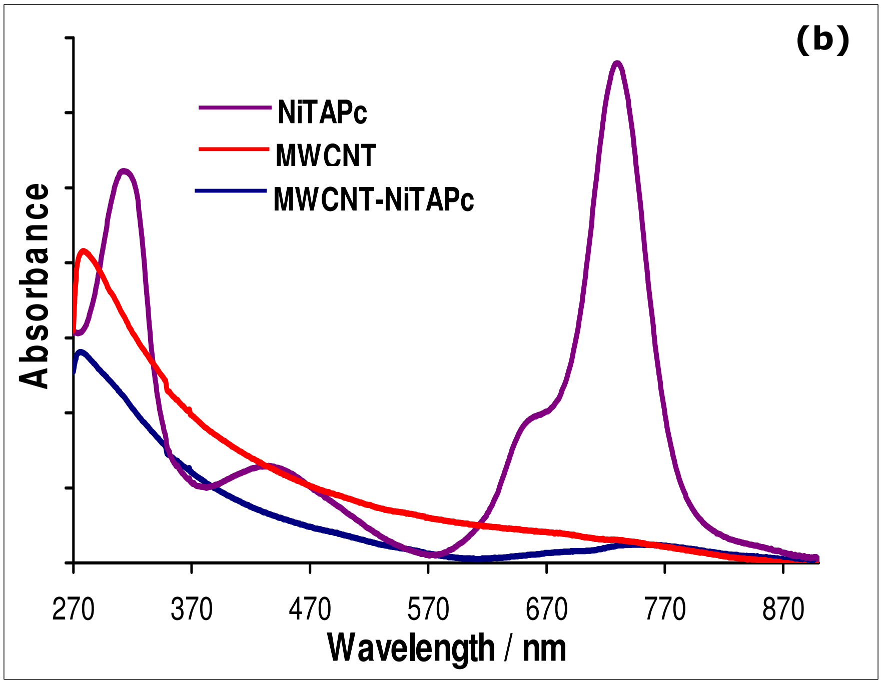

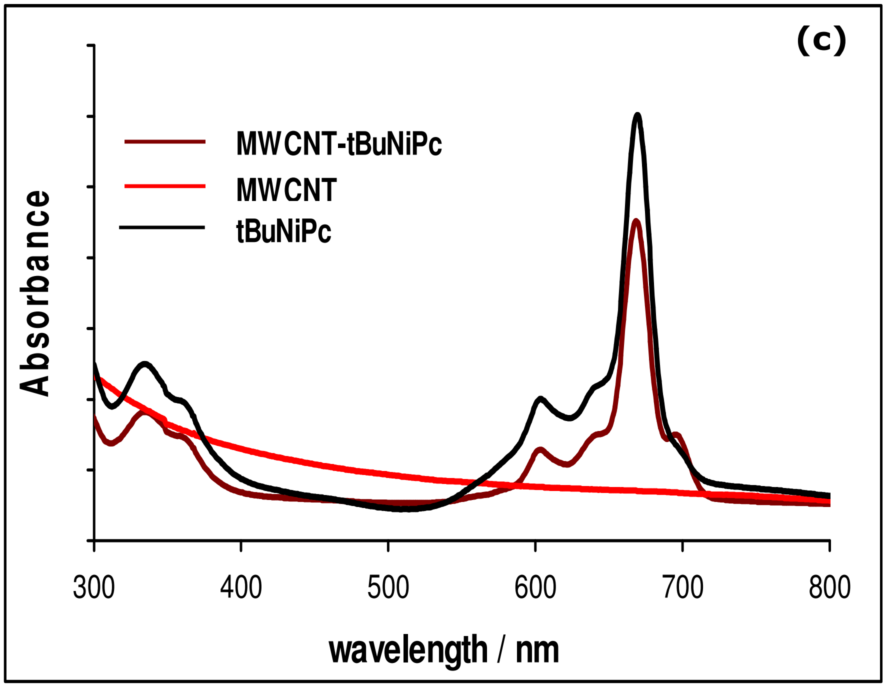

Figure 4.3: Electron absorption spectra of the MWCNT, MWCNT-Ni (II) phthalocyanine composites and Ni (II) phthalocyanine in DMF. **(a)** MWCNT, NiPc and MWCNT-NiPc, **(b)** MWCNT, NiTAPc and MWCNT-NiTAPc, **(c)** MWCNT, tBuNiPc and MWCNT-tBuNiPc.

The spectra of MPc complexes are due to electronic transitions from the highest occupied molecular orbital (HOMO) (π) to the lowest unoccupied molecular orbital (LUMO) (π*). Phthalocyanines have two characteristic bands, the Q band and the B (or Soret) bands. The Soret band is due to an a_{2u} (π)-e_g(π*) transition and the Q-band to an a_{1u}(π)-e_g(π*) transition.[128,129] The Q band appears in the region around 600-700 nm in the far-red end of the visible region. The origins of this band according to Davidson are due to π-π* transition on the phthalocyanine macrocycle.[130]

The B (or Soret) band appears in the region of 300-500 nm. The main suggestion of the large differences occurring in the absorption spectra of the phthalocyanines in this region indicate the presence of a d-band associated with the central metal atom. Upon close examination of figure 4.3.(a) the presence of three peaks in the UV region and a characteristic splitting of the peaks in the visible region is revealed. Due to the electronic interactions between the MWCNTs and the NiPc, the broad peaks in the Q band are slightly shifted towards the blue region. Figure 4.3 (b), shows a peak at 307 nm in the UV region. The other prominent peak, the Q band is observed at 727 nm in the visible region and a shoulder peak at 653nm. This peak has been explained by Davidson in terms of π-π* excitation between bonding and antibonding molecular orbitals.[130]

Upon mixing the phthalocyanine and MWCNT, the broad and most prominent peak in the visible region is reduced significantly to a point where it is almost non-existent. In figure 4.3 (b) the broad peak at 436 nm disappears completely in the MWCNT-NiTAPc spectrum. In the Soret band, the peak at 307 nm shifts to 273 nm and is also reduced in intensity. These results can be explained by the π-π interactions between the MWCNTs and the conjugated system of the Pc backbone. According to Jaegfeldt *et. al*[131] highly aromatic compounds absorb strongly to the basal plane of graphite via π - π stacking . The adsorption of species on to the basal plane of graphite becomes stronger as the number of aromatic rings increases. Chen and co-workers[132] reported the similarity in these strong interactions between polycyclic molecules and carbon nanotubes.

4.1.4 FTIR Analysis

The IR spectrum of the MWCNT-COOH clearly show the presence of COOH groups due peaks at 1373 cm^{-1} and stretching modes of C=O at 1618 cm^{-1} [133].The broad band at 3406 cm^{-1} is due to the –OH stretching vibration. The origin of this peak is attributed to the adsorbed water in the MWCNT pores. Smaller peaks observed at 2847 and 2915 cm^{-1} respectively attributed to the stretching vibrations of the $-CH_2$ and $-CH_3$ groups.[134] On mixing with the Pcs, some peaks from the phthalocyanines are absent in the NWCNT-MPc spectrum especially at wavelengths lower than 1500 cm^{-1}. All three phthalocyanines have notable peaks in the range of 1080-1095 cm^{-1} corresponding to the stretching mode of the C-N bond. The peaks for the C=N bond are also visible at 1481, 1421 and 1454 cm^{-1} for NiTAPc, NiPc and tBuNiPc respectively.

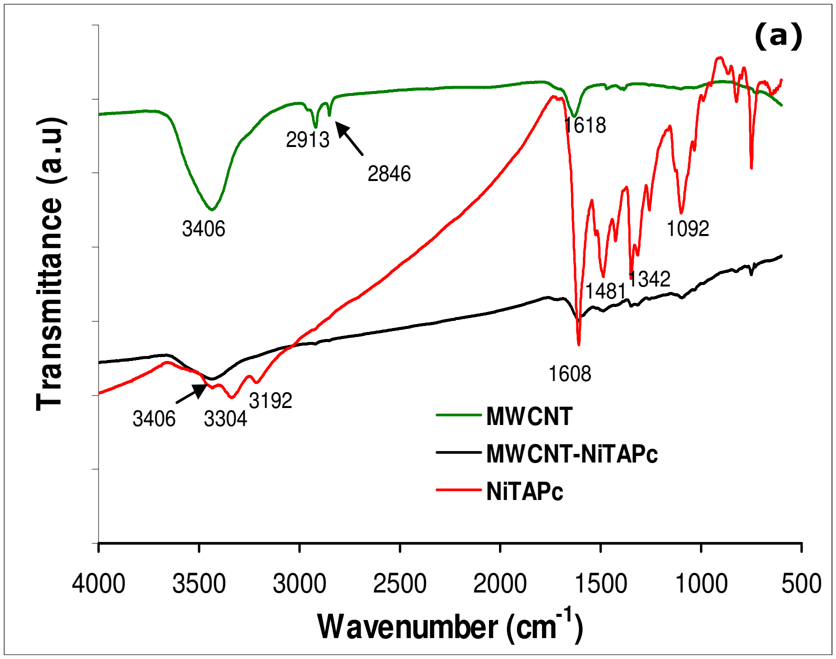

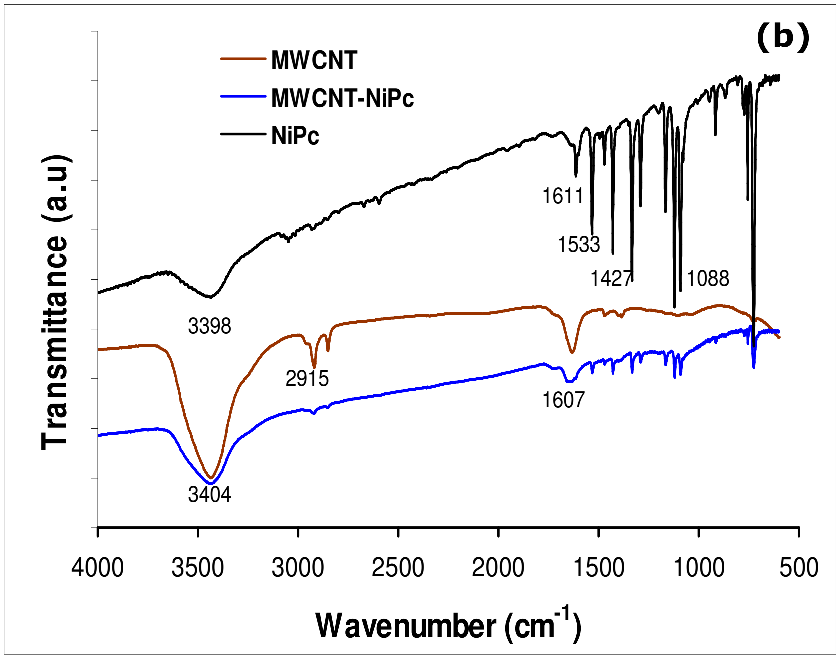

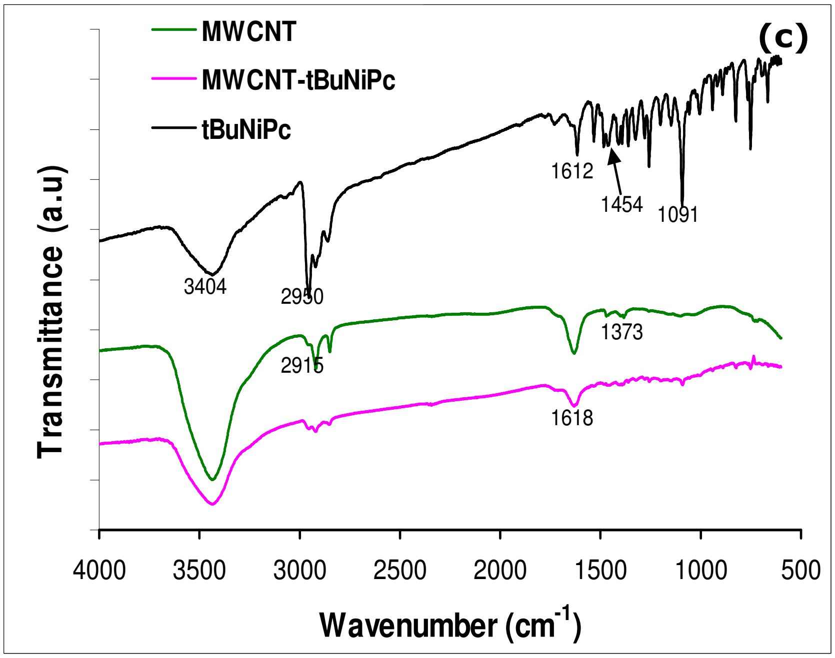

Figure 4.4: FTIR spectra for MWCNT, MWCNT-Ni (II) phthalocyanine composites and Ni (II) phthalocyanine. **(a)** MWCNT, NiTAPc and MWCNT-NiTAPc, **(b)** MWCNT, NiPc and MWCNT-NiPc, **(c)** MWCNT, tBuNiPc and MWCNT-tBuNiPc.

The tBuNiPc spectrum exhibits a strong peak at 2950 cm^{-1} due to the C-H stretching modes of the tert-butyl group. In the NiTAPc molecule, notable peaks are observed at 3304 and 3192 cm^{-1} which could be due to the antisymmetric and symmetric vibrations of the NH_2 groups. In the MWCNT-NiTAPc spectrum, the peaks are hidden by the stronger peak at 3462 contributed by the MWCNTs.[135]

4.1.5 SEM characterisation

CNTs are well known to aggregate together and form bundles due to Van der Waals forces. After functionalization, the MWCNTs are well dispersed and form a unique pore structure due to the spaces that exist between the entangled CNT mats.[136] This is clearly evident from all the pictures in figure 4.5. Figure 4.5 (a) shows the FESEM images of the MWCNT-NiTAPc nanocomposite. Figure 4.5 (a) (inset) clearly reveals the attachment (to a certain extent, via π-π interactions) of the NiTAPc nanoaggregates (50 – 100 nm size) on the nanofibril-like structure of the acid-functionalised MWCNTs.

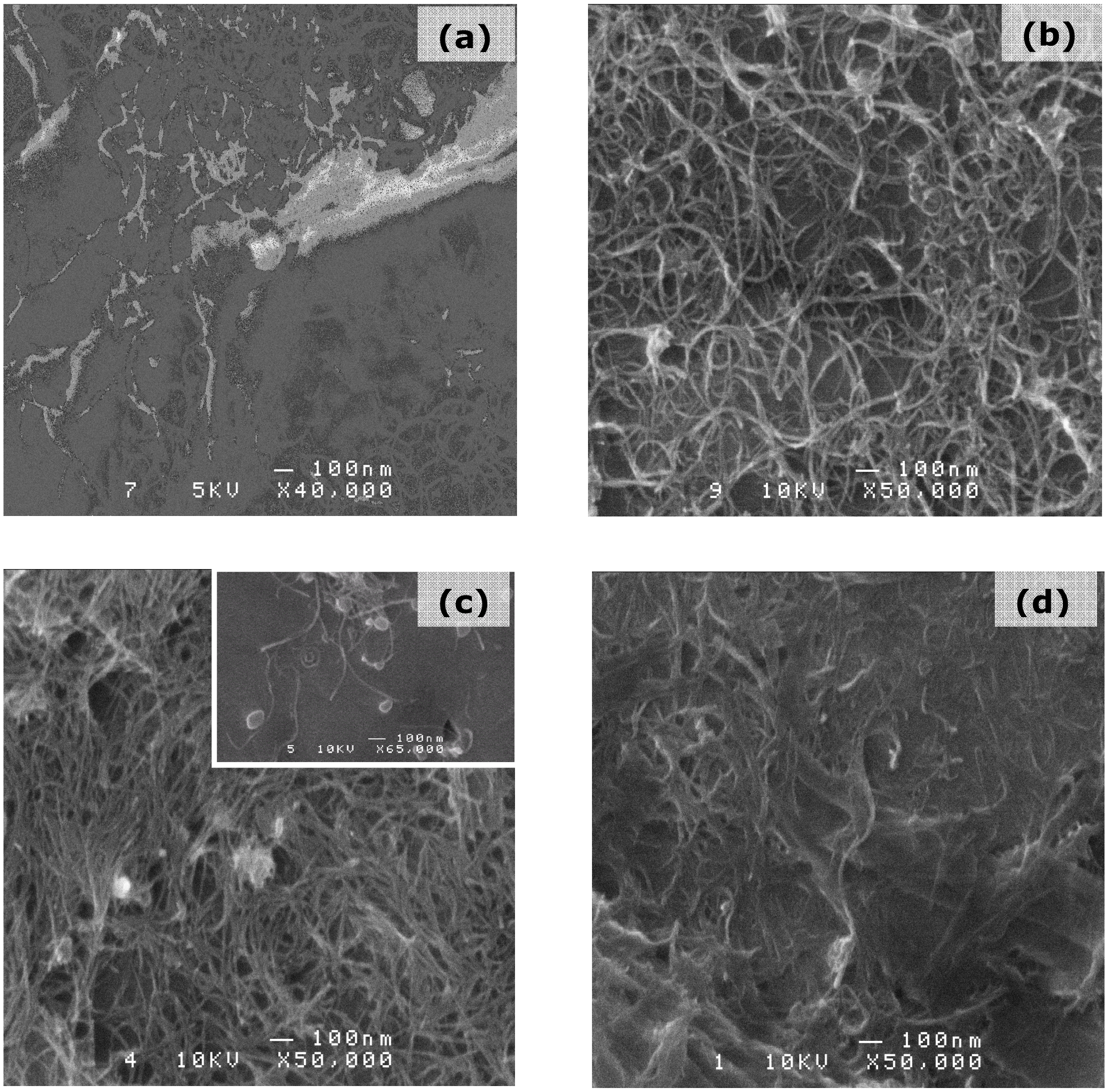

Figure 4.5: Typical SEM images of **(a)** functionalized MWCNTs on basal plane graphite, **(b)** MWCNT-NiPc **(c)** MWCNT-NiTAPc (Inset is a slightly magnified portion showing that some of the NiTAPc molecules are first aggregated before attaching themselves onto the cylindrical structure of the MWCNTs.) and **(d)** MWCNT-tBuNiPc.

The FESEM image of the MWCNT-NiTAPc is different from that reported by Wang *et al*.[126] of a metal-free phthalocyanine (tetra-*tert-butyl* phthalocyanine, *t*BuPcs) species that were uniformly and non-covalently attached to the CNTs via π-π interactions. The authors noted that when the *t*BuPcs was metallated with copper to form the copper (II) tetra-*tert*-*butyl* phthalocyanine (*t*BuCuPcs), these π-π interactions were hindered, which they attributed to the destruction of the aromaticity of the conjugated *t*BuCuPcs backbone due to the formation of the coordinate bond between copper and the nitrogens of the core *t*BuPcs. This explanation may partly hold for our MWCNT-NiTAPc, but their non-covalent attachment cannot be ruled out as other workers [137] have also proved this to be possible with nanocomposites of SWCNTs/metallated porphyrins (compounds structurally-related to phthalocyanines).

4.1.6 TEM images

The HRTEM images in Fig. 4.6 show the effect of functionalization on the length of the CNTs. Functionalization cuts the CNTs into a smaller size thereby enhancing the surface area of the nanostructures. Figures 4.6 (c) and (d) show the interior empty structure of the MWCNTs with the phthalocyanine molecules attached to the walls of the CNTs appearing as little black dots.

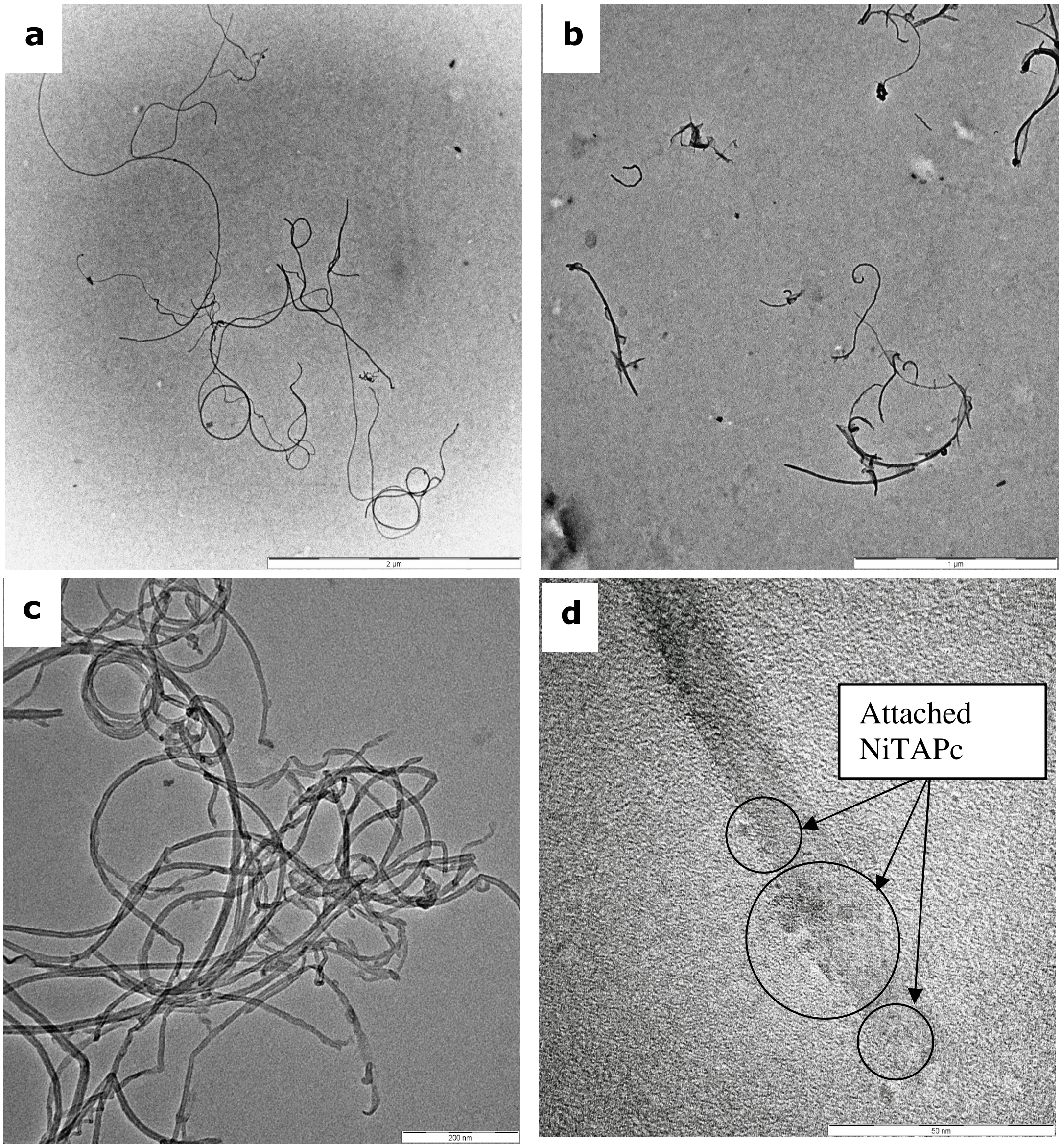

Figure 4.6: TEM images of **(a)** pristine MWCNTs **(b)** acid – cut / functionalised MWCNTs (c) and (d).MWCNT-NiTAPc nanocomposite.

4.2 Electrochemical Characterization

4.2.1 Cyclic Voltammetry

Cyclic voltammetry is a fast and useful method when it comes to the evaluation of electrochemical capacitor properties of electrode materials. The results shown in the diagrams below indicate the capacitive nature of the CNT- phthalocyanine nanocomposites. The electrochemical properties of the hybrids and their constituents were studied by cyclic voltammetry in 1 M H_2SO_4 aqueous solution.

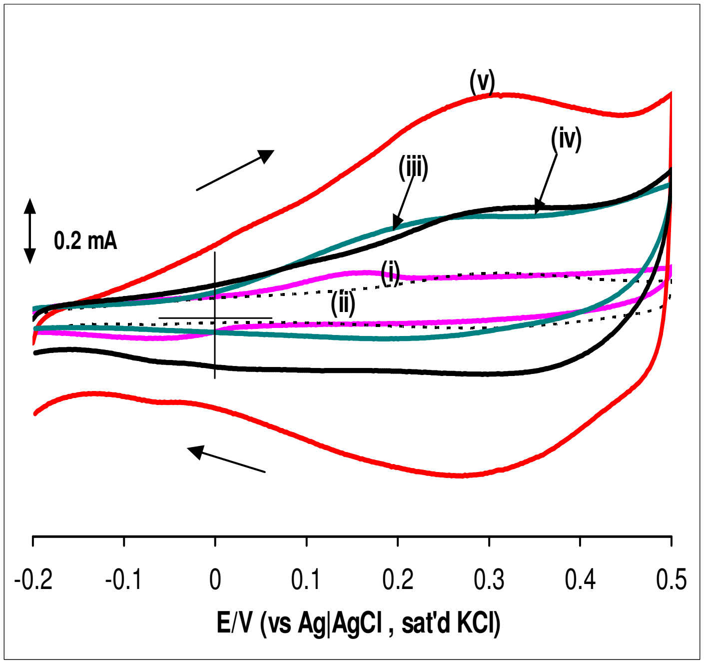

Figure 4.7: Comparative voltammetric evolutions for MWCNT-NiTAPc with different ratios of CNTs: MPc (i) 1:5, (ii) 1:2, (iii) 5:1, (iv) 2:1 and (v) 1:1 at 50 mVs^{-1}.

Preliminary studies to show effect of varying amounts of MWCNTs and NiPc were performed. A ratio of 1:1 (MWCNT:MPc) proved to offer more capacitance when compared to other ratios. Equal masses of MPc and MWCNTs were therefore mixed and sonicated to produce the nanocomposites used for capacitance studies throughout this work.

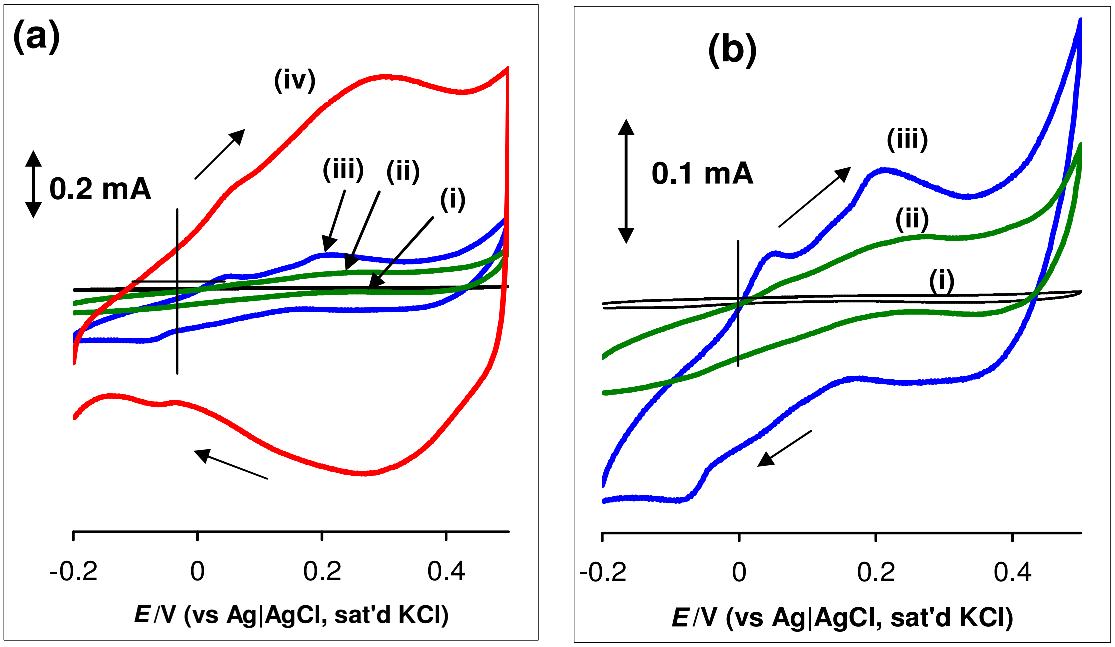

Figure 4.8: (a) Overlaid cyclic voltammograms comparing a bare BPPGE (i), BPPGE-NiTAPc (ii), BPPGE-MWCNT (iii) and BPPGE-MWCNT-NiTAPc (iv) at 50 mV s^{-1}. **(b)** Expansion of the voltammograms of the (i) to (iii). Electrolyte = 1 M H_2SO_4.

The overlaid voltammograms in figure 4.8 show that the MWCNT-NiTAPc nanocomposite exhibits larger capacitance compared to the other electrodes. In acidic medium, pseudocapacitance arises from the redox reactions of the functional groups on the surface of the materials. In the case of acid pretreated MWCNTs these are likely to correspond to the two-electron, two-proton redox process of surface quinones, which are also introduced as surface oxo-groups during acid pretreatment of MWCNTs.[138, 139, 140] These surface quinones give rise to two small, ill-defined, quasireversible redox waves observed at *ca*. 0.2 V vs SCE at low pH, corresponding to both ortho- and para-quinone surface groups.

The larger pseudocapacitance of the MWCNT-NiTAPc nanocomposite compared to that of the MWCNTs or NiTAPc alone, suggests a synergy between these two π-electron species. This positive synergy may have arisen from depositing electroactive-NiTAPc species onto a high conducting and high surface area support (the MWCNTs) resulting in greater double-layer charging and the large Faradaic response. In fact, a closer look at figure 4.8 (a). shows that those peaks observed for the MWCNTs (figure 4.8 (b)) are also present (as weak peaks) at the MWCNT-NiTAPc voltammogram (figure 4.8 (a)). Thus, the broad redox couple (indicative of pseudo-capacitance) of the MWCNT-NiTAPc nanocomposite (4igure 4.8 (a)) at around 0.2 V is related to both the oxygen functionalities of the acid-functionalised MWCNTs as well as the Ni(II)/Ni(III) redox process of the NiTAPc species (equation 23):

$$\mathrm{Ni(II)TAPc} \Leftrightarrow \mathrm{Ni(III)TAPc} + e^{-} \quad \ldots\ldots\ldots\ldots\ldots\ldots\ldots \text{(23)}$$

The participation of the nitrogen-containing groups of the NiTAPc in the electrochemistry may not be completely ruled out. For example, redox chemistry corresponding to immine like groups within the phthalocyanine structure, which is anlogous to the quinonyl redox process discussed above, may also be a contributory factor to the pseudocapacitance observed in figure 4.8.

$$C^{*} = NH + 2e^{-} + 2H^{+} \Leftrightarrow C^{*}H - NH_{2} \text{ .... } (24)$$

According to Hulicova-Jurcakova *et al*. [141] pyrrol and pyridinic nitrogens are electroactive and can enhance supercapacitance. This is because pyrrol or pyrrol-like nitrogen (-NH) improve charge mobility in a carbon matrix by their ability to introduce electron-donor characteristics and enhancing the carbon catalytic activity in electron-transfer reactions, while the pyridinic nitrogen (=N) can provide a lone pair for conjugation with the π-conjugated rings. Although amines bonded to the carbon surface are not expected to affect the electron-donor properties of carbon materials.[141] The contribution to the overall capacitance by the oxyygen containing carboxyl, carbonyl and phenol groups of the acid treated MWCNTs cannot be ignored as reported by Frackowiak.[6,9]

It is a well-established knowledge to the phthalocyanine researchers and electrochemists that the electropolymers of the metallo-tetra-aminophthalocyanine (MTAPc) complexes, notably NiTAPc, can easily be formed on any carbon electrode surface (for electrocatalysis and sensing) using cyclic voltammetry in an appropriate organic solvent (such as DMF) in the presence of a supporting electrolyte salt (e.g., tetrabutyl ammonium phosphate, TBAP). The formation of such MTAPc electropolymers are known to be due to the electroactivity of these peripherally substituted amino groups.[142, 143]

At higher scan rates (figure 4.9 (a)), the observed peak-to-peak separation (ΔE_p) increases slowly (*ca.* 100 mV) and the ratio of anodic and cathodic peak current is almost unity, indicative of fast, electrochemically reversible electron transfer kinetics. A plot of peak (anodic and cathodic) current vs scan rate was linear (figure 4.8 (b)), indicative of a surface bound redox system. Note that despite that we did not employ any binding substance in the fabrication process, the thin film of the MWCNT-NiTAPc nanocomposite on the BPPGE surface still exhibited excellent electrochemical stability, possibly due to the ability of the BPPGE to hold MWCNT-NiTAPc species via π-π interactions.

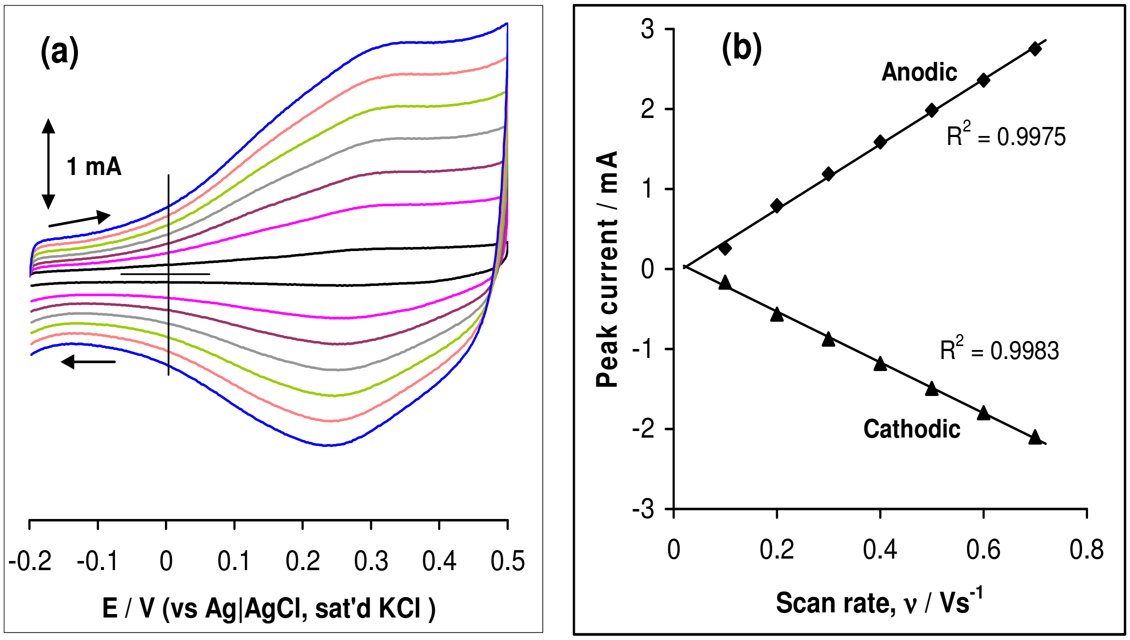

Figure 4.9: (a) Typical cyclic voltammetric evolutions of BPPGE- MWCNT-NiTAPc at varying scan rates 100, 200, 300, 400, 500, 600 and 700 mVs-1 (inner to outer). **(b)** Plot of peak current (anodic and cathodic) vs scan rate. Electrolyte = 1 M H_2SO_4.

At high scan rates the cyclic voltammograms of the three nanocomposites project a clear picture of the differences in capacitance. It is interesting to note that the nanocomposites retain their shape even at high scan rate.

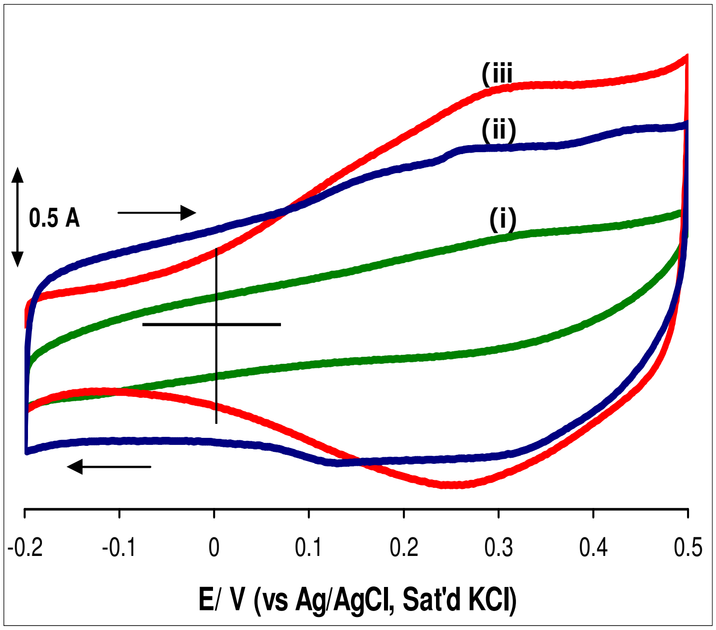

Figure 4.10: Comparative cyclic voltammetric evolutions of BPPGE-MWCNT-NiPc BPPGE-MWCNT-NiTAPc and BPPGE-tBuNiPc at varying scan rates 700 mVs^{-1}.

The cyclic voltammograms are not symmetrical about the zero current axis and their deviation from perfect rectangular shapes is due to pseudocapacitance contribution by the phthalocyanine. It is however interesting to note that the cyclic voltammogram of the MWCNT-tBuNiPc is significantly smaller than that of the other two nanocomposites. The resulting low capacitance of the MWCNT-tBuNiPc hybrid is probably due to the presence of the large t-Butyl groups. The large alkyl groups reduce the hydrophilicity of the hybrid in DMF. More importantly, the protons are hindered from accessing the MWCNT support. The cyclic voltammograms for the MWCNTs did not exhibit the typical rectangular shape expected for an ideal EDLC.This behaviour should certainly be expected considering the long digestion period employed in the functionalisstion of the MWCNTs.

4.2.2 Impedance spectroscopy characterisation

Unlike cyclic voltammetry or galvanostatic discharge methods, electrochemical impedance spectroscopy is the least reliable and accurate technique for determining the supercapacitive properties of materials, especially those related to conducting polymeric substances.[144-149] Figure 4.11 shows typical comparative Nyquist plots of the electrodes.

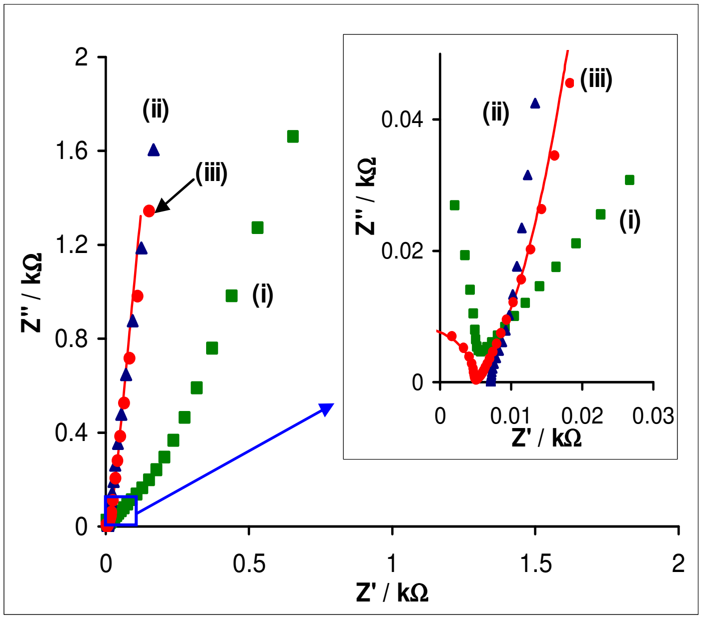

Figure 4.11: Comparative Nyquist plots of BPPGE-NiTAPc (i), BPPGE-MWCNT (ii) and BPPGE-MWCNT-NiTAPc (iii) in 1 M H_2SO_4 at 0.30 V, between 100 kHz and 1 Hz. Inset: The expanded portion of the high frequency region, showing the fitted line for the BPPGE-MWCNT-NiTAPc.

The low-frequency differential capacitance (C_d) for each of the electrodes can be obtained from the slope ($1/2\pi C_d$) of the plot of the imaginary component of the impedance versus the reciprocal of the frequency (i.e., $-Z''$ vs $1/f$).[149-151] The values of the specific capacitances for the three modifiers were less than 500 F g^{-1}, indicative of strong deviation from the data obtained from the CV and galvanostatic methods. At 40 µg (~2 mg cm^{-2}) loading mass fixed at 0.3 V, NiTAPc, MWCNT and the MWCNT-NiTAPc nanocomposite had capacitances of 13, 64 and 340 Fg^{-1} respectively. This strong discrepancy has also been observed by several workers for conducting polymeric substances, [144-149] and the origin of which has long been a subject of some controversy for more than two decades. For example, Murray and co-workers[144] have suggested the involvement of some physico-chemical heterogeneities; Tanguy and co-workers[27] attributed such phenomenon to "deeply trapped" counter ions which remain immobile during impedance experiment; while Kalaji and Peter[148] described it as the consequence of slow conformational changes occurring in the polymer network.

Later, Ren and Pickup[149] performed further experiments that claimed to support the arguments on conformational changes. It should be noted that recent workers have also observed this discrepancy and attributed it to "redox-switching hysteresis" associated with conducting polymers, [152] or the hindrance that accompanies the penetration of alternating current into the bulk electrode.[153] As also observed in figure 4.17, the SC value of the different mass loading of the MWCNT-NiTAPc decreases significantly from the lowest mass loading (~ 586 Fg^{-1} at 20 µg) to the highest mass (~ 180 Fg^{-1} at 80 µg). Thus, it is very likely that one or more of these interpretations by other workers may also hold in our case, especially considering that thick films are prone to inhibiting facile current flow and exacerbating the trapping and / or immobility of ions. Since this behaviour has mainly been reported for the conducting polymers, it suggests that the MWCNT-NiTAPc nanocomposites exhibit some properties of conducting polymeric substances.

Despite the paucity of EIS in establishing reliable data on the supercapacitive data, it still remains a powerful technique for providing valuable insights into processes that occur at the electrode/solution interface. As seen in figure 4.11, the BPPGE-MWCNT shows near-vertical line as expected for pseudocapacitor. The BPPGE-MWCNT-NiTAPc (inset) shows smaller incomplete semi-circle in the high frequency region (describing the ESR or charge transfer resistance across the electrode/electrolyte interface), compared to the BPPGE-NiTAPc, followed by a near-vertical line at low frequency region, which is typical of capacitive behaviour.

The transition point between the high frequency and low frequency component, referred to as the "knee" or "onset" frequency (f_o) describes the maximum frequency at which the capacitive behaviour is dominant, and is a measure of the power capability of a supercapacitor; the higher the f_o the more rapidly the supercapacitor can be charged and discharged or the higher the power density that can be achieved from the supercapacitor.[154,155] The values of the f_o were about 4 Hz for NiTAPc and MWCNTs, and 720 Hz for the MWCNT-NiTAPc. Accordingly, the higher f_o value of the MWCNT-NiTAPc confirms its higher power property compared to the individual NiTAPc and MWCNTs, which is consistent with the comparative CV data shown in figure 4.2.2 (a). The reciprocal of the f_o is the response time of the capacitor. Note that the f_o of MWCNT- NiTAPc is about 1.4 ms, suggesting that most of its stored energy is still accessible at frequencies as high as 720 Hz. Most commercially available supercapacitors, including those specifically designed for higher power applications operate at frequencies less than 1 Hz.[156]

The impedimetric behaviour of MWCNT-NiTAPc could be satisfactorily modelled by the electrical equivalent circuit comprising the modified Randles circuit with one voigt RC element (Figure 3.12), involving a solution resistance (R_s = −11.7 Ω), a double-layer capacitance (C_{dl} =95 nF), an electron-transfer resistance (R_{ct1} = 16.6 Ω and R_{ct2} = 18 Ω) and constant-phase elements (CPE_1 = 10.5 mF with n_1 = 0.95 and CPE_2 = 33.6 mF with n_2 = 0.55).

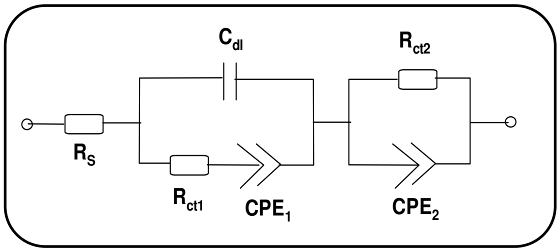

Figure 4.12: Electrical equivalent circuit used in fitting the experimental EIS data obtained at the BPPGE-MWCNT-NiTAPc.

As already stated in chapter one, the impedance of CPE is defined as

$$Z_{CPE} = \frac{1}{[Q(j\omega)^n]} \quad \text{...} \quad (22)$$

The CPE_1 that replaced the diffusion impedance (Z_W) in the ideal Randles circuit is associated with a high n_1 value (0.95), describing the high porous nature of the electrode. The n_2 value (0.55) is approximately equal to the ideal Warburg behaviour of $n = 0.5$, describing the diffusion of ions through the thin film.[150] From the Bode plot (log $|Z|$ vs. log f (figure 4.13), the high frequency region yielded a slope of close to zero, characteristic of pure resistor, while the low frequency region yielded a slope of <1.0, characteristic of pseudocapacitor.

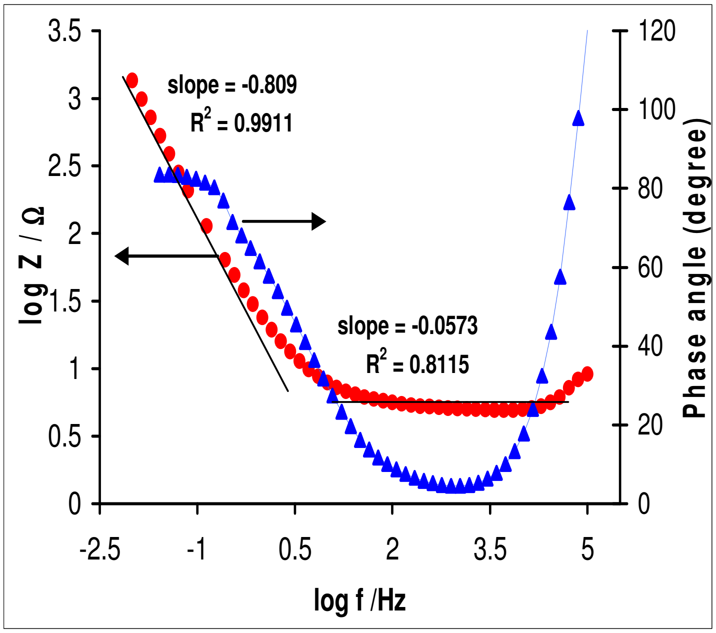

Figure 4.13: Bode plots for the BPPGE-MWNCT-NiTAPc electrode.

In general, these data clearly suggest that the impedance of this electrode varies from a pure resistor at high frequency to pseudocapacitor at low frequency region. Surprisingly, all attempt to replace the ideal C_{dl} with a CPE (a real application situation) in the modeling circuit proved unsuccessful. As has elegantly been described recently by Orazem and Tribollet,[157] the behaviour occurs as a result of distribution of time constants along either the area of the electrode surface (involving a 2-dimensional aspect of the electrode) or along the axis normal to the electrode surface (involving a 3-dimensional surface).

It is noteworthy that a 2-D distribution presents itself as an ideal RC behaviour, meaning that impedance measurements are very useful in distinguishing whether the observed global CPE behaviour is due to a 2-D or 3-D distribution or both.Thus, we may conclude that the observed impedimetric behaviour of the BPPGE-MWCNT-NiTAPc likely involve time constant distributions occurring along the area of the electrode as well as along the axis normal to the electrode. Also, from the other type of Bode plot (i.e., –phase angle (θ) vs. log f, (figure 4.13), the θ was about 80^{o}, which is less than the 90^{o} expected of ideal capacitive behaviour, thus further confirming the presence of CPE and pseudocapacitive nature of the BPPGE-MWCNT-NiTAPc.

Impedance spectroscopy was also performed for the MWCNT-tBuNiPc and the unsubstituted MWCNT-NiPc nanocomposites. The overall picture was the same as that for the MWCNT-NiTAPc hybrid where they all exhibit a shape characteristic of porous electrodes. The diagrams in figure 4.14 show the Nyquist and Bode plots for the MWCNT-NiPc nanocomposite. The phase angle for the hybrid is ca. 80° indicative of an almost ideal supercapacitor. The synergy between the MWCNT and unsubstituted NiPc (figure 4.14 (b)) and tBuNiPc is also observed in the comparative Nyquist plots where the Pc and MWCNT contribute to a near-vertical line at low frequencies. The result is best shown by the Bode plots where the phase angle for the hybrids is close to 90°

implying that the electrode reaction is dominated by double layer capacitance.

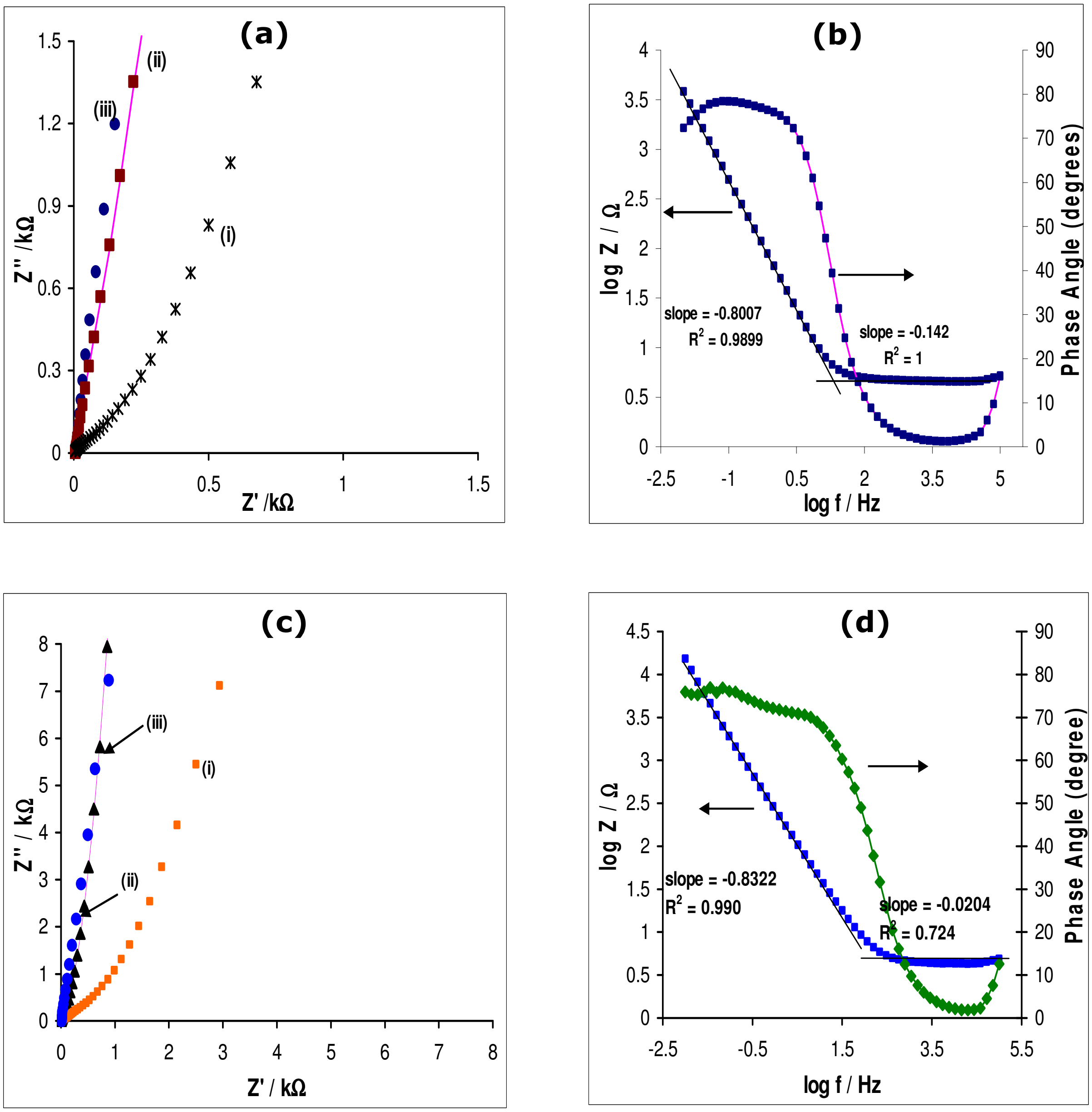

Figure 4.14: (a) Comparative Nyquist plots of BPPGE-NiPc (i) BPPGE-MWCNT-NiPc (ii) and BPPGE-MWCNT (iii) in 1M H_2SO_4 at 0.30 V, between 100kHz and 10mHz. **(b)** Bode plots for fitted BPPGE-MWCNT-NiPc data in 1M at 0.30 V. Comparative Nyquist plots of BPPGE-tBuNiPc **(c)** and Bode plots for the BPPGE-MWCNT-tBuNiPc **(d)**

4.2.3 Galvanostatic Charge/Discharge

The three hybrid supercapacitor electrodes were all tested under galvanostatic conditions. The electrodes were subjected to constant current charge/discharge cycling in the voltage range of -0.2 to 0.5 V at different current densities of 1 A g^{-1} to 30 A g^{-1}. It is well documented that galvanostatic discharge is the most reliable and accurate method for evaluating the supercapacitance of electrodes.[153,158,159] Figure 4.15 shows typical galvanostatic charge / discharge measurements obtained for the BPPGE-MWCNT (i) and BPPGE-MWCNT-NiTAPc (ii) at a current density of 1 A g^{-1}; first charged to 0.5 V and then discharged to -0.2 V. The specific capacitance (SC), specific power density (SP) and specific energy (SE) based on the active materials (MWCNT, or NiTAPc or MWCNT-NiTAPc) were easily estimated from the discharge process using the established equations.(equations 14,15 and 16 from chapter 1)

$$SC(F/g) = \frac{[i(A)\times\Delta t(s)]}{[\Delta E(V)\times m(g)]} \quad \text{.............................} \quad (14)$$

$$SE(Whkg^{-1}) = \frac{[i(A)\times t(s)\times\Delta E(V)]}{m(kg)} \quad \text{........................} \quad (15)$$

$$SP(Wkg^{-1}) = \frac{[i(A)\times\Delta E(V)]}{m(kg)} \quad \text{...........................} \quad (16)$$

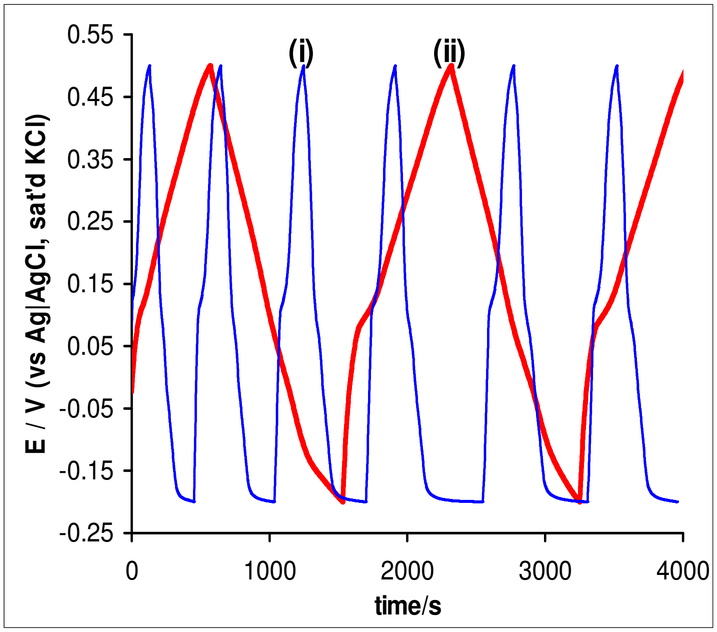

Figure 4.15: Typical charge-discharge cycles obtained at the BPPGE-MWCNT (i) and BPPGE-MWCNT-NiTAPc (ii) at 1 Ag^{-1}.Supporting electrolyte = 1 M H_2SO_4.

It is well known that in an aqueous electrolyte, capacitance is predominantly determined by the hydrophilicity of the electrode materials, the stronger the affinity of the electrode materials; the higher the double layer capacitance.[160] The high specific capacitance recorded for the MWCNTs should perhaps not be surprising considering the stringent acid-treatment procedure adopted in this work to functionalise our MWCNTs. For example, by merely stirring MWCNTs in 3:1 mixture of H_2SO_4/HNO_3 for just an hour, Kim *et al*.[160] reported the capacitance of MWCNTs immobilized onto a Ni mesh using PVDF solution in N-methylpyrolidine as binder (and a 3-electrode system) to be 51.3 F g^{-1} in 1 M H_2SO_4. On the other hand, Frackowiak and co-workers[9] did not employ the long functionalisation times as used in our case, however, they reported values from 70 to 120 Fg^{-1} in 6 M KOH for a 2-electrode system and using PVDF binder.

Therefore, if we consider that we did not employ organic binders (which, to a certain extent, can impact negatively on the flow of ions and hence on the observed capacitance) and that capacitance value of a 2-electrode system is about 4 times less than for a 3- electrode system, the values reported by these authors [160] are in close proximity to ours. Different masses were also loaded onto the electrode and the capacitance measured using CD and EIS to obtain an insight into the impact of different mass loadings (20-80 µg range) on capacitance. As seen in figure 4.16, the specific capacitance decreased slightly from the lowest mass loading (~1320 Fg^{-1} at 20 µg) to the highest mass (~907 Fg^{-1} at 80 µg).

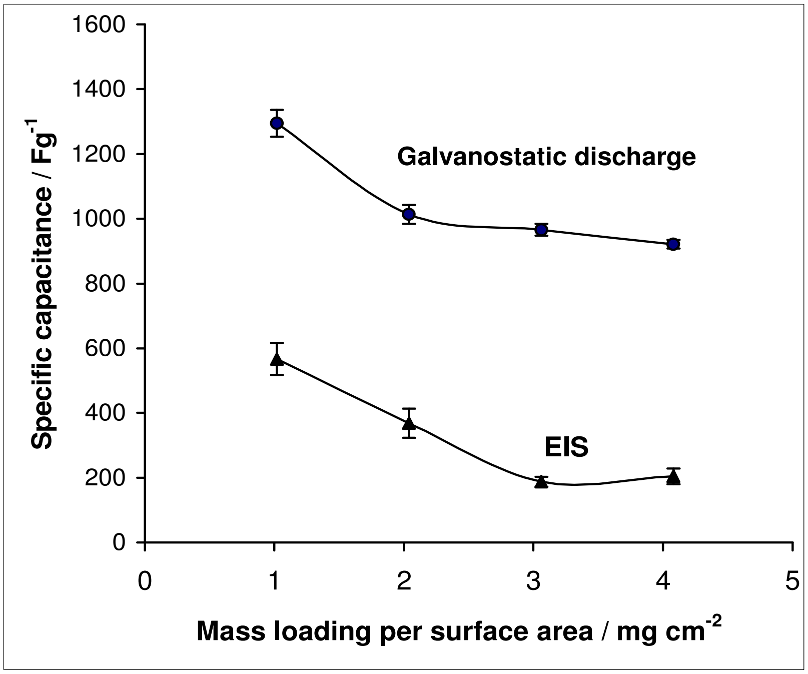

Figure 4.16: Plot of specific capacitance versus mass loading of the MWCNT-NiTAPc determined from the **(a)** galvanostatic discharge at 1 Ag^{-1}, and **(b)** electrochemical impedance spectroscopy at 0.3 V vs Ag|AgCl (sat'd KCl).Supporting electrolyte 1M H_2SO_4.

It is interesting to observe from figure 4.16 that, within the limits of experimental errors, the SC of the MWCNT-NiTAPc nanocomposite is approximately 1000 Fg^{-1} at all mass loadings studied. The decrease in the SC at higher mass loadings (> 20 μg) may be attributed to the thickness of the film on the small geometric area electrode (0.196 cm^2) employed in this study. In fact, with the exception of the 20 μg loading, all subsequent loadings had to be carried out at several "drop-dry times" to get all the materials loaded on the electrode. Thick film is disadvantageous to pseudocapacitive behaviour. As the material loading increases more of the electroactive species are buried within the thick film and become 'redox-silent'. In addition, there will be problems with distribution of potentials within this thick surface-confined modified CNT material. Thus, as a compromise, we used 40 µg (~ 2 mg cm^{-2}) to compare the SC values of the three materials.

The maximum supercapacitive parameters were obtained at 1 A g^{-1} and are summarised in Table 4.1. For the MWCNT-NiTAPc (n = 6, 95% confidence level) the following were obtained: SC = 981 ± 57 Fg^{-1} or 200 ±12 Fcm^{-2}; SP = 701 ± 1 W kg^{-1} and SE = 134 ± 8 Wh kg^{-1}. These values are more than twice higher than those of the MWCNTs alone.

Table 4.1: Supercapacitive properties of basal plane pyrolytic graphite electrode (BPPGE) modified with NiTAPc, acid-functionalised MWCNTs and MWCNT-NiTAPc**.**

Electrode	Supercapacitive parameters			
	SC (F g^{-1})	SC (mF cm^{-2})	SP (W kg^{-1})	SE (Wh kg^{-1})
BPPGE-NiTAPc	198 ±13	40 ± 3	703 ± 1	27 ± 2
BPPGE-MWCNTs	335 ± 18	68 ± 4	700 ± 1	46 ± 3
BPPGE-MWCNT-NiPc	760 ± 15	95 ± 1	700 ± 3	134.6 ± 5
BPPGE-MWCNT-tBuNiPc	440 ± 23	44.9 ± 1	700 ± 2	33.4 ± 7
BPPGE-MWCNT-NiTAP	981 ± 57	200 ± 12	701 ± 1	134 ± 8
[1] Specific capacitance (F cm^{-2}) calculated per geometric area of the electrode, not the electroactive area.				

From Table 4.1, the values of the specific capacitance are comparable to our estimated CV data. However, the values recorded with the galvanostatic discharging are more reliable given their low errors. In general, the SC value for the BPPGE-MWCNT-NiTAPc is indeed greater than most other half-cell or three electrode counterparts reported in the literature.[161-163] For example, using the same experimental conditions as ours (i.e., 1 A g^{-1}, 1 M H_2SO_4 with a 3-electrode system), Hulicova Jurcakova *et al.*[21] recently reported a value of 1117 µFcm^{-2} for the nitrogen-enriched carbon electrode.

It is interesting to note that our supercapacitance value of 135 m Fcm^{-2} (200 Fcm^{-2} using 40 µg) is two orders of magnitude or more than a hundred-fold greater than the value described as ‘extraordinary supercapacitance’.[21] The excellent supercapacitive behaviour of the MWCNT-NiTAPc may be related to the high surface area and porous nature of the nanocomposite that enhance the penetration of solution ions. Importantly, the thin film nature (small active mass used in this study) of the hybrid is advantageous as it shortens the distance which ions and electrons would have to travel to reach the electrode. In addition, the incorporation of pendant amine groups, capable of protonation at this low pH incorporates more positive charges into the NiTAPc macrocyle structure than simply the Ni(II)/Ni(III) metal centre, thus enhancing the interaction with electrolyte anions at the electrolyte-electrode interface and increasing the observed double-layer capacitance compared to macrocylces without such additional charged groups.

Also, at all current densities of 1 – 30 A g^{-1} (i.e., 0.1 – 3 mF cm^{-2}) studied, the charge processes of the MWCNT-NiTAPc showed mirror images of their corresponding discharging counterparts, with no detectable IR drop even at much higher discharge current densities, suggesting a very small equivalent series resistance (ESR) of the electrode. The energy deliverable efficiency (η / %) was obtained from equation 17 (from chapter 1). The energy deliverable efficiency of the MWCNT-NiTAPc nanocomposite at the ~2 mg cm^{-2} was ~ 121 % at 1 A g^{-1} and up to ~ 100 % at 1 A g^{-1}.

$$\eta\ (\%) \quad = \frac{t_{\mathrm{d}}}{t_c}\,\mathrm{x}100 \qquad \text{.......................................} \ (17)$$

To obtain an insight into the impact of phthalocyanine ring substituents on the supercapacitive behaviour, similar CV and CD experiments for NiTAPc-MWCNT were also performed with unsubstituted nickel (II) phthalocyanine (NiPc) and nickel (II) tetra-*tert-butyl* phthalocyanine (*t*BuNiPc). Interestingly, the NiTAPc gave superior capacitive data. As an example, at a current density of 1 Ag^{-1} (for ~ 20 µg loading) the specific capacitance decreases as NiTAPc (~ 243 Fg^{-1}) > NiPc (~ 176 Fg^{-1}) > *t*BuNiPc (~ 126 Fg^{-1}). This trend is accordance with the nitrogen contents of the three phthalocyanine species. In addition, the poorer value of the *t*BuNiPc may be related to the absence of nitrogens with any doner lone pairs to protonate at this acidic pH used in this work or the bulky *t*ert-butyl group that may deform the phthalocyanine framework, thus reducing the supercapacitance. In addition, Kim *et al*.[160] proved that alkyl chains reduce supercapacitance. Also, the NiTAPc-MWCNT is more stable on the BPPGE and highly reproducible galvanostatic data than the other nickel phthalocyanines studied. More importantly, NiPc and *t*BuNiPc and their MWCNT composites are less soluble in DMF than the NiTAPc based electrodes. This superior performance of the NiTAPc is not fully understood at this moment, but may be related to its nitrogen-containing groups, which have recently been observed to greatly enhance supercapacitive behaviour. [141,164]

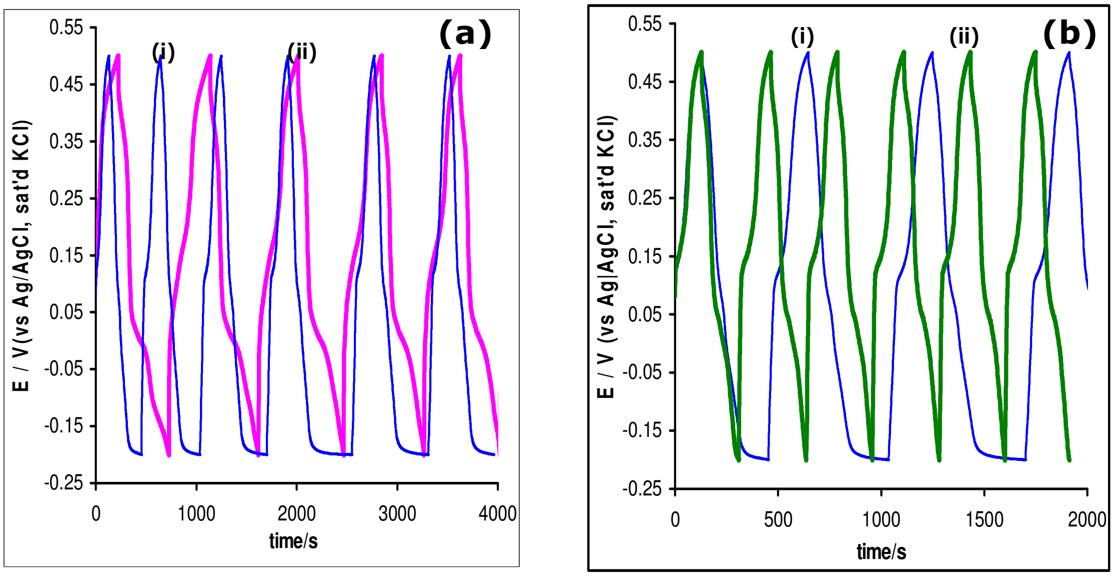

Figure 4.17: Typical charge-discharge cycles obtained at the **(a)** BPPGE-MWCNT (i) and BPPGE-MWCNT-NiPc (ii), **(b)** BPPGE-MWCNT (i) and BPPGE-MWCNT-tBuNiPc at 1 Ag^{-1} (0.1 mA cm^{-2}).Supporting electrolyte = 1 M H_2SO_4.

The plots given in Figure 4.18 show the relationship between specific capacitance and current density. For the three materials, the highest specific capacitance was observed at low current densities and decreased significantly with increase in current density. This can be explained by the limited access of the pores for charge storage at high current densities by the ions. The contribution by the smaller pores to the overall capacitance is limited. The three kinds of material are therefore suitable for supercapacitors in lower current densities than 5 Ag^{-1}. A levelling of the curves is observed at high current densitites.

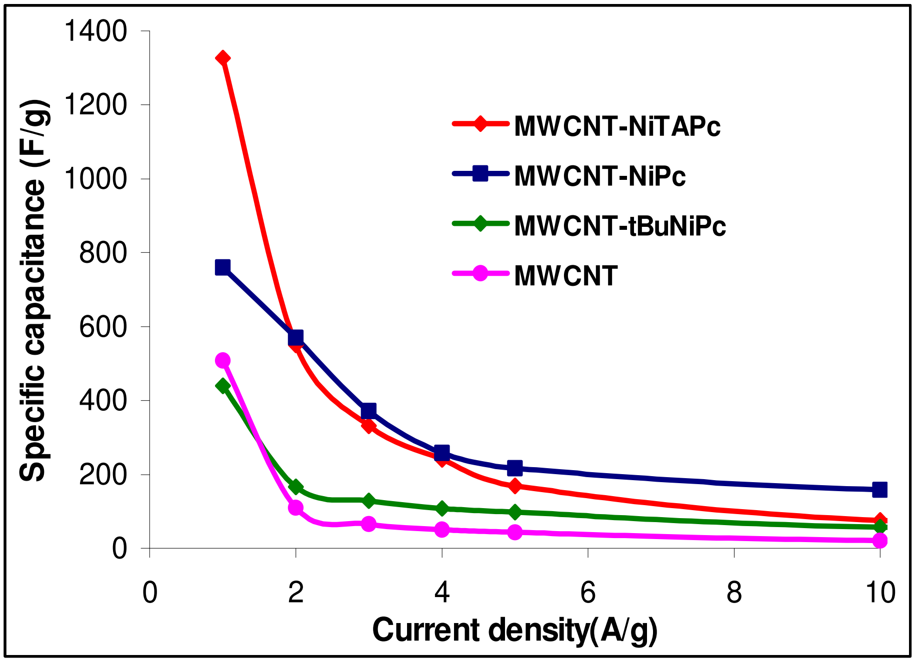

Figure 4.18: Specific capacitance values as a function of current density.

4.2.4 Stability studies

The MWCNT-Nickel(ii) phthalocyanine electrodes were tested for stability at high current and were all found to possess remarkable stability over 1000 charge-discharge cycles.The stability of the nanocomposites were tested by continuous cycling at high current density (1mA/cm^2). A typical repetitive charge-discharge cycling for 1500 cycles is shown in figure 4.20. The figure clearly shows that the electrode is able to charge and discharge continuously without any significant loss in capacitance.

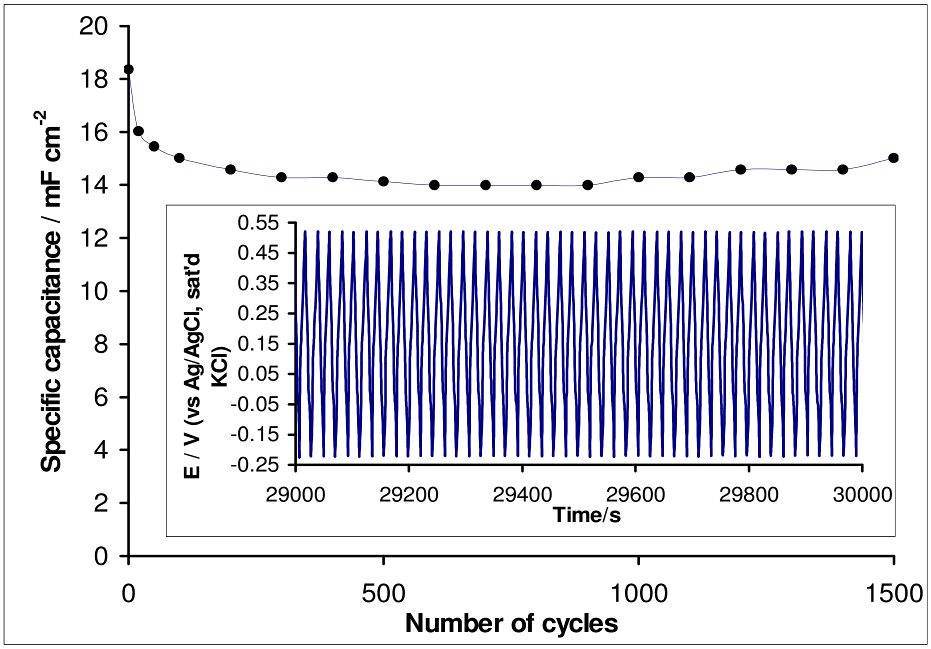

Figure 4.20: Variation of specific capacitance with the number of cycles at 10 A g^{-1} (1mA cm^{-2}). Inset is a portion of the charge-discharge curves. Supporting electrolyte = 1 M H_2SO_4.

A small decrease in the specific capacitance is observed for the MWCNT-NiTAPc nanocomposite in the first 100 cycles. A decrease in specific capacitance of 16.7% was observed. In the subsequent 500 cycles a decrease of 6% was observed.

4.3 Supercapacitive properties of electropolymerized film of Nickel (ii) tetra-aminophthalocyanine

Electropolymerized metalloporphyrin and metallophthalocyanine-coated electrodes have been reported expansively as efficient electrocatalysts for chemical, photochemical and analytical applications.[165-170] Nickel macrocyclic complexes have received a lot of attention as conducting polymer films.[171,172] Interestingly enough, despite the huge literature on the conductive ability and electrocatalytic properties of electropolymerized nickel phthalocyanine complexes, no report on nickel phthalocyanine polymers as potential supercapacitor electrode materials has been made. Motivated by the results in chapter 3.2 where a composite mixture of nickel (II) tetra-aminophthalocyanine (NiTAPc) and multi-walled carbon nanotubes (MWCNTs) exhibit supercapacitive behaviour, this section explores, for the first time, the capacitive properties of the electropolymeric films of NiTAPc supported on a MWCNT platform.

4.3.1 Cyclic Voltammetry

Figure 4.21 shows typical electropolymerisation process of the NiTAPc on BPPGE, showing growth of scan. As the scan number increases, typical features of electropolymerisation process become evident. The electropolymerisation process has been reported to occur via the oxidation of the amino groups and the N-N coupling resulting in an electroactive polymer on the electrode surface.[173] Well defined peaks appear at around 0.45 V are observed.

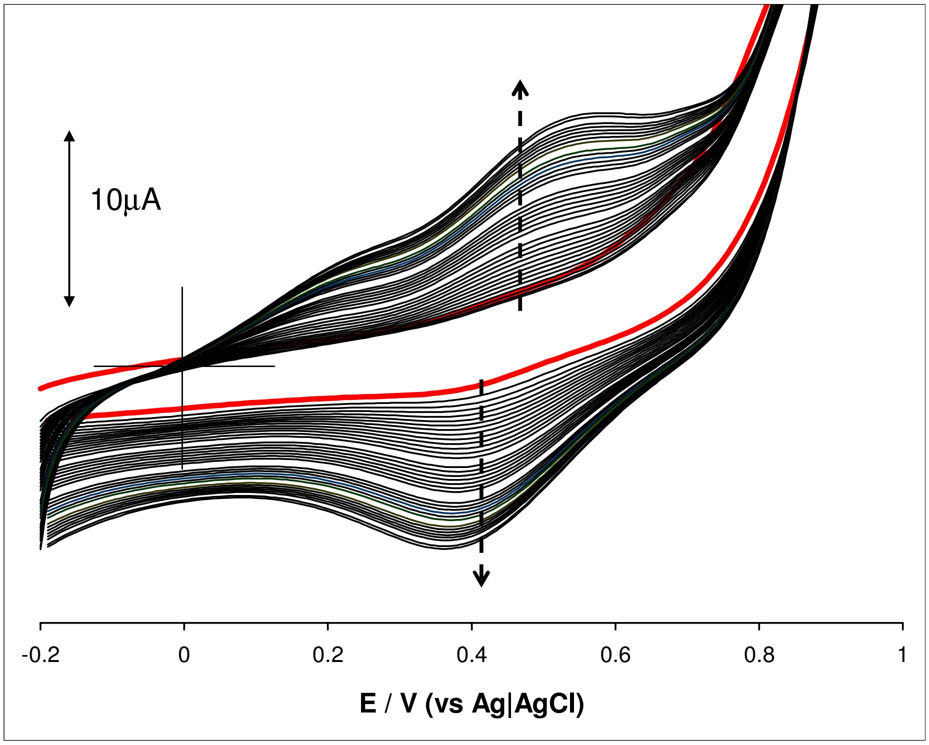

Figure 4.21: Cyclic voltammogram of 10 mM NiTAPc in DMF at 100 mVs^{-1} (50 scans increasing from inner to outer)

The same feature is also observed for the BPPGE-MWCNT-polyNiTAPc.

Figure 4.22 shows the CV evolutions of the BPPGE-polyNiTAPc on continuous cycling in 0.1 M NaOH. As the cycling continues, the peaks grow steadily until they reach a steady state where no further growth is observed.

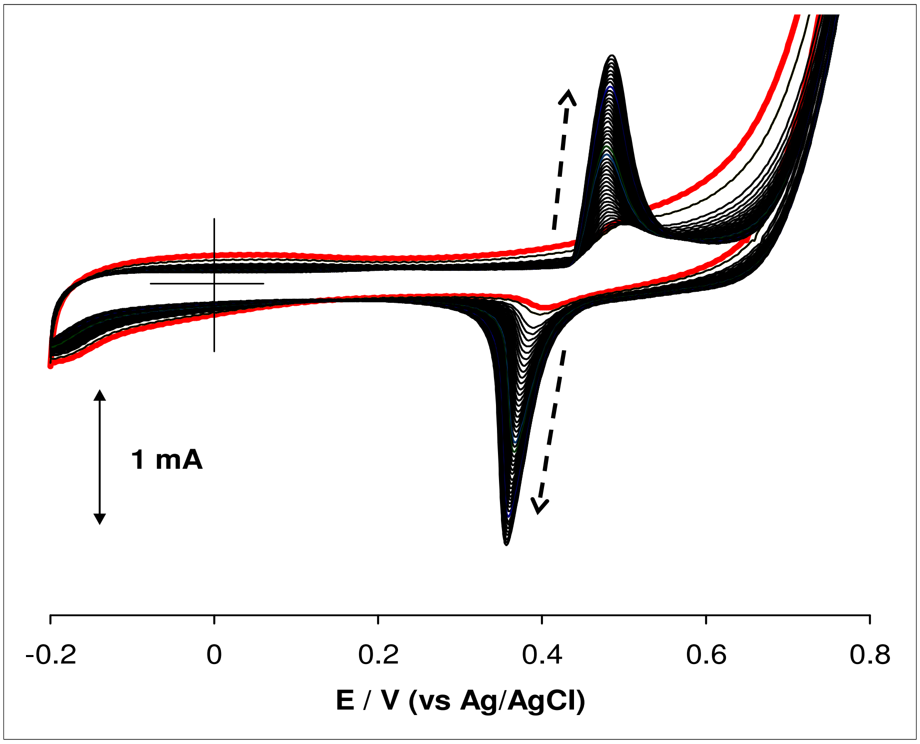

Figure 4.22: Modified CVs of BPPGE-MWCNT-polyNiTAPc, after 50 scans (increasing from inner to outer) from -0.2 V to 0.8 V in aqueous NaOH 0.1 mol L^{-1} solution at 100 mV $^{s-1}$.

This is typical of cyclic voltammograms recorded for electroformed nickel macrocyclic-based films in alkaline solution and shows that the film has been formed as a result of the anodic polymerization of the macrocyclic complex.[173] As the cycling continues, the peaks grow steadily until they reach a steady state where no further growth is observed as shown in figure 4.22. The CV shows one redox couple with formal potential ($E_{1/2}$) at ~0.42 V vs Ag|AgCl, which is assigned to the Ni(II)/Ni(III) redox process of the nickel centre of the NiTAPc. The appearance of this signature redox couple confirms the successful integration of the polyNiTAPc onto the electrode. The same feature is observed for the MWCNT-polyNiTAPc electrode, except for the higher current response observed for the BPPGE-MWCNT-polyNiTAPc. It has been postulated that the polymerization of nickel macrocyclic complexes in alkaline media is very similar to that of the nickel hydroxide electrode.[173] The nickel-nitrogen tetra coordination of the complex is thought to be lost in the polymerization process. Another postulate by Roslonek and Taraszewka proposes that upon electropolymerisation, the complexes are attached *via* oxo-bridges.[174] Cyclic voltammetry study was carried out for all the electrodes in both acid (1 M H_2SO_4) and alkaline (1 M NaOH) conditions. Figure 4.23 presents typical cyclic voltammetric evolutions obtained.

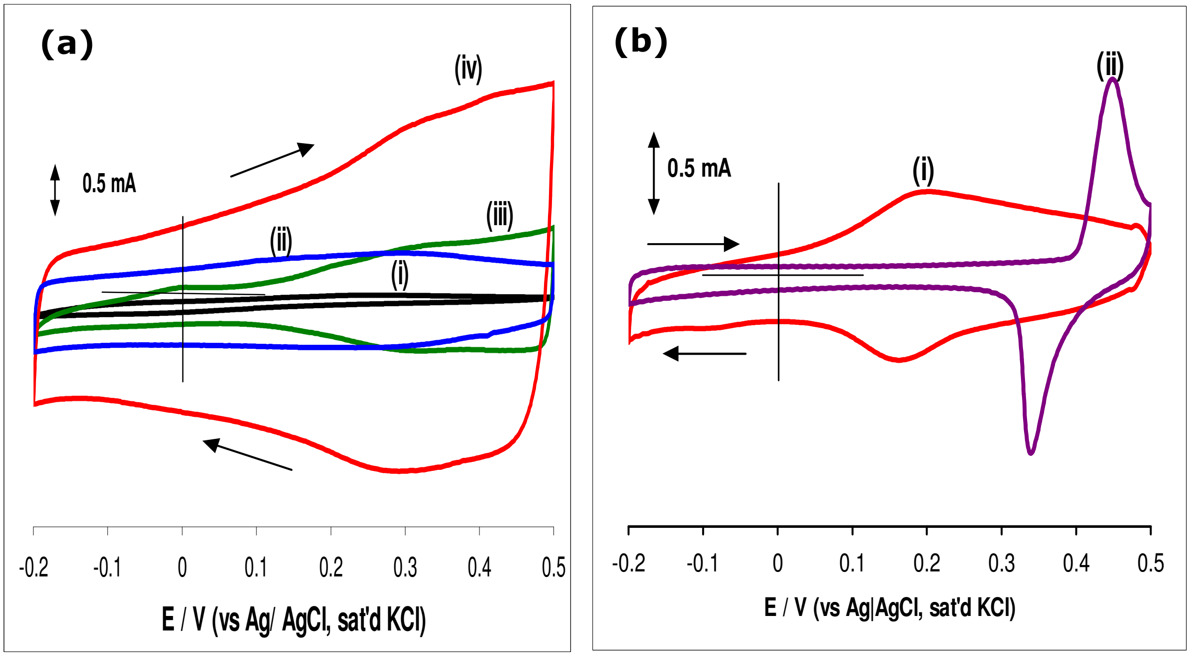

Figure 4.23: (a) Comparative CV's for bare BPPGE (i), BPPGE-MWCNT (ii), BPPGE-polyNiTAPc (iii) and BPPGE-MWCNT-polyNiTAPc (iv) in 1 M H_2SO_4. **(b)** Effect of electrolyte on capacitance: BPPGE-MWCNT-polyNi(OH)TAPc in acid (i) and in alkali (ii).

The capacitance of the polymeric film per unit area of the electrode ($C_{polym.}$/F cm^{-2}) was estimated in both the faradaic (ca 0.35 V) and the non-Faradaic regimes (-0.1 V versus Ag/AgCl) using equation (25) [175,176]

$$C_{polym}\ (Fcm^{-2}) = \frac{I_{ch}}{\nu A} \quad \text{..............................} \ (25)$$

where I_{ch} is the charging current, ν the scan rate and A the geometric area of the electrode. The capacitance was calculated for both the anodic and cathodic charging current and the average values reported. From the comparative CVs in acidic medium, the capacitive behaviour of the electrodes follows as MWCNT-polyNiTAPc (97 mF cm^{-1}) > MWCNT-polyNi(OH)TAPc (50 mF cm^{-1}) > MWCNT (35 mF cm^{-1}) > polyNiTAPc (21.9 mF cm^{-1}). Figure 4.23 (b) shows the impact of electrolyte on the capacitance, where BPPGE-MWCNT-polyNi(OH)TAPc in acid medium is better than obtained in alkaline. Clearly, the CV recorded in acid has a lager current separation as compared to that recorded in alkaline medium.

The overall capacitance in acidic media is therefore higher than that observed in alkaline medium. Recently, Hulicova *et al.*[141] observed a similar phenomenon for nitrogen-doped carbon materials studied for supercapacitor and found that these materials exhibit enhanced capacitive behaviour in 1 M H_2SO_4 than in 1 M KOH solution. The authors interpreted the situation in terms of the nitrogen functionalities exhibiting stronger interactions with the H_3O^+ than with the K^+ resulting in higher capacitance. The same explanation may also hold in our case, possibly due to the interaction between the nitrogen groups of the phthalocyanine ring and the H_3O^+ of the H_2SO_4 electrolyte. Based on this observation, further studies were carried out with the more reliable galvanostatic charge-discharge method to unequivocally determine the capacitance values. Scan rate studies were also performed for the MWCNT-polyNiTAPc electrode

4.3.2 Galvanostatic charge-discharge experiments

It is well established that galvanostatic discharge represents the most accurate and reliable strategy for probing the supercapacitance of materials. Figure 4.24 shows the galvanostatic charge-discharge curves obtained. The specific capacitance (SC) was evaluated from the discharge curve using equation 14 from chapter 1 with the mass of the electrode being replaced by electrode area in cm^2:

$$SC\ (Fcm^{-2}) = \frac{I \times \Delta t}{\Delta E \times A} \qquad \text{..............................} \ (14)$$

The specific capacitance follows the same trend as the CV data: BPPGE-MWCNT-polyNiTAPc (112 mFcm^{-2}) >BPPGE- MWCNT-polyNi(OH)TAPc (84.9 mFcm^{-2}) > BPPGE-MWCNT (38.7 mFcm^{-2}) > BPPGE-polyNiTAPc (27.2 mFcm^{-2}). Also, as in the CV, the capacitance of the BPPGE-MWCNT-polyNiTAPc obtained in acid is higher than obtained in the alkaline medium.

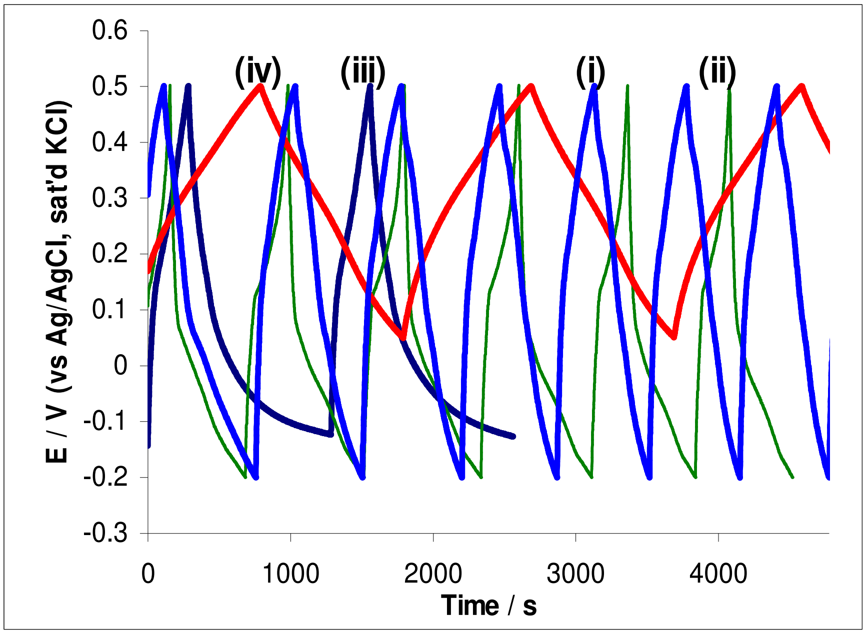

Figure 4.24: Comparative CD's for the BPPGE-MWCNT (i), BPPGE-polyNi(OH)TAPc (ii), BPPGE-MWCNT-polyNi(OH)TAPc (iii),BPPGE-MWCNT-polyNiTAPc (iv) at 0.5 mAcm^{-2} in 1M H_2SO_4.

The enhanced capacitance of the MWCNT-polyNiTAPc in acid medium may be interpreted in terms of the synergism between MWCNT and polyNiTAPc species (also observed in the CV profiles). It indicates that this electrode possesses features (mainly, conductivity and porosity) that permit free movement of the solution ions to and from the electrode/solution interface. The porous nature of the MWCNT-polyNiTAPc electrode is also observed in figure 4.25. Upon introduction of the MWCNTs, the globular structure of the polyNiTAPc is still evident in figure 4.25 (c) and the deposit shows a network between the MWCNTs and the polyNiTAPc in 4.25 (d).

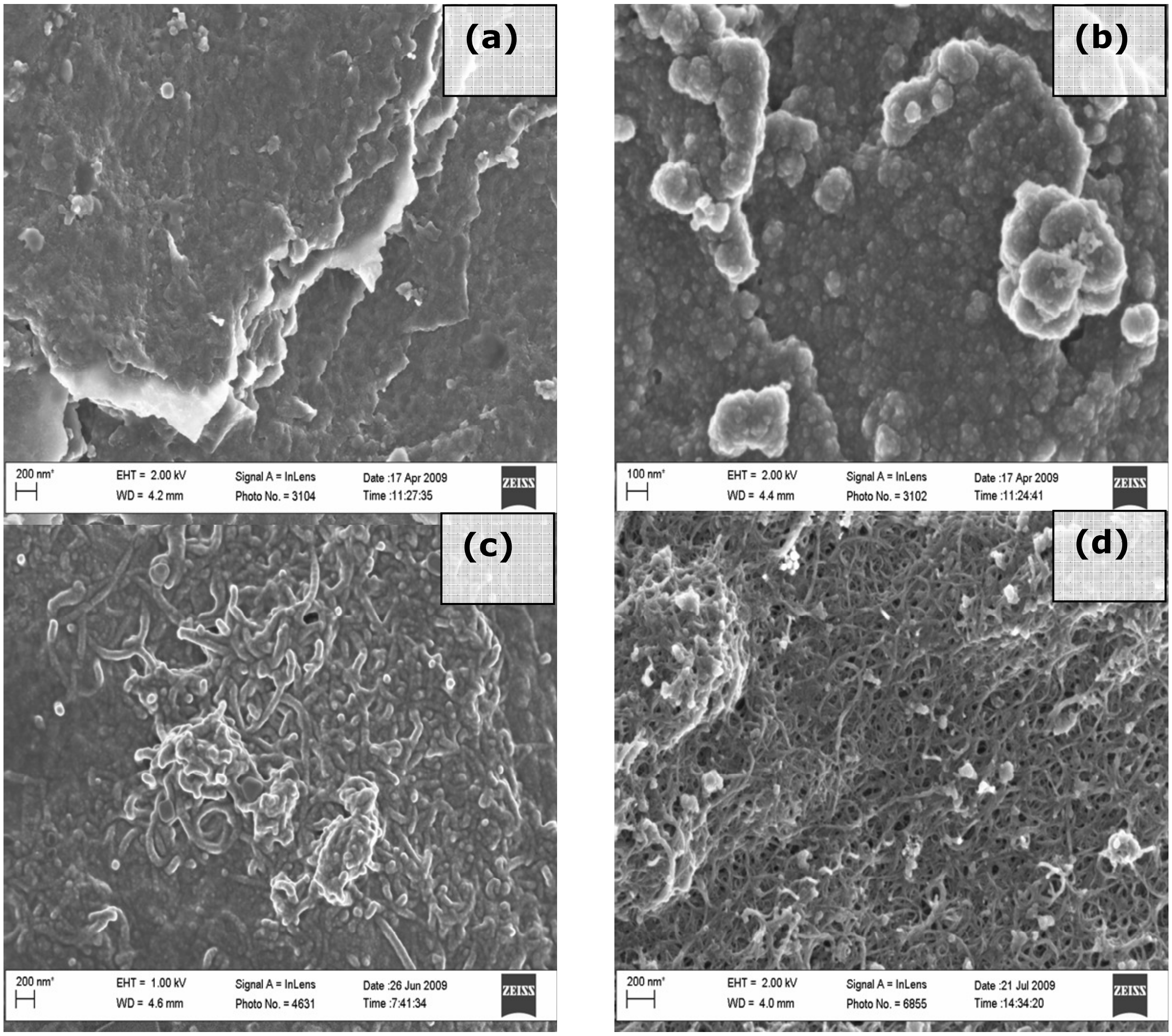

Figure 4.25: SEM image of (a) bare BPPGE, (b) BPPGE-polyNiTAPc, (c) BPPGE-MWCNT-polyNi(OH)TAPc and (d) BPPGE-MWCNT-polyNiTAPc electrode surfaces.

The energy deliverable efficiency (η / %) was obtained from equation 17 in chapter 1.

$$\eta\ (\%) = \frac{t_d}{t_c} \times 100 \ \ldots\ldots\ldots\ldots\ldots\ldots\ldots\ldots\ldots\ldots\ldots\ldots (17)$$

The energy deliverable efficiency for BPPGE-MWCNT-polyNiTAPc is 105 ± 11%. The long-term cycling stability of the same electrode as potential supercapacitor material was also investigated. A typical repetitive charge-discharge cycling for 1000 cycles is shown in figure 4.26. It is clear from this figure that MWCNT-polyNiTAPc is capable of undergoing continuous charge and discharge with little or no significant loss in capacitance. This observation also suggests that MWCNT-polyNiTAPc material does not show significant structural changes during the course of charge-discharge processes.

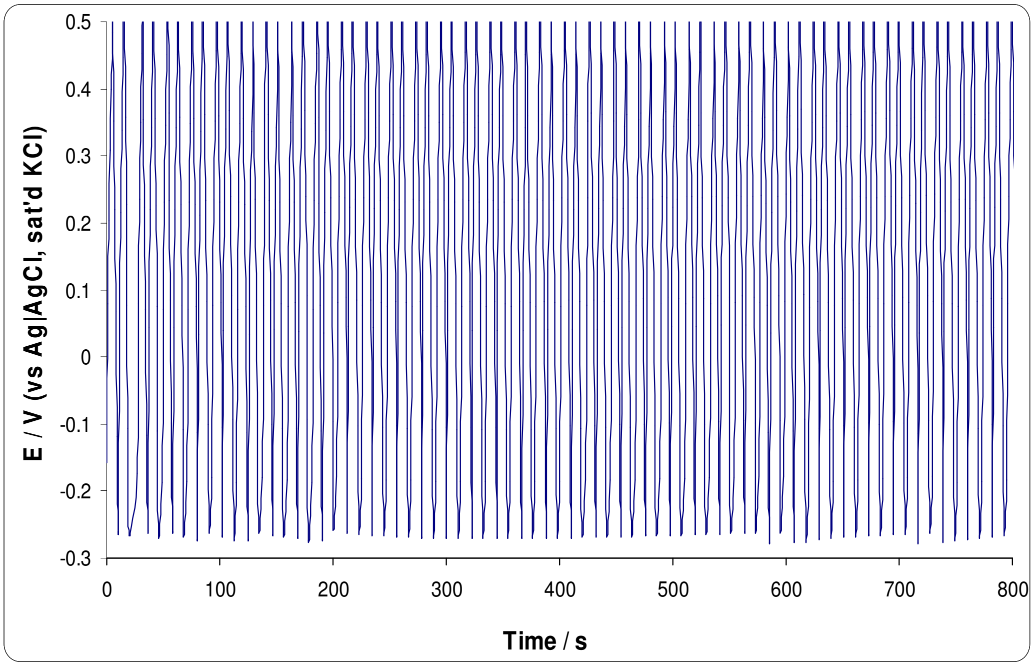

Figure 4.26: Typical portion of the charge-discharge curves obtained during a repetitive cycling of the BPPGE-MWCNT-polyNiTAPc electrode at 10 mA cm^{-2} in 1 M H_2SO_4 solution, showing excellent stability.

4.3.3 Electrochemical Impedance Spectroscopy experiments

To obtain further insights into the impact of the MWCNTs on the capacitive behaviour of the polyNiTAPc, a comparative EIS experiments were carried out for the BPPGE-polyNiTAPc, BPPGE-MWCNT and BPPGE-MWCNT-polyNiTAPc electrodes in 1 M H_2SO_4 conditions. The low-frequency differential capacitance ($C_d = 1/2\pi f Z''$) for each of the electrodes was obtained by running a single potential EIS experiment (biased at 0.25 V) MWCNT, polyNiTAPc and MWCNT-polyNiTAPc at a frequency range of 10 mHz – 100 kHz in 1 M sulphuric acid (Figure 4.27). In all cases, the maximum specific capacitance was obtained at ~ 0.25 V vs Ag|AgCl, with values decreasing as BPPGE-MWCNT-polyNiTAPc (~ 13.2 mF cm^{-2}) > BPPGE-MWCNT (~ 10 mF cm^{-2}) > BPPGE-polyNiTAPc (~ 3.17 mF cm^{-2}). This trend again agrees with CV and CD data. Clearly, the EIS data strongly deviate from the data obtained from the galvanostatic method, and are characteristic of conducting polymeric substances.[147] The deviation in specific capacitances calculated from CD and EIS have been explained in section 4.2.2 of this chapter.

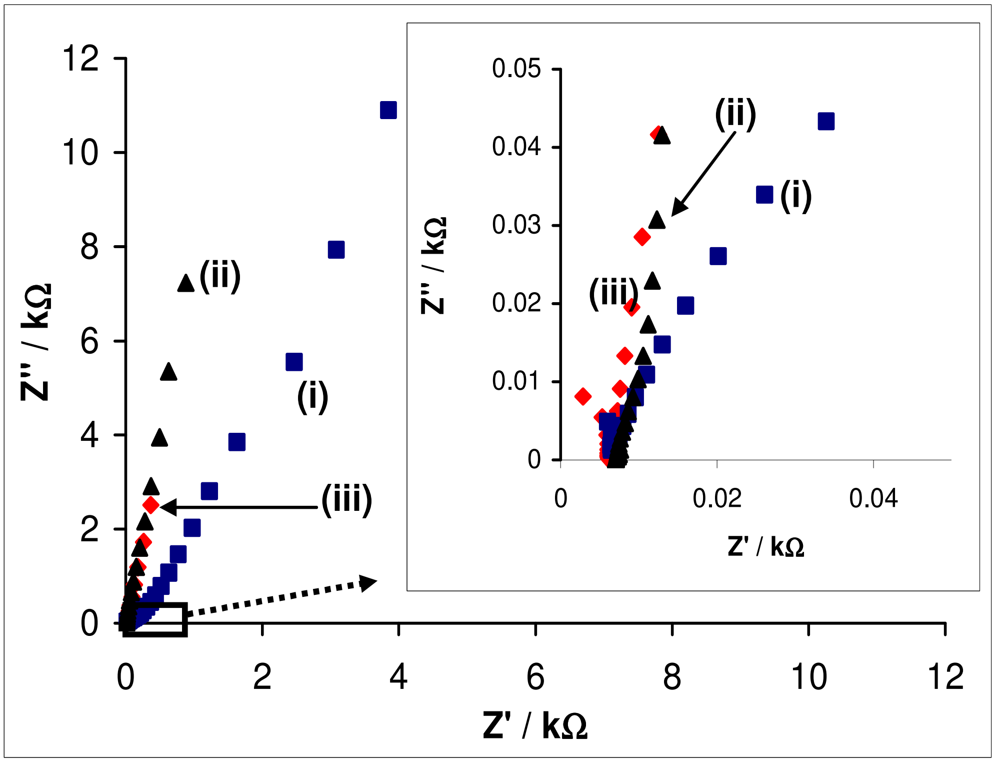

Figure 4.27: Comparative Nyquist plots for BPPGE-polyNiTAPc (i) and BPPGE-MWCNT-polyNiTAPc (ii) and MWCNT (iii) electrodes at 0.25 V. Inset: The expanded portion of the high frequency region.

The impedance spectrum was satisfactorily modeled using the electrical equivalent circuit involving the modified Randles circuit shown in figure 4.28. The circuit (R (Q [RQ]) used to fit the EIS data involved a solution resistance (R_s = -17.6 Ω), a constant phase element (CPE_1 = 2.2 μF with n_1 = 1), an electron transfer resistance of (R_2 = 23.78 Ω) and constant phase element (CPE_2 = 4.8 mF with n_2 = 0.9). The CPE_1 that replaced the diffusion impedance (Z_w) in the ideal Randles circuit is associated with a high n_1 value (n_1 = 1), describing the high porous nature of the electrode.

The n_2 value (0.90) is approximately equal to the ideal capacitive behaviour of n = 1.

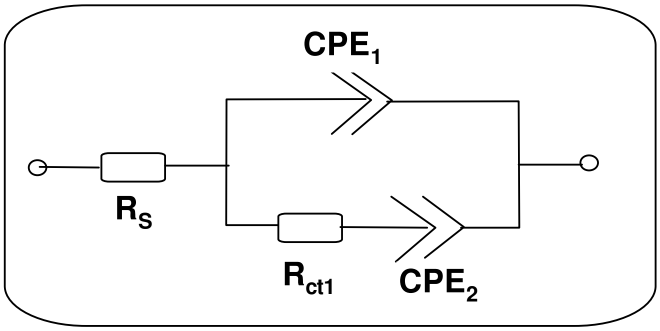

Figure 4.28: Electrical equivalent circuit used in fitting the experimental EIS data obtained for the BPPGE-MWCNT-polyNiTAPc.

As seen in Figure 4.27, the MWCNT-polyNiTAPc shows near-vertical line as expected for pseudocapacitor. The “knee” or “onset” frequency (f_o), which is a measure of the power capability of a supercapacitor, decreases as MWCNT-polyNiTAPc (1.604 kHz). The response time of the capacitor is about 0.6 ms, suggesting that most of the stored energy of MWCNT-polyNiTAPc as a capacitor material is accessible at frequencies as high as 1.604 kHz. This is very interesting considering that most commercially available supercapacitors, including those specifically designed for higher power applications, operate at frequencies less than 1 Hz.[156]

CHAPTER FIVE

CONCLUSIONS

The capacitive behaviour of three different carbon nanotube-nickel (ii) phthalocyanines nanocomposites have been investigated for the first time in 1M H_2SO_4. CNT-MPc modified electrodes showed excellent supercapacitive behaviour and remarkable stability. When compared to unsubstituted NiPc/MWCNT or nickel (II) tetra-*tert-butyl*phthalocyanine (tBuNiPc)/MWCNT, NiTAPc/MWCNT exhibited superior supercapacitive behaviour.

The effect of substituent groups on the phthalocyanine macromolecule was also observed. The MWCNT-NiTAPc electrode had the highest capacitance possibly due to the contribution by the nitrogen groups located at the periphery of the phthalocyanine molecule. The contribution by pseudocapacitance effects to the overall capacitance values cannot be overlooked. Alkyl groups on the tBuNiPc macromolecule however have been shown to block the pores in the nanocomposite essential for charge storage. The results also show the contribution by the MWCNTs to the overall capacitance.

Electropolymeric film of a phthalocyanine polymer, supported on MWCNTs platforms, has also been interrogated for the first time. Cyclic voltammetry, galvanostatic charge-discharge cycling and impedimetric techniques confirmed that the MWCNT-polyNiTAPc based electrode exhibit excellent supercapacitance, which may be ascribed to the positive synergism between the MWCNT and polyNiTAPc. The finding reported in this work is crucial as it could open doors for the investigation of many other electropolymers of metal tetraaminophthalocyanine (MTAPc) complexes and related metal N4 macrocyclic organometallic complexes for application in supercapacitors.

Given the high number of existing MPc complexes and new ones constantly reported in the literature, and the importance of supercapacitors in energy development, we envisage that this novel study is likely to spark research interests in the supercapacitive properties of CNT-MPc hybrid electrodes. Although we have managed to reach a few important conclusions in this work, several aspects still need to be further investigated.Listed below, are some of the suggestions for future work:

1. The effect of different substituent groups on the phthalocyanine molecule and contribution to overall capacitance. e.g $–SO_3$,phenyl groups etc.
2. The effect of different electrolytes on the capacitive properties of the MWCNT-MPc nanocomposites such as ionic liquids and alkaline medium need also be investigated.
3. The growth of carbon nanotubes on the electrode surface by CVD can produce uniform surface coverage and a desired mesoporous surface by controlling the pore size and pore distribution thus providing a high conducting and high surface area support.

4. Since nirogen groups have been reported to increase capacitance in carbon material,functionalisation of the MWCNTs with an aim to increase the number of nitrogen groups on the CNT walls may enhance the supercapacitance .
5. An increased electrode surface area and the employment of the more practical two electrode system should be explored.

References

1) L. Li, H. Song, Q. Zhang, J. Yao and X. Chen, *J. Power Sources*, 2009, **187**, 268

2) H. E. Becker, U.S. Patent 2, 800, 616 9 To General Electric

3) Batteries and Energy Technology (2007) *Brief history of supercapacitors* [Online] Available: http://www.cantecsystems.com/ccrdocs/brief-history-of-supercapacitors.pdf [accessed 10 August 2008]

4) M. Winter, R. J. Brodd, *Chem. Rev*., 2004, **104**, 4245

5) R. Kötz, M. Carlen, *Electrochim. Acta*., 2000, **45**, 2483

6) E. Frackowiak, F. Beguin, in: *Recent Advances in Supercapacitors*, (Ed.: V. Gupta) Transworld Research network, Kerala, India, 2006, Chapter 5, pp. 79-114

7) A. J. Bard and L. R. Faulkner, *Electrochemical Methods, Fundamentals and Applications (2nd)*, John Wiley & Sons, Inc, 2001

8) B. E. Conway, V. Birss, L. Wojtowice, *J. Power Sources,* 1997, **1**, 6

9) E. Frackowiak, F. Béguin, *Carbon,* 2001, **39**, 937

10) V. V. N Obreja, *Physica E.,* 2008, **40**, 2596

11) Marin S. Halper, James C. Ellendogen (2006) *Supercapacitors: A brief Overview*, [Online] Available: http://www.mitre.org/work/tech_papers/tech_papers.../06_0667.pdf [accessed 3 October 2008]

12) S. I. Pyun, C. H. Kim, S. W. Kim, J. H. Kim, *J. Mater. Electrochem., Syst.* 2002, **5**, 289

13) K. H. An, W. S. Kim, Y. S. Park, J. M. Moon, D. J. Bae, S. C. Lim, Y. S. Lee, Y. H. Lee, *Adv. Funct. Mater*., 2001, **11**, 387

14) C-W. Huang, Y-T. Wu, C-C. Hu, Y-Y. Li, *J. Power Sources,* 2007, **172**, 460

15) H. Shi, *Electrochim. Acta,* 1996, **41,** 1633

16) T. Osaka, X. Liu, M. Nojima, T. Momma, *J. Electrochem. Soc.,* 1999, **146** (5), 1724

17) M. F. Rose, C. Johnson, T. Owen, B. Stephens, *J. Power Sources,* 1994, **47**, 303

18) L. Bonnefoi, P. Simon, J. F. Farvaque, C. Sarrau, A. Dugust, *J. Power Sources,* 1999, **80**, 149

19) C. Niu, E. K. Sichel, R. Hoch, D. Moy, H. Tennent, *Appl. Pys. Lett*., 1997, **70**, 1480

20) E. Frackowiak, K. Meitenier, V. Bertagna and F. Beguin, *Appl. Phys. Lett*., 2000, **77**, 2421.

21) H. A. Andreas and B. E. Conway, *Electrochim. Acta,* 2006, **51,** 6510

22) H. Y. Lee, J. B. Goodenough, *J. Solid State Chem*., 1999, **144,** 220

23) S. C Pang, M. A. Anderson, T. W. Chapman, *J. Electrochem. Soc*., 2000, **147,** 444

24) C.C. Hu, Y. H. Huang, K. H. Chang, *J. Power Sources,* 2002, **108,** 117

25) J. P. Zheng, T. R. Jow, *J. Electrochem. Soc*., 1995, **142**, L6

26) T. C. Liu, W. G. Pell, B. E. Conway, *Electrochim. Acta,* 1997 , **42**, 3541

27) V. Srinivasan, J. W. Weidner, *J. Electrochem. Soc*., 1997, **144**, L210

28) K.C. Liu, M. A. Anderson, *J. Electrochem. Soc*., 1996, **143,** 124

29) Y. Zheng, M. Zhang and P. Gao, *Materials Research Bulletin,* 2007, **42,** 1740

30) T. Arikado, C. Iwaruka, H. Tamura, *Electrochim. Acta*., 1977, **22**, 513

31) J. Y. Lee, K. Liang, K. H. An, Y. H. Lee, *Synh. Met*., 2005, **150**, 153

32) N-L. Wu, Y-P. Han, S–Y. Wang, L–R. Shiue. Proceedings-Electrochemical Society 2002, 2002-7 (Electrochemical capacitor and Hybrid Power Sources), 95

33) M. Wohlfahrt-Mehrens, J. Schenk, P.M. Wilde, E. Abdelmula, P. Axmann, J. Garche, *J. Power Sources,* 2002, **105,** 182

34) V. Gupta, N. Miura, *Mater. Lett.,* 2006, **60**, 1466

35) T. C. Girirja, M. Sangaranayanan, *J. Power Sources,* 2006, **156**, 705

36) E. Frackowiak, K. Jurewicz, S. Delpeux, F. Beguin, *J. Power Sources,* 2001, **97-98**, 822

37) A. Rudge, I. Raistick, S. Gottesfeld, J. P. Ferraris, *Electrochim. Acta,* 1994, **39**, 273

38) K. Naoi, Extended Abstracts, 49th Annual Meeting of the International Society of Electrochemistry, Kitakyushu, Japan, September, pp. 647, 1998.

39) D. E. Stilwell, S. M. Park, *Electrochem. Soc*., 1988, **135**, 2491

40) L. Li, H. Song, Q. Zhang, J. Yao, X. Chen, *J. Power Sources,* 2009, **187**, 268

41) B.E. Conway. *Electrochemical Supercapacitors, Scientific Fundamental and technological Applications,* Plenum Publishers, 1999.

42) C. Arbizzani, M. Mastragostino and L. Meneghello, *Electrochim. Acta,* 1996, **41**, 21

43) M. Mastragostino, C. Arbizzani and F. Soavi, *Solid State Ionics,* 2002, **148**, 493

44) K. H. An, K. K. Jeon, J. K. Heo, S. C. Lim, D. J. Bae and Y. H. Lee, *J.Electrochem. Soc,* 2002, **149**, A1058

45) M. Mastragostino, C. Arbizzani and F. Soavi, *J. Power Sources,* 2001, **97-98**, 812

46) L. Jurewicz, S. Delpeux, V. Bertagna .F. Béguin and E. Frackowiak, Chem. *Phys. Lett*., 2001, **347**, 36

47) G. A. Snook, G. Z. Chen, D. J. Fray, M. Hughes, M. Shaffer. *J. Electroanaly. Chem*., 2004**, 568**, 135

48) C. Arbizzani, M. Mastragostino and F. Soavi, *J. Power Sources,* 2001, **100**, 164

49) G. G. Amatucci, F. Badway, A. Du Pasquier, and T. Zheng, *J. Electrochem. Soc*., 2001, **148**, A930

50) S. Iijima, *Nature,* 1991, **363,** 56

50a) L.V. Radushkevich, V. M Lukyanovich, *Zurn Fisic Chim.* 1952, **26**, 88

50b) P. G. Wiles, J. Abrahamson, *Carbon,* 1989, **6**, 341

51) S. Iijima, T. Ichihashi, *Nature,* 1993, **363,** 603

52) A. Thess, R. Lee, P. Nikolaev, H. Dai, P. Petit, J. Robert, C. Xu, Y. H. Lee, S. G. Kim, A. G. RInzler, D. T. Colbert, G. E. Scuseria, D. Tomanek, J. E. Fischer, R. E. Smalley, *Science,* 1996, **273**, 483

53) M. S. Dresselhaus, *Carbon,* 1995, **33**, 871

54) Q. Jiang , M. Z. Qu, G. M. Zhou, B. L. Zhang, Z. L. Yu, *Mater. Lett.,* 2002, **57,** 988.

55) T. W. Odom, J - L. Huang, P. Kim, and C. M. Lieber, *J. Phys. Chem. B.,* 2000, **104***,* 2794

56) V. N. Popov, *Material Science and Engineering R.,* 2004, **43**, 61.

57) G. de la Torre, W. Blau and T. Torres, *Nanotechnol.,* 2003, **14**, 765.

58) E. W. Wong, P. E. Sheehan, and C. M. Lieber, *Science,* 1997, **277**, 1971.

59) A. Peigney, C. Laurent, E. Flahaut, R. R. Basca and A. Rousset, *Carbon,* 2001,**39**,507.

60) L. Agüí, P. Y-Sedeño, J. M. Pingarrón, *Anal.Chim.Acta,* 2008, **622**, 11.

61) J. Wang, M. Musameh, Y. Lin, *J. Am. Chem. Soc*., 2003, **125**, 2408

62) J. Xu, J. Zhu, Q. Wu, Z. Hu and H. Chen, *Electroanal*., 2005, **17**, 89

63) M. Zhang and W. Gorski, *J. Am. Chem. Soc*., 2005, **127**, 2058

64) K. I. Ozoemena, T. Nyokong, D. Nkosi, I. Chambrier, M. J. Cook, *Electrochim. Acta,* 2007, **52**, 4132.

65) J. Pillay, K. I. Ozoemena, *Electrochim. Acta,* 2007, **52**, 3630

65a) R. R. Moore, C. E. Banks, R. G. Compton, *Chem. Commun*., 2004, **16**, 1804

65b) C. E. Banks, A. Crossley, C. Salter, S. J. Wilkins, R. G. Compton, *Angew. Chem*., 2006, **118**, 2595

66) E. Frackowiak and F. Béguin, *Carbon,* 2002, **40**, 1775

67) E. Frackowiak, S. Gautier, H. Gaucher, S. Bonnamy, F. Beguin, *Carbon,* 1999, **37**, 61.

68) C. Nützenadel, A. Zuttel, D. Chartouni, L. Schlapbach, *Electrochem. Solid –State Lett.,* 1999, **2**, 30.

69) A. G. Dandridge, H. A. Drescher and J. Thomas (Scottish Dyes Ltd.), British Patent. 332, 169, November 18, 1929.

70) N. B McKeown ; Phthalocyanine Materials: Synthesis, Structure and Function Cambridge University Press 1998 page 1.

71) K. I. Ozoemena (Editor), Recent Advances in Analytical Electrochemistry (2007) Transworld Research Network.

72) J. E. Kuder, *Imaging Sci.,*1988, **32**, 51.

73) D. Wörle, D. Meissener, *Adv. Mater*., 1991, **3**, 129.

74) K. I. Ozoemena, T. Nyokong, Electrochemical Sensors Based on Phthalocyanine and Related Complexes. In *Encyclopedia of Sensors*; Grimes, C. A; Dickey, E. C.; Pishko, M. V., Eds.; American Scientific Publishers: California, 2006 : Vol. 3, chapter E, pp. 157 - 200

75) A. B. P. Leznoff, M. R. Hempstead, C. C. Leznoff, W. Lui, M. Melnik, W. A Nevin and P. Seymour, *Pure Appl. Chem*., 1986, **58**, 1467.

76) H. M. Rietveld, *J. Appl. Crystallogr*., 1969, **2**, 65.

77) University of New Mexico (1999) *Basics of X-ray Diffraction*, [Online] Available: http://epswww.unm.edu/xrd/xrdbasics.pdf [accessed on 11 July 2008]

78) Stanley Whittingham,(1989-1997) *X-ray Analysis of a Solid*, [Online] Available:http://materials.binghamton.edu/labs/xray/xray.html [accessed on 11 July 2008]

79) A. K. Hassan, R. D. Gould, *Phys. Stat. Sol* (A)., 1992, 132, 91

80) D. Qu, *J. Power Sources,* 2002, **109**, 403

81) J. R. Ferraro, L. J. Basile, Fourier Transform Infrared Spectroscopy, vol.3, (1982) Academic Press, New York.

82) J. M. Goddard, J. H. Hotchkiss, *Prog. Polym. Sci*., 2007, **32** , 698.

83) H. –H. Perkampus, *UV-Vis Spectroscopy and its Applications*, Springer-Verlag, Berlin Heidelberg (1992)

84) D.A. Skoog, F. J. Holler, S. R. *Crouch., Principles of Instrumental Analysis*, Thomson Brooks/Cole, 6th Edition, 2007, pg337

85) F.C. Strong, *Anal. Chem*., 1952, **24,** 338

86) University of Nebraska-Lincoln (nd) *Transmission Electron Microscope* (TEM) [Online] Available :http://www.unl.edu/CMRAcfem/temoptic.htm [Accessed 2 February 2009]

87) V. J. Morris, A. R. Kirby, A. P. Gunning; *Atomic force Microscopy for Biologists*, Imperial College Press, London (1999)

88) J. Wang, *Analytical Electrochemistry*, VCH Publishers Inc. New York, 1994

89) Zoltan Nagy (2008) *Electrochemistry Encyclopedia* [Online] Available:http://electrochem.cwru.edu/ed/encycl/art-i02-introduction.htm [Accessed 2 February 2009]

90) P.T. Kissinger, W.R. Heineman, *J. Chem. Ed*., 1983, **60**, 702

91) R. Compton and C. Banks, *Understanding Voltammetry*, World Scientific Publishing Co. Inc., Singapore (2007)

92) Reilley, C.N. *J. Chem. Ed*., 1962, **39**, A853

93) R.S. Nicholson, I. Shain, *Anal. Chem*., 1964, **36**, 707

94) D.H. Evans, K. M. O'Connell, R.A. Petersen and M. J. Kelly., *Journal of Chemical Education,* 1983, **60**, 290

95) S-J Bao, C.M. Li, C-X Guo, Y Qiao, *J .Power Sources,* 2008, **180**, 676

96) M. Lakatos-Varsanyi and D. Hanzel, *Corros. Sci.,* 1999, **41,** 1585.

97) S. Rudenja, C. Leygraf, J. Pan, P. Kulu, E. Tallimets, V. Milki, *Surf. Coat. Technol.,* 1999, **114**, 129

98) L. Cunha, M. Andritschky, L. Rebouta, K. Pischow, *Surf. Coat. Technol.,* 1999, **116-119**, 1152

99) J. A. Gonzalez, E. Otero, A. Bautista, E. Almeida, M. Morcillo, *Prog. Org. Coat.,* 1998, **33**, 61

100) P.L. Bonora, F. Deflorian, L. Fedrizzi, *Electrochim. Acta,* 1996, **41**, 1073

101) A. Chu, P. Braatz, *J. Power Sources,* 2002, **112**, 236

102) H-K. Song, Y-H. Jung, K-H Lee, L. H. Dao, *Electrochim. Acta,* 1999, **44**, 3513

103) P. N. Mashazi, K. I. Ozoemena, T. Nyokong, *Electrochim. Acta,* 2006, **52**, 177

104) I. Navrátilová, P. Skládal, *Bioelectrochem*., 2004, **62**, 11

105) C. Khaldi, H. Mathlouthi, J. Lamloumi, *J. Alloys and Compounds,* 2009, **479**, 284

106) F. Lufrano,P. Staiti, *Electrochim. Acta,* 2004, **49**, 2683

107) T. Shinomiya, V. Gupta, N. Miura, *Electrochim. Acta,* 2006, **51**, 4412

108) Gamry Instruments (28 December 2007) *Fundamentals of Electrochemical Impedance Spectroscopy* [Online] Available: http://www.gamry.com/App_Notes/EIS_Primer/EIS_Primer.htm#Data%20Presentation [Accessed 4 November 2008]

109) J. R. Macdonald, W. B. Johnson in: E. Barsoukov, J. R. Macdonald (Eds.), *Impedance Spectroscopy, 2nd ed*. John Wiley and Sons Inc. 2005

110) E. Barsoukov, J. R. Macdonald (Eds.),*Impedance Spectroscopy, 2nd ed*. John Wiley and Sons Inc. 2005

111) C. Du, N. Pan, *Nanotechnology,* 2006, **17**, 5314

112) B. A. Boukamp, *J. Electrochem. Soc*., 1995,**142**, 1885

113) P. Zoltowski, *J. Electroanal. Chem*., 1998, **443**, 149

114) J. Bisquert, G. garcia-Belmonte, P. Bueno, E. Longo, L. O. S. Bulhões, *J. Electroanal. Chem*., 1998, 452, 229

115) J-B. Jorcin, M. E. Orazem, N. Pébére, B. Tribollet, *Electrochim. Acta*, 2006, **51,** 1473

116) J.Liu, G. Rinzler, H. Dai, J. H. Hafner, R. K. Bradley, P. J. Boul, A. Lu, T. Iverson, K. Shelimov, C. B. Huffman, F. Rodriguez-Macias, Y-S. Shon, T. R. Lee, D. T. Colbert, R. E. Smalley, *Science,* 1998, **280**, 1253.

117) Z-L. Yang, H-Z. Chen, L. Cao, H-Y. Li, M. Wang, *Mater. Sci. Eng. B.,* 2004, **106**, 73

118) M. Siswana, K. I. Ozoemena, T. Nyokong, *Electrochim. Acta,* 2006, **52**, 114.

119) K. I. Ozoemena, T. Nyokong, *Inorg. Chem. Commun*., 2003, **6**, 1192

120) T – F. Kang, G – L. Shen. R – Q. Yu, *Anal. Chim. Acta,* 1997, **356**, 245

121) A. Goux, F. Bedioui, L. Robbiola, M. Pontie, *Electroanalysis,* 2003, **15**, 969.

122) G. Roslonek and J. Taraszewka, *J. Electroanal. Chem*., 1992, **325**, 285

123) Q. Jiang, M. Z. Qu, G. M. Zhou, B. L. Zhang, Z. L. Yu, *Mat. Lett.,* 2002, **57**, 988

124) S. Nakamura, H. Amatatsu, T. Ozaki, S. Yamaguchi and G. Sawa, *Jpn. J. App. Phys*., 1987, **26**,1878

125) M. -S. Wu, H.-H. Hsieh, *Electrochim. Acta,* 2008, **53,** 3247

126) X. Wang, Y. Liu, W. Qiu and D. Zhu, *J. Mater. Chem*., 2002, **12**, 1636.

127) M. J. Stillman and T. N. Nyokong, *in* “Phthalocyanines: Properties and Applications,” (C. C. Leznoff, and A. B. P. Lever, Eds.), Vol. 1, Chap. 3, p. 133. VCH, New York, 1989

128) Gouterman, M. In The Porphyrins; Dolphin, D., Ed.; Academic Press: New York, 1978; Vol. III, Part A, Physical Chemistry.

129) B. Ortiz, S.-M. Park, N. J. Doddapaneni, *Electrochem. Soc.,* 1996,**143**, 1800

130) A. T. Davidson, *J Chem Phys*., 1982, **77**, 162

131) H. Jaegfeldt, T. Kuwana and G. Johansson, *J. Am. Chem. Soc*., 1983, **105**, 1805

132) R. Chen, Y. Zhang, D. Wang, H.Dai, *J. Am. Chem. Soc*., 2001, **123**, 3838

133) H.-L. Hsu, J.-M. Jehng, L.-C. Wang, S.-R. Yang, *Materials Chemistry and Physics,* 2008, **109**, 148

134) J. Li, X. Wang, Q. Huang, S. Gamboa, P.J. Sebastian, *J. Power Sources,* 2006, **158**, 784

135) G. De la Torre, W. Blau and T. Torres, *Nanotechnol.,* 2003 ,**14**, 765

136) C. Du, N. Pan, *Nanotechnol.,* 2006, **17**, 5314

137) H. Murakami, T. Nomura, N. Nakashima, *Chem. Phys. Lett*., 2003, **379**, 481

138) C. A. Thorogood, G. G. Wildgoose, A. Crossley, R. M. J. Jacobs, J. H. Jones, R. G. Compton, *Chem. Mater.*, 2007, **19**, 4964

139) C. A. Thorogood, G. G. Wildgoose, J. H. Jones, R. G. Compton, *New J. Chem.*, 2007, **31**, 958

140) G. G. Wildgoose, P. Abiman, R. G. Compton, *J. Mater. Chem.*, 2009, **19**, 4875

141) D. Hulicova-Jurcakova, M. Kodama, S. Shiraishi, H. Hatori, Z. H. Zhu, G. Q. Lu, *Adv. Funct. Mater*., 2009, **19**, 1.

142) K. I. Ozoemena, T. Nyokong in *Encyclopedia of Sensors*, Vol. 3 (Eds.: C.A. Grimes, E.C. Dickey, M.V. Pishko), American Scientific Publishers, California, 2006**,** Chapter E, pp. 157-200.

143) F. Bedioui, S. Griveau, T. Nyokong, A. J. Appleby, C. A. Caro, M.Gulppi, G. Ochoa and J. H. Zagal, *Phys. Chem. Chem. Phys*., 2007 , **9**, 3383.

144) B. J. Feldman, P. Burgmayer, R. W. Murray, *J. Am. Chem. Soc*., 1985, **107**, 872.

145) N. Mermilliod, J. Tanguy, F. Petior, *J. Electrochem. Soc.,* 1986, **133**, 1073.

146) J. Tanguy, N. Mermilliuod, M. Hoclet, *J. Electrochem. Soc.,* 1987, **134**, 795.

147) T. Tanguy, M. Slama, M. Hoclet, J. L. Baudin, *Synth. Me*t., 1989, **28**, C145.

148) M. Kalaji, L. M. Peter, *J. Chem. Soc., Faraday Trans*., 1991, **87**, 853.

149) X. Ren, P. G. Pickup, *J. Electroanal. Chem*., 1994, **372**, 289.

150) V. Ganesh, S. Pitchumani, V. Lakshminarayanan. *J. Power Sources*, 2006, **158**, 1523

151) T. C. Girija, M.V. Sangaranarayanan, *J. Appl. Electrochem*., 2006, **36**, 531

152) G. Xu, W. Wang, X. Qu, Y. Yin, L. Chu, B. He, H. Wu, J. Fang, Y. Bao, L. Liang, *Eur. Polym. J.* 2009, doi : 10.1016/j.europolymj.2009.05

153) V. Gupta, T. Shinomiya, N. Miura in: *Recent Advances in Supercapacitors,* (Ed.: V. Gupta) Transworld Research Network, Kerala, India, 2006, chapter 2, pp.17-28.

154) C. Du, N. Pan, *J. Power Sources,* 2006, **160**, 1487

155) C-W. Huang, Y-T. Wu, C-C. Hu, Y-Y. Li, *J. Power Sources*, 2007, **172**, 460.

156) J. R Miller, Proceedings of the Electrochemical Society Meeting, Chicago, October, 1995, 246

157) M. E. Orazem, B. Tribollet, Electrochemical Impedance Spectroscopy, John Wiley & Sons Inc, Hoboken, NJ., 2008, Chapter 13.

158) T. Shinomiya, V. Gupta, N. Miura, *Electrochim. Acta,* 2006, **51,** 4415

159) K. Kierzek, E. Frackowiak, G. Lota, G. Gryglewicz, J. Machnikowski, *Electrochim. Acta*, 2004, **49**, 515

160) Y-T. Kim, Y. Ito, K. Tadai, T. Mitani, *Appl. Phys. Lett*., 2005, **87,** 234106.

161) V. Gupta, N. Miura, *J. Power Sources*, 2006, **157**, 616

162) H. Zhang, G. Cao, Z. Wang, Y. Yang, Z. Shi, Z. Gu, *Electrochem. Commun*., 2008, **10**, 1056

163) V. Gupta, S. Gupta and N. Miura, *J. Power Sources*, 2008, **177**, 685

164) E. Frackowiak, G. Lota, J. Machnikowski, C. Vix-Guterl, F. Béguin, *Electrochim. Acta,* 2006, **51**, 2209

165) J. Wang, P. Tuzhi, *Anal. Chem*., 1986, **58**, 3257

166) F. Bedioui, S. Gutierrez Granados, C. Bied-Charreton, *Recent Res. Devel. Electrochem*., 1999, **2**, 91

167) A. B. P. Lever, *J. Porph. Phthal*., 1999, **3**, 488

168) M. Biesaga, K. Pyrzynska, M. Trojanowicz, *Talanta,* 2000, **51**, 209

169) M. M. El-Nahass, A. M. Farag, K. F. Abd El-Rahman, A. A. A. Darwish, *Opt. Laser Technol*., 2005, **37**, 513

170) S. Trevin, F. Bedioui, M. G. Gomez Villegas, C. Bied-Charreton, *J. Mater. Chem*., 1997, 7, 923

171) F. Bedioui, J. Devynck and C. Bied-Charreton, *Acc. Chem. Res*., 1995, **28**, 30

172) A. Deronzier and J. C. Moutet, *Coord. Chem. Rev*., 1996, **147**, 339

173) A. Goux, F. Bedioui, L. Robbiola, M. Pontie, *Electroanalysis,* 2003, **15**, 11, 969

174) G. Roslonek and J. Taraszewka, *J. Electroanal. Chem*., 1992, **325**, 285

175) J. Pillay, K. I. Ozoemena, *Chem. Phys. Lett.,* 2007, **441**, 72

176) M. S. Wu, H-H Hsieh, *Electrochim. Acta,* 2008, **53**, 3427